TRABAJO FINAL DE MÁSTER

TÍTULO

RELEVANCE OF HYDRO-MECHANICAL-CHEMICAL PROCESSES INVOLVED IN THE CONSTRUCTION AND OPERATION OF COPPER HEAP LEACH PADS

AUTOR

MAYU ALBERTO TINCOPA HEREDIA

TUTOR

ALBERTO LEDESMA

ESPECIALIDAD

INGENIERÍA GEOTÉCNICA

FECHA

JUNIO 2013

Dep. de Ingeniería del Terreno, Cartográfica y Geofísica
E.T.S. Ingenieros de Caminos, Canales y Puertos
UNIVERSIDAD POLITÉCNICA DE CATALUÑA

ABSTRACT

Heap leaching in the mining industry had become a fairly sophisticated practice at least 500 years ago. It is defined as a mineral processing technology whereby large piles of crushed Run-of–Mine (ROM) rock are leached with various chemical solutions to extract the valuable minerals.

The main goal of this work is to contribute to the understanding of the behavior of a heap leach pad by using coupled Hydro-Mechanical-Chemical (HMC) simulations and optimize its design by improving the pad stability and the ore recovery efficiency.

The methodology of the work has been the following. First, an exhaustive review of the state of the art of heap leach pad construction is included, describing the coupled equations of the involved physical and chemical phenomena. Then, the implementation of numerical methods to solve the complete system of equations is described. The commercial Finite Element (FE) code COMSOL Multiphysics has been used as a numerical tool. Afterwards, several benchmark examples involving the different physics are solved to check the proper implementation of these numerical tools. Finally, a simulation of a general heap leach pad with a complete system of equations is performed.

The numerical tool used in this work is able to solve simultaneously unsaturated flow, soil mechanics and reactive transport in porous media. The changes in porosity, permeability due to mineral dissolution/precipitation and irrigation time affect significantly the hydromechanical behavior of the heap leach pad. The stability of the pad and the ore recovery efficiency improves because the variable saturation and the mechanical deformation are considered during the construction and operation process.

AGRADECIMIENTOS

Dedico estas líneas a mis padres, hermanos y familiares por la inspiración que representan, la motivación y el apoyo incondicional durante el transcurso de mi vida.

A todos mis amigos por los buenos momentos compartidos que me brindan con su compañía, amistad y durante el día a día de estar viviendo fuera de mi país.

A mi tutor Alberto Ledesma por su tiempo y consejos tanto profesionales como de persona.

A la empresa Amphos21 por la apuesta y apoyo económico durante el desarrollo de la tesis con especial énfasis a mi mentor Albert Nardi y Jorge Molinero por sus enseñanzas, dedicación y motivación que me han trasmitido durante este tiempo tanto profesionalmente y como personas.

CONTENT

Figures

Tables

Annexes

1.0 INTRODUCTION

1.1 Background

Heap leaching is a mineral processing technology whereby large piles of crushed Run-of-Mine (ROM) rock are leached with various chemical solutions that extract valuable minerals (Thiel, 2004). This is one of several alternative processes for treating precious metal ores and it is selected primarily to take advantage of its low capital cost relative to other methods (Kappes, 2002).

There are many critical aspects in heap leach pad construction and operations. At least two of them could be improved by an appropriate design and management: the mechanical stability and the mineral recovery efficiency. They are of paramount importance for two main reasons: (1) they could play an important role on the safety of the operation and; (2) they are keys for the metallurgical process efficiency, especially in the mid-long term.

Heap leach pad simulation practice is becoming more relevant because its possible impact on the efficiency and on the security which could increase the benefits of the industry. However, an accurate modeling of all the processes involved is not a simple task since there are several interrelations between them that make the system very complex.

As an example of such a complex coupled physics behind the heap leaching process, it may be mentioned that geotechnical stability of the heap depends on the liquid pressures distribution, which is related to the permeability through Darcy's law. In its turn, permeability will be affected by porosity changes, which depend on the compaction state and the dissolution/precipitation of minerals. Obviously, hydrometallurgical performance of the heap ore is also strongly linked with the abovementioned coupled processes.

1.2 Motivation

It is quite common to find models in the literature related to geotechnical, hydrogeological and geochemical disciplines, but it is not so easy to find all of them coupled in a real engineer problem. Usual approaches for heap leaching models solve the different phenomena in an uncoupled or just partially coupled way due to its resolution complexity. Some of the existing approaches were formulated to solve hydrodynamics and solute transport (Decker, 1999), and soil mechanics and hydrodynamics (Pacheco, 2011)

In last years some efforts about incorporating the chemistry in Hydro-Mechanical (HM) problems (Liu, 2004), (Mata, 2005), (Mohajeri, 2011) have been done, but most of them only considered simple geochemical models over synthetic cases. Also some attempts to solve the THMC equations in the context of the design of radioactive waste facilities have been reported as well (Guimarães, 2002).

Improving the design of heap leach pads requires performing an integrated analysis of the HMC phenomena. The key aspects of the construction and operation such as mechanics stability and mineral recovery efficiency cannot be estimated accurately without taking into

account multiple coupling of a complex chemistry, the soil mechanics and the hydrodynamics.

1.3 Objectives

We distinguish two types of objectives: the main objective and the specific objectives.

1.3.1 Main objective

The main objective of this work is:

- Improve the understanding of a heap leach pad behavior by using a coupled hydro-mechanical-chemical model in order to optimize its design and operation. The pad stability and the ore recovery efficiency are studied with special emphasis.

1.3.2 Specific objectives

The following objectives are also part of this work:

- Simulate HMC problems over heap leach pads including the effects of the construction and operation procedure.
- Calculate a more accurate and realistic safety factor of the heap leach pad by taking into account the link between the HMC phenomena in the model.
- Investigate the influence of the pad irrigation on the mineral recovery efficiency.

1.4 Methodology

To achieve the marked objectives, the following tasks have been planned:

- A general review of the state of art in order to know the results, recommendations and limitations of previous studies.
- The description of the governing equations of fluid flow, mechanical and reactive solute transport.
- Adaptation of two numerical existing tools (COMSOL and PHREEQC) to solve the described coupled phenomena, taking into account the different stages of the heap leach pad construction and its operation.
- Tool validation by the resolution of four benchmarks.
- Simulation of a typical heap leach pad demonstrative case.

1.5 Organization of the document

The thesis is divided into eight chapters.

- The first chapter presents a review of the state of the art, the motivation and the approach followed in the study.
- The second chapter introduces the heap leaching practice in mining and focuses on two key aspects: the pad stability and the ore recovery efficiency.
- The third chapter describes the physical-chemical phenomena and the governing equations involved in the heap leaching process.
- The fourth chapter presents the numerical tools to solve the described equations (COMSOL-PHREEQC interface), paying special attention to the nature of the coupling between phenomena.
- The fifth chapter presents the validation of the numerical tool by the resolution of four benchmarks.
- In the sixth chapter an application of a realistic heap leach pad case is developed.
- The seventh chapter presents the conclusions and recommendations.
- Finally, in the eighth chapter is presented the future works.

2.0 HEAP LEACH PAD DESCRIPTION

2.1 General description

Heap leaching is a mineral processing technology whereby large piles of crushed or Run-of-Mine (ROM) rock are leached with various chemical solutions that extract valuable minerals. Mining operation often has several civil structures for mineral recovery; heap leach pad is one of them. An example of a typical mining operation is shown in Figure 2.1.

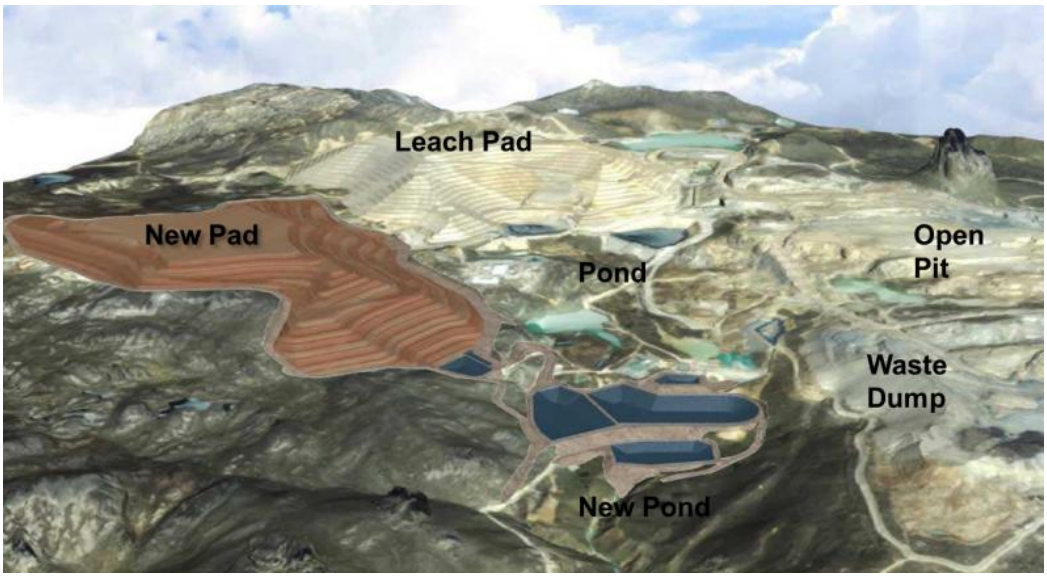

Figure 2.1: Typical civil structures found in a mining operation.

Mining engineering is devoted to find economical operations of metal recovery. In the context of heap leaching, that means that a large percentage of the available metal should be recovered during a reasonable period of time.

According to Thiel, et al., (2004) leach pads can be divided into four categories:

- **Conventional** or **"flat"** pads have relatively flat slopes and the ore is stacked in relatively thin lifts typically of 5 to 15 m.
- The **Dump** leach pads system is similar to the flat one but it can include rolling terrain. The term "dump" usually means that the lifts are much thicker (up to 50 m).
- The **Valley** fills systems are placed in natural valleys using either a buttress dam at the bottom of the valley or a leveling fill within the valley.
- The **on/off** pads are also known as dynamic heaps. A relatively flat pad is built using a robust liner and overliner system. Then a **single** lift of ore, from 4 to 10 meters thick, is loaded and leached. At the end of the leach cycle the spent ore ("ripios" in most mining literature) is removed for disposal and the pad recharged with fresh ore. Usually, loading is automated using conveyors and stackers.

Pictures with examples of these types of leach pad are shown in Figure 2.2.

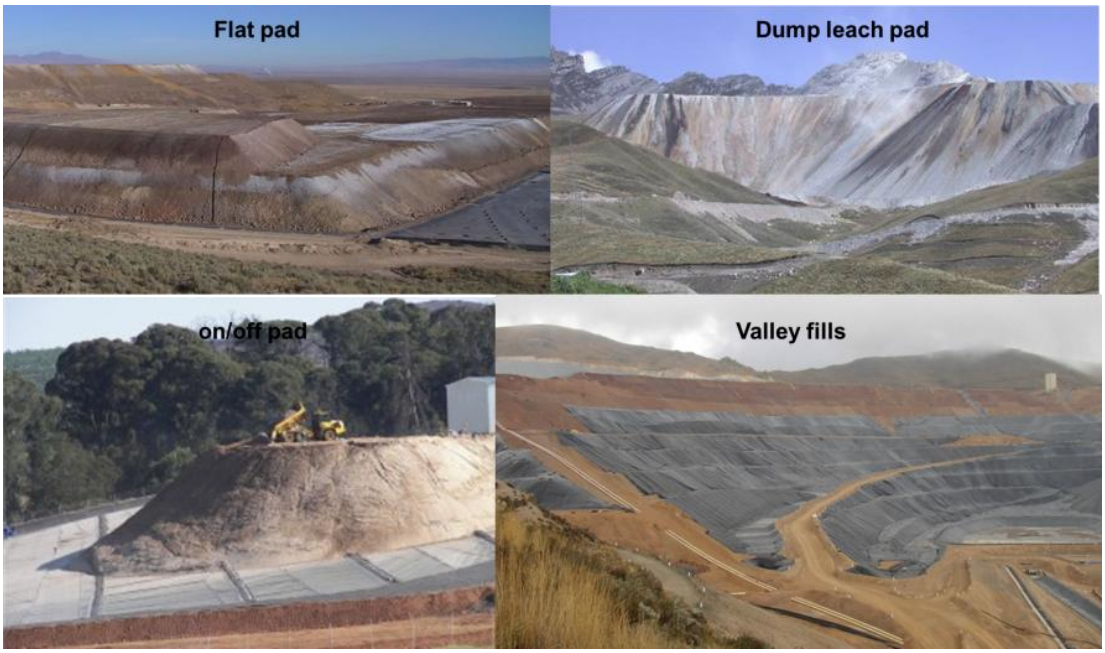

Figure 2.2: Types of heap leach pad according to Thiel et al. (2004).

Heap leaching has become a widely used method of mining low-grade gold, silver, copper and uranium ores around the world because the following advantages: it has a comparatively shorter start up time and it allows to economically mine deposits too small for conventional processing methods.

2.2 Heap construction and operation

A typical pad consists of several layers of relatively dry ore material (sometimes the crushed ore is brought under an agglomeration process before leaching, which provides the material of the layers a given humidity degree). The layers are deposited from bottom to top at their angle-of-repose.

Ideally, the pad-site is set on a uniformly sloping area with a slope of 0,5% to 2,0% in the direction of the process ponds. This provides the pad a gradient to collect the solution that has leached through the ore. However, in practice the pad gradient is rarely uniform.

A sketch of the typical layer construction process is shown in Figure 2.3. There can be seen different parts: the foundation where the pad is placed, the drainage/liner system (underliner soil, geomembrane or liner and overliner drain) for solution recollection, and the ore material placed in two layers.

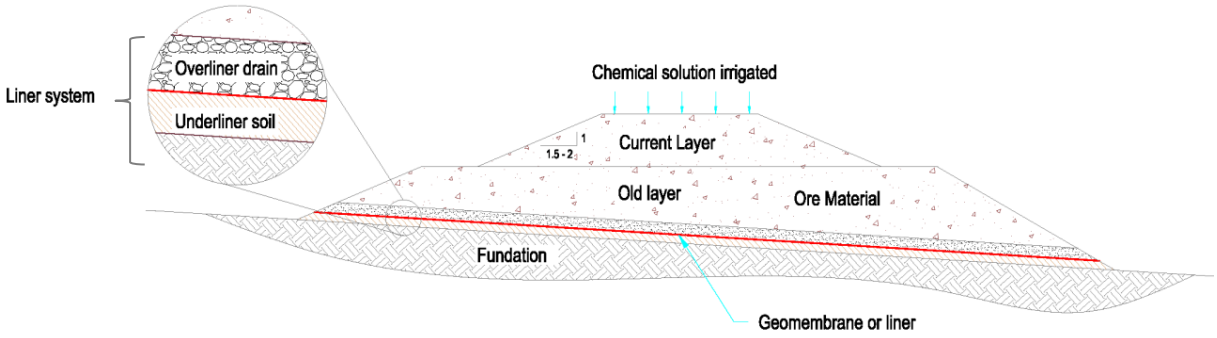

Figure 2.3: Transversal section sketch of a typical heap leach pad. Notice that the pad gradient and ore slopes are exaggerated.

The heap is generally constructed in successive lifts. Each lift is irrigated with a leaching solution before the subsequent lift is placed. The heap ore lifts are typically stacked at 5 to 10 meters in thickness and leaded to typical maximum heights in the range of 30 to 60 meters, but in the Andes of South America, the highest heap stacks to date exceed 300 meters above the pad foundation.

Each ore lift surface is wetted uniformly during the leaching by using irrigation drip emitters or spray sprinklers. Leaching is generally conducted in 30 to 120 day or longer leach cycles with barren or recirculated alkaline (gold and silver) or acidic (copper) process solutions.

Steeply dipping layers of fine, coarse and well-graded material commonly exist in leaching heaps as a result of segregation that occurs during heap construction. These layers can become preferential flow paths that channel the leaching solution through the heap. Solution channeling causes some regions within the heap to be poorly leached resulting in reduced metal recovery.

Problems with compaction normally result when heavy dump trucks and dozers are used for heap construction. In these situations trucks driving on top of the pile cause the compaction. This problem can be mitigated somewhat by “ripping” the haul paths with a dozer.

2.3 Key aspects of heap leach

Engineers should consider especially the following aspects:

2.3.1 Pad liner system

The pad liner system used in the current heap leaching practice is a composite liner with an overlying drain cover fill (Breitenbach, 1999). The primary purpose of the composite pad liner is to prevent the loss of pad and pond process solutions from the lined facilities. This helps to improve the leaching efficiency while fitting environmental requirements. The composite liner consists of a low permeability subgrade soil that is in direct contact with the geomembrane liner (see Figure 2.3).

Underliner soil is a fine-grained bedding fill that provides a secondary containment barrier for leach solutions and also protects the overlying geomembrane liner from subgrade rock puncture.

A geomembrane liner beneath heap leach stack provides a primary containment barrier for leach solutions. The selected leach pad geomembrane liner must prevent leakage. Some of the more important engineering aspects in liner selection include geomembrane liner resistance to rock puncture, adequate liner friction strengths for slope stability, elongation capacity to withstand foundation settlements under high heap loads, and long-term exposure to climatic conditions.

The overliner drain cover fill provides protection to the exposed geomembrane liner and is generally supplemented with drain pipes at controlled spacing. Relatively clean crushed ore materials are often used as drain cover fill. The drain cover fills and drain pipes provide rapid drainage recovery of the pregnant solutions to the process pond and plant facilities and allow maintaining low hydraulic heads above the pad liner.

2.3.2 Ore material characteristics

The maximum rock size of the granular ore materials ranges from large run-of-mine cobble and boulder rock fragments to fine crushed sand and gravel particles. The crusher operations may include agglomeration as needed to provide a more uniform distribution of fines (minus No. 200 sieve size material). This improves the permeability of the heap and the recovery of the target metals. The individual ore lifts are offset with benches along the exterior slope, as required for establishing the overall stable design slopes for operations.

Insufficient heap permeability is one of the most common causes of failure of heap leaching projects. Poor permeability means slow solution flow and results in uneconomic leach cycle times. In addition, recovery is reduced due to incomplete wetting of the heap. Low permeability also limits air ingress, a necessity for bacterial leaching operations. On the other hand, if heaps are too permeable the solution-ore contact time will be insufficient also resulting in reduced or slow recovery.

Heap permeability problems also arise in heaps where the ore has been compacted due to careless or inadequate material placement practices. Consolidation of the heap material during the life of a pile will also lead to permeability issues.

2.3.3 Chemical solution application

The two common means used to apply heap leach solution are sprinklers and drip emitters. The operation of these devices can produce flow barriers within the heap or seal the heap surface. In either case, a significant reduction in metal recovery will result as portions of the heap remain unleached.

The chemistry for leaching gold and silver from their ores is essentially the same for both metals. A dilute alkaline solution of sodium cyanide dissolves these metals without dissolving many other ore components (e.g. copper, zinc, mercury and iron, which are the most common soluble impurities).

Typical application rates in most heap leach operations range from 7 to 10 l/hr/m^2. It is also common applying 1.3 tonnes of leach solution per tonne of ore during a 70-day primary leach cycle.

For some field heaps, notably where the ore is fine crushed and the ore leaches quickly, the solution/ore ratio is a more important factor than the overall leach time. However, for the majority of heap leaches, time seems as important as specific application rate (Kappes, 2002).

2.3.4 Stability

The safe operation of a heap leach greatly depends on its stability. Safety factors can be used for local and overall assessment of the slope stability of a heap leach pad. Instability typically occurs because the geomembrane is used to cover the pad foundation. This causes that the shear strength on interface (underliner-geomembrane-overliner) decreases below the shear strength of the ore. As a result, potential slip surfaces are developed through the upper or the lower face of the geomembrane.

Also, instability can be due to other reasons:

- The stability of the first-lift is affected by lift thickness (5m to 50m) and stacking direction (Smith, 2000).
- The ore degradation caused by mineral dissolution and bacterial action through the leaching process can provoke the decrease in shear strength of the ore and along the geosynthetic interfaces.
- The earthquake-induced failures which introduce worse conditions on the slope stability.

There are several uncertainties associated to heap leach pad operations. Classical studies for the design and prediction of the operation do not take into account the HMC coupling properly and, consequently, pad stability and ore recovery efficiency are not well assessed. The present work proposes a modeling methodology to address these issues by an integrated analysis of the HMC phenomena involved in heap leaching.

3.0 MATHEMATICAL DESCRIPTION

In this chapter we provide a detailed description of the mathematical expressions considered to model the phenomena involved in heap leaching construction and operation.

Compact notation is used in writing Partial Differential Equations (PDEs).

3.1 Basic assumptions

The basic assumptions are:

- The atmospheric pressure is set at zero because we consider an open system.
- The variation of the liquid pressure (suction) with the liquid content of the ore in the heap is represented by a soil-water retention curve function. Hysteretic behaviour of the curve is not considered.
- Liquid and solid particles are assumed as incompressible phases.
- Thermal effects on soil mechanics, liquid flow, and reactive transport are neglected.

The primary variables for soil mechanics, liquid flow, and reactive transport are the displacement vector ($\boldsymbol{u}$), the liquid pressure (p_l) and the concentration vector ($\boldsymbol{c}$), respectively.

3.2 Governing equations for soil mechanics

The soil mechanics of a heap leach pad is governed by equilibrium and compatibility equations, as well as constitutive laws describing the material behavior. These governing equations and constitutive relationships are described separately below.

A scheme of the dependencies between variables and boundary conditions in the case of static analysis are shown in Figure 3.1.

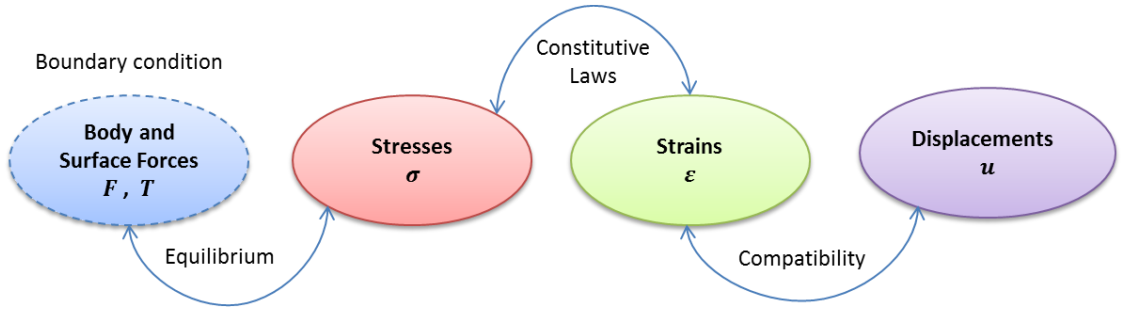

Figure 3.1: Dependencies between variables in a static analysis of soil mechanics.

We will follow the sign convention of continuum mechanics (Chen, 1990) that considers positive tensile stresses. This means that principal stresses often have a negative sign and are sorted as $\sigma_1 > \sigma_2 > \sigma_3$.

3.2.1 Equations of equilibrium

The equation of equilibrium relates the stress tensor with the body forces through the called Cauchy's equation.

To quantify how forces are transmitted through a continuum, engineers use the concept of stress (force/unit area). The magnitude and direction of a stress and the manner in which it varies spatially indicates how the forces are transferred. However, these stresses cannot vary randomly but must obey certain rules, which is described in the Eq. 1.

The equilibrium equations for a soil under unsaturated conditions, in terms of total stress are given by:

$$\nabla \cdot \boldsymbol{\sigma} = -[(1-n)\rho_s + nS_l\rho_l]\boldsymbol{g} \tag{1}$$

where n is the porosity of the medium ($m^3 \cdot m^{-3}$), ρ_s is the soil particle density ($kg \cdot m^{-3}$), ρ_l is the liquid density ($kg \cdot m^{-3}$), S_l is the degree of liquid saturation ($m^3\ m^{-3}$) and $\boldsymbol{g}$ is the acceleration gravity vector ($m \cdot s^{-2}$). The symmetric tensor of total stress, $\boldsymbol{\sigma}$ ($N \cdot m^{-2}$) is defined by:

$$\boldsymbol{\sigma} = \begin{bmatrix} \sigma_x & \tau_{xy} & \tau_{xz} \\ \tau_{xy} & \sigma_y & \tau_{yz} \\ \tau_{xz} & \tau_{yz} & \sigma_z \end{bmatrix} \tag{2}$$

where σ_x, σ_y, σ_z and τ_{xy}, τ_{xz}, τ_{yz} are normal and shear stresses ($N \cdot m^{-2}$), respectively.

In a variable saturated porous medium the effective stress $\boldsymbol{\sigma}'$ ($N \cdot m^{-2}$) controls the soil behavior. Some constitutive material model incorporates the effect of suction when soil is unsaturated (Alonso, 1990). The suction (s) is defined by:

$$s = (p_a - p_l) \tag{3}$$

where s is the suction ($N \cdot m^{-2}$), p_a is the air pressure ($N \cdot m^{-2}$) and p_l is the liquid pressure ($N \cdot m^{-2}$). The effective saturation S_e ($m^3 \cdot m^{-3}$) is defined by:

$$S_e = \frac{\theta - \theta_r}{\theta_s - \theta_r} \tag{4}$$

where θ is the volumetric liquid content ($m^3 \cdot m^{-3}$), θ_r is the residual volumetric liquid content ($m^3 \cdot m^{-3}$), and θ_s is the saturated volumetric liquid content ($m^3 \cdot m^{-3}$). The volumetric liquid content is related with the porosity n and the degree of liquid saturation S_l by:

$$\theta = nS_l \tag{5}$$

3.2.2 Equation of compatibility

The equation of compatibility relates the normal (ε_x, ε_y, ε_z,) and shear (γ_{xy}, γ_{yz}, γ_{xz}) strains with the displacements u, v and w in the x, y and z directions, respectively (Timoshenko, et al., 1951):

$$\begin{aligned} \varepsilon_x &= -\frac{\partial u}{\partial x} & \varepsilon_{xy} &= \gamma_{xy} = \frac{\partial u}{\partial y} + \frac{\partial v}{\partial x} \\ \varepsilon_y &= -\frac{\partial v}{\partial y}; & \varepsilon_{yz} &= \gamma_{yz} = \frac{\partial v}{\partial z} + \frac{\partial w}{\partial y} \\ \varepsilon_z &= -\frac{\partial w}{\partial z} & \varepsilon_{xz} &= \gamma_{xz} = \frac{\partial w}{\partial x} + \frac{\partial u}{\partial z} \end{aligned} \quad (6)$$

To express the shear strain, the tensor form ε_{xy}, ε_{yz}, ε_{xz}, or the engineering form γ_{xy}, γ_{yz}, γ_{xz} can be used. The symmetric strain tensor $\boldsymbol{\varepsilon}$ (m·m^{-1}) can then be expressed in terms of normal and shear strain components:

$$\boldsymbol{\varepsilon} = \begin{bmatrix} \varepsilon_x & \gamma_{xy} & \gamma_{xz} \\ \gamma_{xy} & \varepsilon_y & \gamma_{yz} \\ \gamma_{xz} & \gamma_{yz} & \varepsilon_z \end{bmatrix} \quad (7)$$

3.2.3 Shear strength equation

The shear strength of a **saturated** soil is described using the Mohr-Coulomb failure criterion and the effective stress concept (Terzaghi, 1936).

$$\tau = c' + (\sigma - p_l)\tan\varphi' \quad (8)$$

where τ is the shear stress on the failure plane at failure (N·m^{-2}), c' is the "effective cohesion" (N·m^{-2}), $(\sigma - p_l)$ is the effective normal stress on the failure plane at failure (N·m^{-2}), φ' is the effective angle of internal friction.

The shear strength of an **unsaturated** soil can be formulated in terms of independent stress state variables (Fredlund, 1978). The stress state variables, $(\sigma - p_a)$ and $(p_a - p_l)$, have been shown to be the most advantageous combination for practice. Using these stress variables, the shear strength equation is written as follows:

$$\tau = c' + (\sigma - p_a)\tan\varphi' + (p_a - p_l)\tan\varphi^b \quad (9)$$

where c' is the cohesion at zero matric suction and zero net normal stress (N·m^{-2}), $(\sigma - p_a)$ is the net normal stress state on the failure plane at failure (N·m^{-2}), $(p_a - p_l)$ is the matric suction on the failure plane at failure (N·m^{-2}), φ^b is the angle indicating the rate of increase in shear strength relative to the matric suction.

A comparison of the Eq. 8 and 9 reveals that the shear strength equation for an unsaturated soil is an extension of the shear strength equation for a saturated soil. For an unsaturated soil, two stress state variables are used to describe its shear strength, while only one stress state variable (i.e., effective normal stress $(\sigma - p_l)$) is required for a saturated soil.

3.2.4 Constitutive laws

Constitutive laws are needed to describe the material behavior. In short, these constitutive laws represent the stress-strain behavior of the soil and provide a link between equilibrium and compatibility equations. These relations can be expressed as:

$$\Delta\boldsymbol{\sigma}' = \boldsymbol{D}\Delta\boldsymbol{\varepsilon} \quad (10)$$

where $\boldsymbol{D}$ is the constitutive relationship or stiffness matrix which represents the current stress state and past history of the soil (N·m^{-2}). In (Eq. 10) $\Delta\boldsymbol{\sigma}'$ is the incremental effective stress vector (N·m^{-2}) and $\Delta\boldsymbol{\varepsilon}$ is the incremental deformation vector (m·m^{-1}).

The constitutive relationships considered in this work are briefly described below.

3.2.4.1 Linear Elasticity

The linear elastic model is based on Hook's law of isotropic elasticity. It may be used to model stiff volumes in the soil, such as concrete walls or intact rock formations.

Figure 3.2 shows a simple graph displaying the stress and strain path in a linear elasticity model.

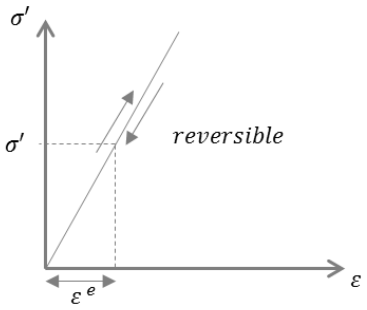

Figure 3.2: Basic idea of a linear elastic model, σ' is the effective stress (N·m^{-2}) and ε^e is the reversible elastic deformation (m·m^{-1}).

Two basic elastic parameters are necessary to calculate the stiffness matrix ($\boldsymbol{D}$): Young's modulus E and Poisson's ratio v.

3.2.4.2 Elastic plastic Mohr-Coulomb

This model is based on the failure criterion of Mohr-Coulomb which represents an approximation of "first-order" for the soil or rock behavior. Simple graphs representing the stress and strain path in an elastic plastic perfect model is shown in Figure 3.3.

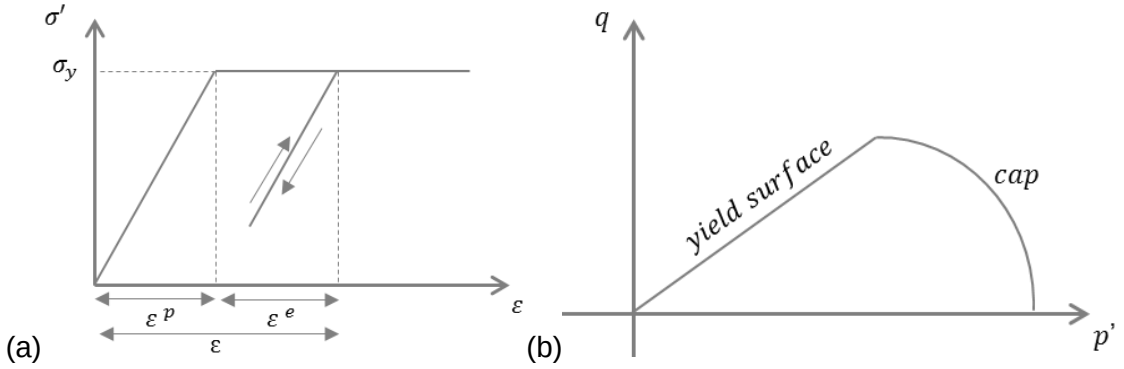

Figure 3.3: (a) The path of stress-deformation and (b) deviator-mean stress are represented for a perfectly elastic plastic model. ε^e is the reversible elastic deformation (m·m^{-1}), ε^p is the irreversible plastic deformation (m·m^{-1}), σ_y is the yield stress (N·m^{-2}), p' is the mean effective stress (N·m^{-2}) and q is the deviator stress (N·m^{-2}).

The stiffness matrix ($\boldsymbol{D}$) of this model depends on five parameters: the Young's modulus E and Poisson's ratio v for soil elasticity; friction angle φ and cohesion c for soil plasticity and dilatation angle.

3.2.4.3 Modified Cam-Clay

The Modified Cam-Clay model is a well known model in soil modelling literature i.e. (Wood, 1990). It is focused primarily for the modelling of near normally-consolidated clay type soils.

The diagrams shown in Figure 3.4 represent the stress and strain path in a Modified Cam Clay model.

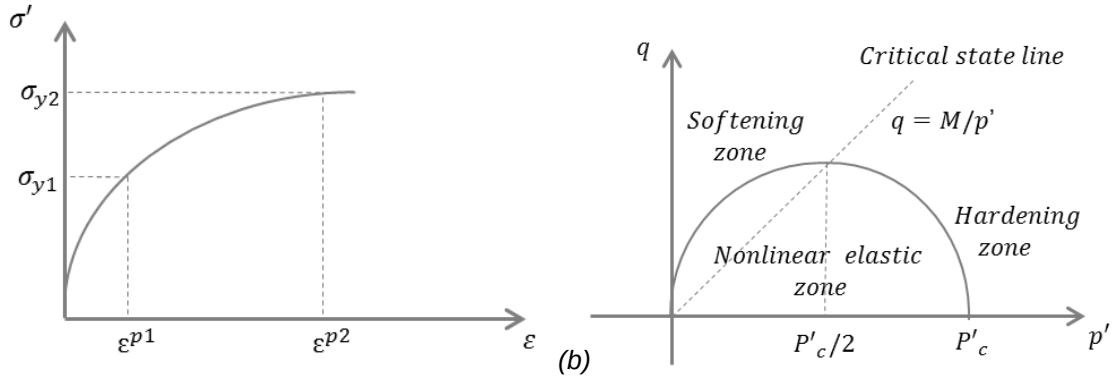

Figure 3.4: (a) The path of stress-deformation and (b) deviator-mean stress are presented for a Modified Cam Clay model. ε^p and σ_y are the plastic deformation and yield stress, respectively and P'_c is the initial pre-consolidation pressure ($N{\cdot}m^{-2}$).

The stiffness matrix ($\boldsymbol{D}$) of this model to involve six input parameters: Young's module E, Poisson's ratio v, swelling index κ, compression index λ, initial void ratio e_0 and slope of critical state M, which depend of friction angle.

3.2.4.4 Summary of constitutive models

A summary of constitutive models and the $\boldsymbol{D}$ dependencies are shown in Table 3.1.

Table 3.1: Summary of constitutive models used in this work.

Constitutive model	Material	Application case	Dependent parameters
Linear Elasticity	Concrete and intact rock	Initial stress	$\boldsymbol{D}(E, v)$
Mohr Coulomb	Soil and Rock	Slope stability	$\boldsymbol{D}(E, v, \varphi, c, \psi)$
Modified Cam Clay	Soft clay	Settlement and stability	$\boldsymbol{D}(E, v, \kappa, \lambda, e_0, \varphi)$

3.3 Governing equation for flow in porous media

In porous media flow, Darcy's law and liquid mass balance must be satisfied. These phenomena are considered separately below.

Interrelationships between processes are shown schematically in Figure 3.5.

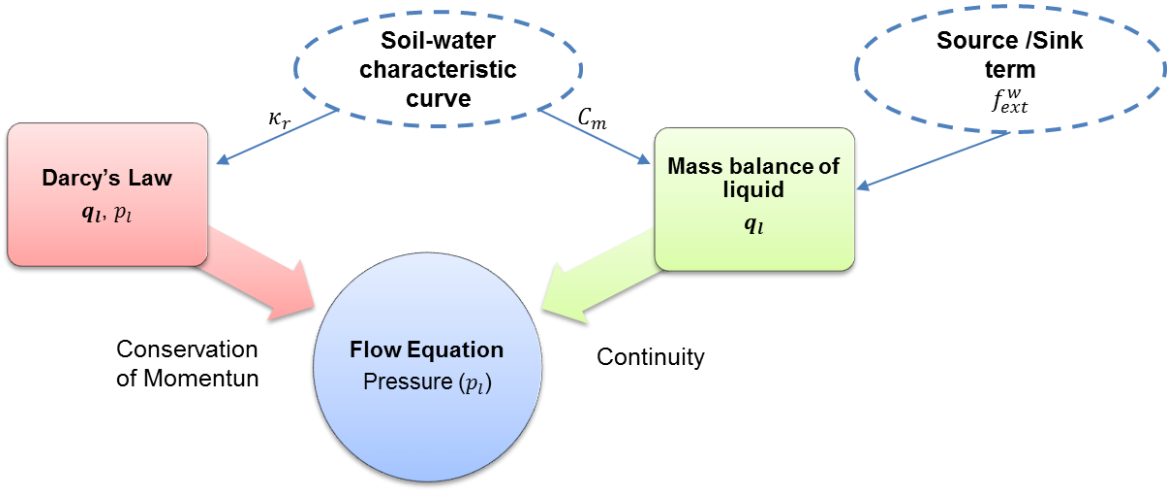

Figure 3.5: Interrelationships between variables in groundwater flow.

3.3.1 Mass balance of liquid

The mass balance equation for unsaturated soil can be written as:

$$\partial_t(nS_l\rho_l) = -\nabla\cdot(\rho_l\boldsymbol{q_l}) + f_{ext}^{w} \tag{11}$$

where $\boldsymbol{q}_l$ is the Darcy flow vector ($m^{3}\cdot s^{-1}\cdot m^{-2}$) and f_{ext}^{w} is an external supply of liquid ($kg\cdot m^{-3}\cdot s^{-1}$). The left-hand side term of the Eq. 11 can be expressed also as:

$$\partial_t(nS_l\rho_l) = \rho_l[\partial_p(nS_l) + S_l(nX_f + (1-n)X_p)]\partial_t(p_l) \tag{12}$$

where X_f is fluid compressibility (Pa^{-1}) that is equal to $\left(\frac{1}{\rho_l}\right)\partial_p(\rho_l)$ and X_p is the effective compressibility of soil matrix (Pa^{-1}) that is equal to $\left(\frac{1}{1-n}\right)\partial_p(n)$.

The following storage term S (Pa^{-1}) can be used to simplify the Eq. 12.

$$S = nX_f + (1-n)X_p \tag{13}$$

Assuming constant liquid, solid density and saturated condition, the advective term of the Eq. 11 can be expressed for liquid and solid as:

$$\nabla\cdot(\rho_l n\boldsymbol{v_l}) = \nabla\cdot(n(\boldsymbol{v_{rel}} + \boldsymbol{v_s})) = 0 \tag{14}$$

$$\nabla\cdot(\rho_s(1-n)\boldsymbol{v_s}) = \nabla\cdot(\boldsymbol{v_s}) - \nabla\cdot(n\boldsymbol{v_s}) = 0 \tag{15}$$

where $\boldsymbol{v_l}$ is the real liquid velocity ($m \cdot s^{-1}$). The soil particle velocity $\boldsymbol{v_s}$ ($m \cdot s^{-1}$) can be written as $\partial_t(\boldsymbol{u})$. Adding the two equations (14 and 15) results in:

$$\nabla \cdot (n\boldsymbol{v_{rel}}) + \nabla \cdot (\partial_t(\boldsymbol{u})) = 0 \tag{16}$$

where $\boldsymbol{v_{rel}}$ is the relative liquid velocity ($m \cdot s^{-1}$) and represents to $\frac{\boldsymbol{q_l}}{n}$ for saturation condition. Moreover, the volumetric deformation ε_{vol} is equal to displacement tensor divergence ($\nabla \cdot (\boldsymbol{u})$). This Eq. 16 can be rearranged to

$$\nabla \cdot (\rho_l \boldsymbol{q_l}) = \rho_l \nabla \cdot (\boldsymbol{q_l}) + \rho_l \partial_t(\varepsilon_{vol}) \tag{17}$$

Finally, the equation formulation to solve is the following:

$$\rho_l [C_m + S_l S] \partial_t(p_l) = -\rho_l \nabla \cdot (\boldsymbol{q_l}) - \rho_l \partial_t(\varepsilon_{vol}) + f_{ext}^w \tag{18}$$

where C_m is the specific moisture capacity (-) that is equal to $\partial_p(\theta)$.

3.3.2 Darcy's law

Darcy's law describes the velocity of a fluid though a porous medium. It can be written in term of pressure as follow:

$$\boldsymbol{q}_l = -\frac{\boldsymbol{\kappa}\kappa_r}{\mu}(\nabla p_l - \rho_l \boldsymbol{g}) \tag{19}$$

where $\boldsymbol{q}_l$ is the Darcy flow vector ($m^3 \cdot s^{-1} \cdot m^{-2}$), $\boldsymbol{\kappa}$ is the intrinsic permeability tensor (m^2), μ is the dynamic viscosity (Pa·s) and κ_r (-) denotes the relative permeability (between 0 and 1) which depends on the degree of liquid saturation.

3.3.1 Soil-water characteristic curve

The soil-water characteristic curve (SWCC) for a soil is defined as the relationship between volumetric liquid content (θ) and suction ($p_a - p_l$).

Several mathematical expressions for these relationships can be found in literature. The most widely known are the proposed by (Van Genuchten, 1980) and (Brooks, 1964).

The relative permeability κ_r function can also be related to the volumetric liquid content or suction. Often, these relationships are deduced from the SWCC and the capillary bundle theory. Experimental SWCC and permeability functions also can be formulated.

3.4 Reactive solute transport

Reactive transport problems are related with the solute transport and chemical reactions through porous media.

Interrelationships between the relevant processes are shown schematically in Figure 3.6.

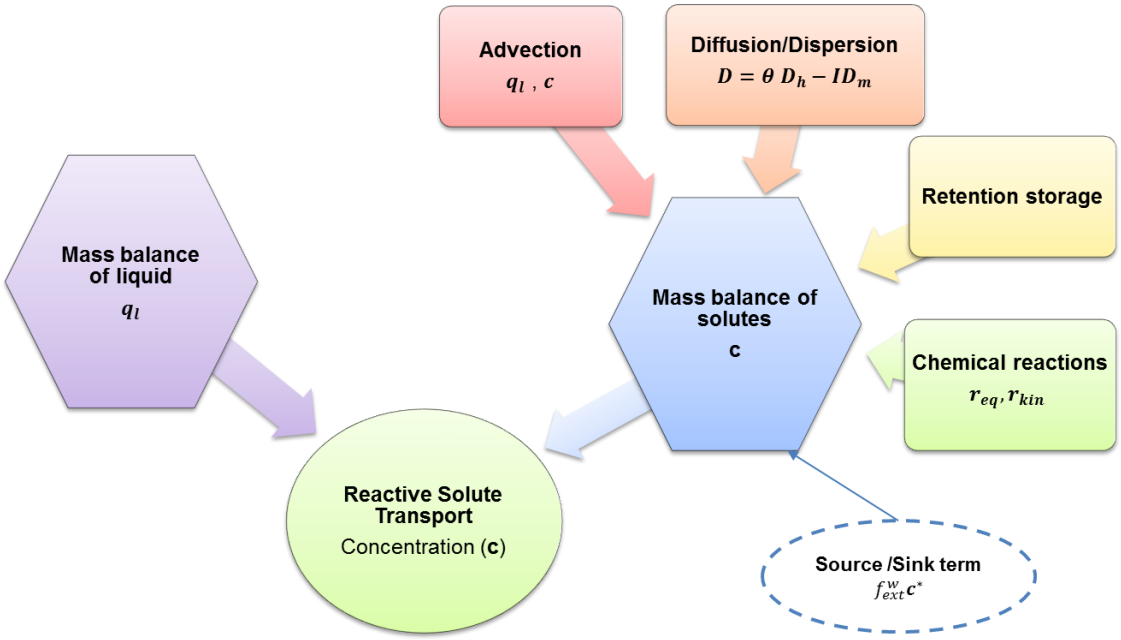

Figure 3.6: Interrelationships between processes in reactive solute transport problems.

3.4.1 Mass balance of reactive solute species

The mass balance equation for a reactive chemical species is described by:

$$\partial_t(\omega \boldsymbol{c}) = -\nabla \cdot (\rho_l(\boldsymbol{J_{adv}} + \boldsymbol{J_{dif}} + \boldsymbol{J_{dis}})) + \omega \boldsymbol{r_{eq}} + \omega \boldsymbol{r_{kin}} + f_{ext}^{w} \boldsymbol{c}^* \quad (20)$$

where $\omega = nS_l\rho_l$ is an auxiliary variable used for notation convenience, $\boldsymbol{c}$ is the concentration vector of species (mol·kg^{-1}), $\boldsymbol{c}^*$ is the vector of external concentration of species (mol·kg^{-1}), $\boldsymbol{r_{eq}}$ is the reaction rate due to equilibrium reactions (mol·kg^{-1}·s^{-1}) and $\boldsymbol{r_{kin}}$ is the reaction rate due to kinetic reactions (mol·kg^{-1}·s^{-1}).

3.4.1.1 Advection

Advection is the process by which moving groundwater carries with it dissolved solutes. The rate of flowing groundwater is given by the advective flux vector $\boldsymbol{J_{adv}}$ (m·s^{-1} mol·kg^{-1}):

$$\boldsymbol{J_{adv}} = \boldsymbol{q_l c} \quad (21)$$

3.4.1.2 Diffusion/Dispersion

The **diffusion** is the process by which both ionic and molecular species dissolved in water move from areas of higher concentration (i.e., higher chemical activity) to areas of lower concentration. The diffusion of a solute through water is described by Fick's laws as:

$$\boldsymbol{J_{dif}} = D_m \nabla \boldsymbol{c} \tag{22}$$

where $\boldsymbol{J_{dif}}$ is the diffusion flux vector ($m^2 \cdot s^{-1}$ $mol \cdot kg^{-1}$) and the diffusion coefficient D_m ($m^2 \cdot s^{-1}$) is defined by.

$$D_m = -\theta \tau D_0 \tag{23}$$

where τ is tortuosity (-) and D_0 is the liquid phase diffusion coefficient ($m^2 \cdot s^{-1}$). This formulation assumes the same liquid phase diffusion for all the chemical species.

The process of **dispersion** acts to dilute the solute and lower its concentration. The dispersion of a solute through a porous medium can be described by Fick's law:

$$\boldsymbol{J_{dis}} = \boldsymbol{D_h} \nabla \boldsymbol{c} \tag{24}$$

where $\mathbf{D_h}$ is the tensor of mechanical dispersion ($m^2 \cdot s^{-1}$) and $\boldsymbol{J_{dis}}$ is the dispersion flux vector ($m^2 \cdot s^{-1}$ $mol \cdot kg^{-1}$).

The mechanical dispersion tensor $\boldsymbol{D_h}$ ($m^2 \cdot s^{-1}$) is defined as:

$$\mathbf{D}_h = \alpha_L |\boldsymbol{q_l}| + (\alpha_L - \alpha_T) \frac{\boldsymbol{q_l} \boldsymbol{q_l^t}}{|\boldsymbol{q_l}|} \tag{25}$$

where α_L and α_T are the longitudinal and transverse dispersivities (m).

3.4.1.3 Total flux

The total flux of advection, diffusion and dispersion is then obtained by the sum of equations 21, 22 and 24:

$$\boldsymbol{J} = \boldsymbol{J_{adv}} + \boldsymbol{J_{dif}} + \boldsymbol{J_{dis}} = \boldsymbol{q_l c} - \boldsymbol{D} \nabla \mathbf{c} \tag{26}$$

where $\boldsymbol{D}$ is the contraction vector of the dispersion and diffusion coefficient ($m^2 \cdot s^{-1}$).

$$\boldsymbol{D} = \theta \boldsymbol{D_h} - \boldsymbol{I} D_m \tag{27}$$

Finally, the mass balance equation 20 can be rewritten as:

$$\partial_t (\omega \boldsymbol{c}) = -\nabla \cdot (\boldsymbol{q_l c}) + \nabla \cdot (\boldsymbol{D} \nabla \mathbf{c}) \; + \; \omega \boldsymbol{r_{eq}} + \omega \boldsymbol{r_{kin}} + f_{ext}^{w} \boldsymbol{c}^* \tag{28}$$

3.4.2 Non-conservative formulation of reactive transport

The conservative formulation for the reactive transport of a chemical species is described by the mass balance equation 28. An alternative equation can be obtained multiplying Eq. 11 by the vector concentration ($\boldsymbol{c}$) and subtracting it from Eq. 28. This leads to the so called ***non-conservative formulation*** for reactive transport. Details of this derivation can be found for example in the CHEPROO user's guide (Bea Jofré, 2008). The resulting governing equation is expressed as:

$$\omega\partial_t(\boldsymbol{c}) = L_t(\boldsymbol{c_a}) + f_{ext}^w \boldsymbol{c_a^*} + \omega \boldsymbol{r_{eq}} + \omega \boldsymbol{r_{kin}} \tag{29}$$

where $\boldsymbol{c_a^*}$ is the external concentration vector of aqueous species (mol·kg^{-1}).

We define the linear operator of advection, dispersion, diffusion and non-chemical sink-source terms for the liquid phase $L_t(\cdot)$ as:

$$L_t(\cdot) = -\rho_l \boldsymbol{q_l} \cdot \nabla(\cdot) + \nabla \cdot \left(\rho_l \boldsymbol{D} \cdot \nabla(\cdot)\right) - f_{ext}^w(\cdot) \tag{30}$$

The Eq. 29 consists on a system of N_s equations, where N_s is the number of chemical species size). Nevertheless, it can be reduced to a system of size N_c, the number of chemical components, by eliminating the equilibrium reactions. Chemical components are defined as linear combination of species whose mass is not affected by equilibrium reactions (Smith, 1982) (Lichtner, 1985) (Steefel, 1996) (Saaltink, 1998).

$$\omega\partial_t(\boldsymbol{m}) = L_t(\boldsymbol{m}_a) + f_{ext}^w \boldsymbol{m}_a^* + \omega r_{kin} \tag{31}$$

where $\boldsymbol{m}$ is the vector of components (mol·kg^{-1}), which can be decomposed in subcomponents $\mathbf{m}_\mathrm{g}$, $\mathbf{m}_\mathrm{s}$, $\mathbf{m}_\mathrm{a}$ and $\mathbf{m}_\mathrm{d}$ containing the chemical species of the component present in gaseous, mineral, aqueous and sorbed phases, respectively. Notice that $\boldsymbol{m} = \boldsymbol{m}_g + \boldsymbol{m}_s + \boldsymbol{m}_a + \boldsymbol{m}_d$.

3.5 Common processes

Here we refer to common processes as these ones which do not belong to a single phenomenon.

3.5.1 Changes in porosity

The total dynamic porosity n may change due to both chemical and mechanical effects. It can be defined as

$$n^{k+1} = n_0 + \Delta n_{chemical}^{k+1} + \Delta n_{mechanical}^{k+1} \tag{32}$$

Where k is the previous calculated time step, $k+1$ is the current time step, n_0 is the initial porosity, $\Delta n_{mechanical}^{k+1}$ is the mechanical porosity increment and $\Delta n_{chemical}^{k+1}$ is the chemical porosity increment. They are defined in Equations (33) and (34), respectively.

3.5.2 Changes in porosity due to mechanical deformations

The porosity changes due to mechanical effects like compaction phenomenon can be represented by (Wood, 1990).

$$\Delta n_{mechanical}^{k+1} = \varepsilon_{vol}^{k+1} \cdot (1 - n^k) \tag{33}$$

where $\Delta n_{mechanical}^{k+1}$ is the porosity change (-) and ε_{vol}^{k+1} is the volumetric deformation (-).

3.5.3 Changes in porosity due to chemical reactions

The dissolution/precipitation of mineral phases leads to changes in porosity of the medium which also affects its intrinsic permeability. As a consequence, the flow is also affected.

Changes in porosity due to mineral dissolution/precipitation are taken into account after chemical speciation by the following expression:

$$\Delta n_{chemical}^{k+1} = \sum_{s=1}^{N_s} V_s \, c_s^{k+1} \tag{34}$$

where V_s is molar volume ($m^3 \cdot mol^{-1}$) of mineral species s and c_s^{k+1} is the mineral concentration at the current calculation time step ($mol \cdot kg^{-1}$).

3.5.1 Changes in permeability due the porosity

Changes in porosity will affect the permeability of the porous media as well. In real soils and rocks, the permeability varies with porosity (Carman, 1937)

$$\boldsymbol{\kappa} = \boldsymbol{\kappa_0} \left(\frac{n}{n_0}\right)^3 \tag{35}$$

where $\boldsymbol{\kappa_0}$ is the tensor of initial intrinsic permeability (m^2).

4.0 NUMERICAL METHODS

In this chapter we describe the numerical tools used in solving the governing equations. The coupling between the different processes and their implementation in interface used is also explained.

4.1 Coupling description

The interactions between different processes studied in the present work are illustrated in Figure 4.1. It is apparent that there exist two closed related feedback loops: an outer loop (permeability modification – flow velocity-phase transformation) and an inner loop (pore fluid pressure – porosity modification- dissolution/precipitation).

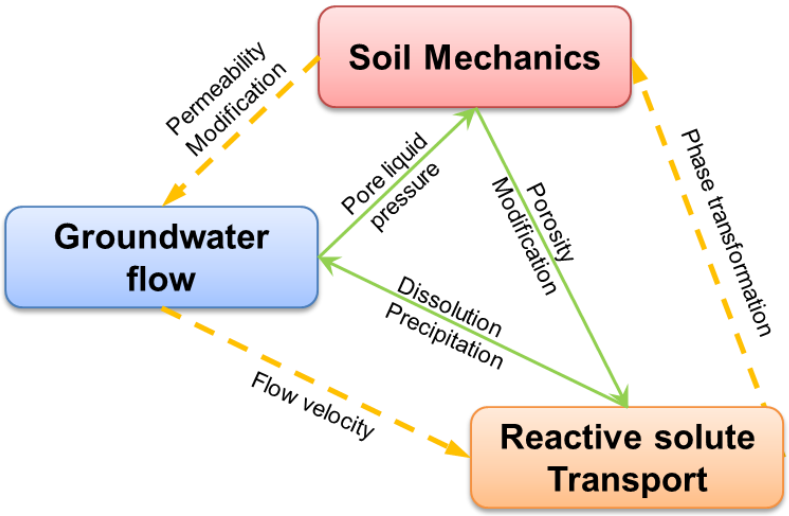

Figure 4.1: Illustration of interactions among different processes of HMC phenomena that can arise in heap leaching problems (inspired in figure from Liu, (2004)).

The total dynamic porosity (Eq. 32) is only affecting groundwater flow and reactive solute transport, but not soil mechanics.

The PDE system of Eq. 31 is highly nonlinear. This is the reason why it is commonly solved using an operator-splitting (OS) approach, where solute transport (Eq. 36) and geochemical reactions (Eq. 37) are solved separately.

$$\omega \partial_t(\boldsymbol{m}_a) = L_t(\boldsymbol{m}_a) + f_{ext}^{w} \boldsymbol{m}_a^{*} \tag{36}$$

$$d_t(\boldsymbol{m}_g + \boldsymbol{m}_m + \boldsymbol{m}_a + \boldsymbol{m}_d) = \boldsymbol{r_{kin}} \tag{37}$$

This OS method can derive on a sequential non-iterative approach (SNIA) or sequential iterative approach (SIA), depending if the system iterates until a desired level of convergence tolerance. More details on the different coupling strategies can be found in the literature of reactive transport (e.g. (Saaltink, 2001)).

In this work, a SNIA has been used. The advantage of the SNIA is its fast computation, since no iteration is performed. The reactive step affects the transport only in lagged mode. Therefore, accurate results require a control of the time step size. The flow diagram of the SNIA implemented in COMSOL-PREEQC is shown in Figure 4.2.

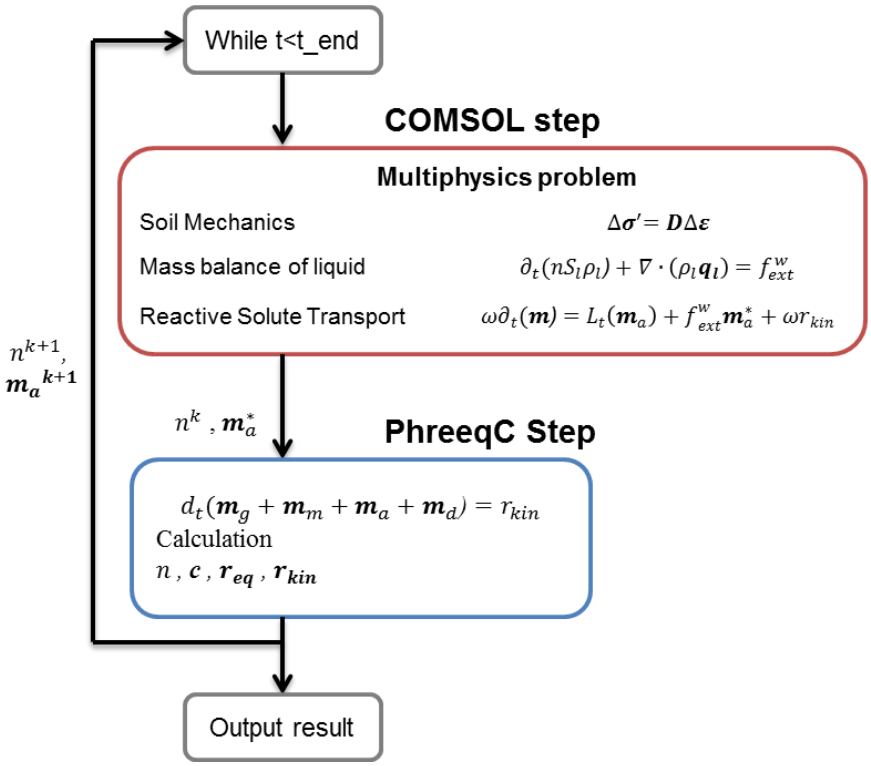

Figure 4.2: Flow diagram of the sequential non-iterative approach implemented in COMSOL-PHREEQC.

Equations 10, 18 and 31 are the set of PDE equations which form the multiphysics problem. They are solved considering as unknowns the variables $\boldsymbol{u}$, p_l and $\mathbf{m}$. PHREEQC solves Eq. 37 for $\mathbf{m}_a$, $\mathbf{m}_m$, $\mathbf{m}_g$, $\mathbf{m}_d$ and also solves the necessary equations to compute the $\boldsymbol{c}$, $\mathbf{r_{kin}}$, $\mathbf{r_{eq}}$ values. From the calculated $\mathbf{m}_m$ value the interface updates the porosity (n) that is returned to COMSOL for the calculation of the next time step.

The COMSOL-PHREEQC was used to perform the simulations. This interface combines the key capabilities of PHREEQC (Parkhurst, 1999) and COMSOL (COMSOL, 2011a) in a single reactive transport (RT) simulator. Figure 4.3 shows the information flows through the COMSOL-PHREEQC interface (Nardi, 2012).

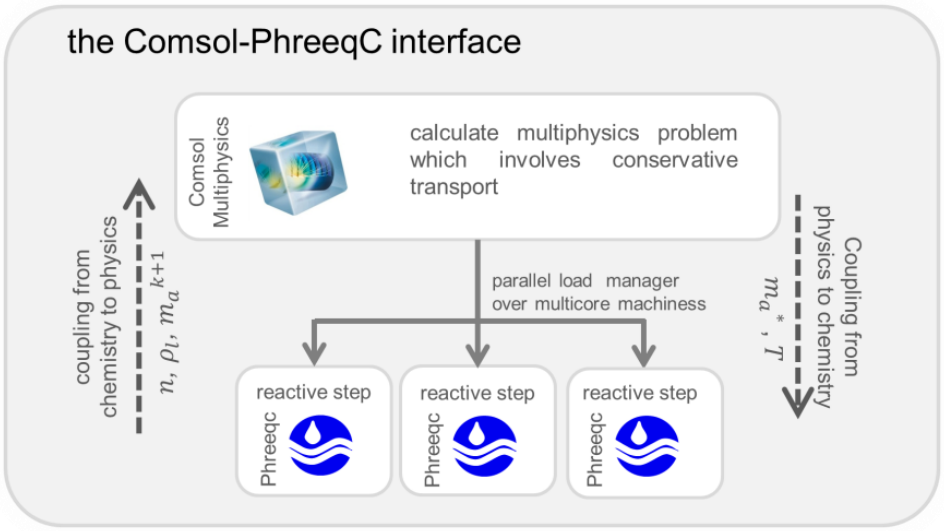

Figure 4.3: Information flow chart between COMSOL, PHREEQC and the Java interface.

A simple sketch that represents the coupling in COMSOL-PHREEC between the relevant physical and chemical processes is shown in Figure 4.4.

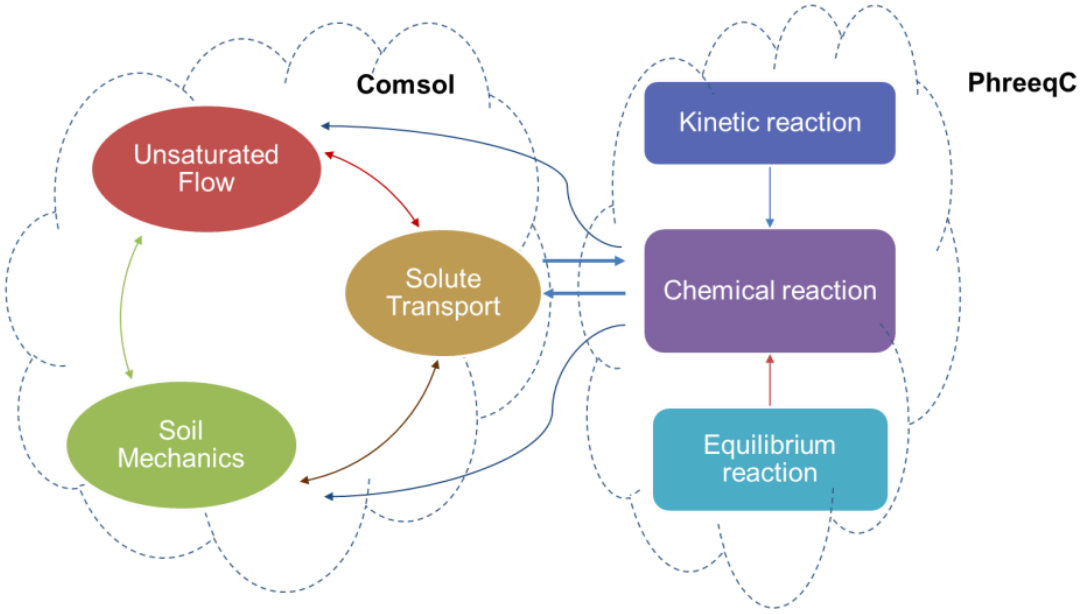

Figure 4.4: Illustration of interactions between different processes of HMC phenomena as implemented in the present COMSOL-PHREEQC interface.

4.2 Constructive process

Modeling the constructive process of a heap is important because two reasons: (i) it allows calibrating the model and (ii) it can help to improve the stability of the heap pad and optimize the mineral recovery efficiency.

The present methodology consists in simulating sequentially each layer that appears during the construction and operation of a heap leach pad (stacking levels). Therefore, this strategy of simulation allows mimicking the sequence of construction of a heap leach pad that is shown in Figure 4.5.

In this sequential simulation approach the results obtained during the calculation of the previous layers are used to define the initial and boundary conditions of the next layer.

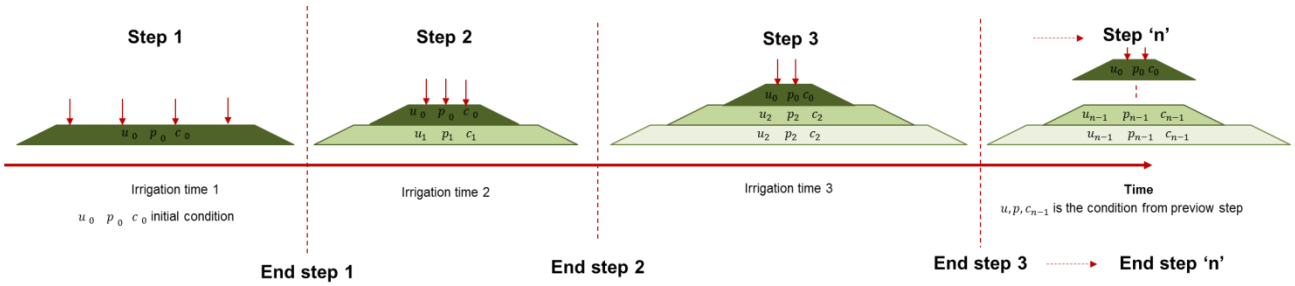

Figure 4.5: Sequence of construction of a heap leach pad layer by layer. The layer "n" is represent by step "n".

4.3 Numerical tools

4.3.1 Introduction

The governing equations described in Chapter 3 have been solved with COMSOL-PHREEQC, a numerical interface developed at Amphos 21 aimed at providing a flexible and efficient platform for the solution of large-scale coupled HMC problems. This interface consists on linking two standalone codes: (i) the commercial Finite Element software Comsol Multiphysics (v4.3), widely used in many different scientific fields for the modelling of processes based on partial/ordinary differential equations (PDE/ODE) and algebraic differential equations (ADE); (ii) the software PHREEQC (v2.0), a popular code within the geochemical scientific community that has been exhaustively tested and verified.

In brief, the tool is based on implementing an operator splitting technique for solving the hydro-mechanical problem (represented by a coupled or uncoupled PDE/ADE system) on COMSOL and the chemical system of algebraic and differential equations on PHREEQC.

A similar coupling approach has been developed recently by (Wissmeier, 2011). The main difference of Comsol-PhreeqC compared with the approach of (Wissmeier, 2011) stems from the parallelization of the geochemical step, which in typical HMC applications is the most CPU demanding process. The parallelization implemented in COMSOL-PHREEQC is achieved by slicing the domain in contiguous subdomains where reactions are solved, using a single Phreeqc process. This provides a remarkable higher computational efficiency to the tool, thus allowing for solving fully-coupled large-scale problems. Other programming differences with the tool of (Wissmeier, 2011) are a more general handling of different geochemical zones and the use of Java instead of Matlab as interface for the Comsol and Phreeqc modules. It is worth mentioning that Java offers a more flexible and maintainable platform and does not require any additional license.

In the next section we give a brief description of the numerical tools and their linking to develop the interface COMSOL-PHREEQC.

4.3.2 Software

4.3.2.1 COMSOL Multiphysics Version 4.3

Comsol Multiphysics version 4.3 (COMSOL, from now on) is a powerful Finite Element software environment for modelling and simulation of a large number of physics-based systems (COMSOL, 2011a). COMSOL is widely used in several scientific and technological applications for the modelling of processes based on PDE/ODE and ADE, allowing to address different coupled and highly non-linear systems.

COMSOL is a standalone product and has an intuitive and flexible graphical user interface (GUI), with flexible configuration options for geometry and mesh generation, setting material properties and different physical processes, setting solver options (parallelized direct and iterative solvers) and post-processing and visualization of the results. It furthermore allows to be accessed by script programming in Java, which is convenient for the purpose of coupling COMSOL to external software packages.

4.3.2.2 PHREEQC Version 2 and IPhreeqc

PHREEQC version 2 (Parkhurst, 1999)is a freely available computer program for simulating chemical reactions and transport processes in aquatic systems (Parkhurst, 1999). It is perhaps the most widely used geochemical code in the scientific community. The program is based on equilibrium chemistry of aqueous solutions interacting with minerals, gases, solid solutions, exchange and sorption surfaces, but also has the capability to model kinetic reactions with rate equations that are completely user-specified in the form of Basic statements. A 1D transport algorithm is included and comprises dispersion, diffusion, and various options for dual-porosity media. However, in this project the PHREEQC 1D transport capability is not used, since transport is solved in COMSOL. Only batch reaction calculations are performed with PHREEQC.

4.3.2.3 Linking PHREEQC to COMSOL

In order to couple PHREEQC with COMSOL we used the IPhreeqc version of the code (Charlton, 2011) IPhreeqc is a version of PHREEQC (Parkhurst, 1999) that has been specifically designed for coupling it to multi-phase flow and multi-component transport simulators to enable complex reactive transport simulations. To that end, PHREEQC was converted into a C++ class, which has a set of a few methods that implement the full reaction capabilities of PHREEQC. Input methods use strings or files to define reaction calculations exactly in the same formats used by PHREEQC. Output methods provide a table of user-selected model results, such as concentrations, activities, saturation indices, etc. Additional methods for data manipulation and communication to the host application have been implemented in the IPhreeqc module.

5.0 VERIFICATION CASES

The objective of this chapter is to validate the present numerical tool developed in COMSOL to solve the coupled phenomena of soil mechanics, unsaturated flow and solute transport.

Several benchmark examples have been solved in COMSOL and compared with analytical solutions and numerical solutions obtained with other finite element codes.

We solved four cases:

- The first case is a consolidation test and was used for validating the coupling between the mechanics and saturated flow.
- The second case refers to a triaxial test and was used to validate effective stress approach of soil mechanics (liquid pressure and total stress). Mohr-Coulomb and Cam-Clay are used as constitutive model.
- The third case is about the dam construction by stages whereby it is followed the construction process. This case was used to validate the displacement and stress evolution.
- The fourth case is about a contamination pond, where unsaturated flow and solute transport are coupled.

5.1 One-dimensional consolidation

5.1.1 Introduction

Consolidation is a transient process of unsteady flow in which there is coupling between flow and volume change as the soil gradually adjusts to a new effective stress regime (Wood, 1990).

The process of consolidation may be explained with the help of a mechanical model as that described in (Potts, 1999). In this problem we are going to use the analytical solution provided by (Biot, 1956).

The purposes of this benchmark are to demonstrate and verify the implementation of the fully coupled stress / liquid pressure formulation to simulate a consolidation test.

The problem of axial symmetrical consolidation can be described by the equations 10 for soil behavior and 18 for flow and certain conditions.

5.1.2 Conceptual model

A consolidation apparatus of 5 cm in diameter and 2 cm in height presses the soil sample from the top by a boundary load (AB) of 100 kPa. A flexible membrane contains the soil radially, allowing changes in radial forces by setting the pressure of the confining liquid.

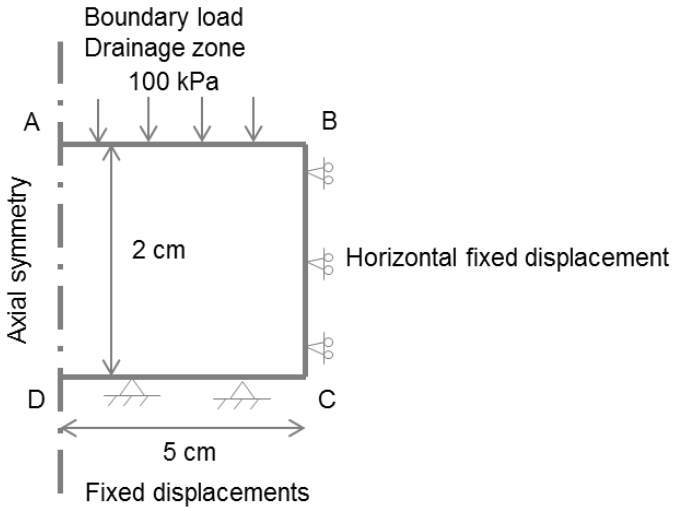

Figure 5.1: Conceptual model of consolidation test.

The boundary conditions of the problem are specified in Table 5.1.

Table 5.1: Summary of boundary conditions assumed to solve the consolidation test problem.

Boundary	Soil mechanics	Liquid flow
AB	$\boldsymbol{\sigma} \cdot \boldsymbol{n} = 100\ kPa$	outflow
BC	$u_x = 0$	$\boldsymbol{q} \cdot \boldsymbol{n} = 0$
CD	$u_x = u_y = 0$	$\boldsymbol{q} \cdot \boldsymbol{n} = 0$
DA	Axial symmetry	Axial symmetry

where $\boldsymbol{n}$ is the normal vector, $\boldsymbol{\sigma}$ is the stress tensor, $\boldsymbol{q}$ is the flux vector and $\boldsymbol{u}$ is the displacement vector

5.1.3 Material properties

The values of the parameters assumed to solve this benchmark are shown in the following table:

Table 5.2: Summary of material properties used to solve the consolidation test benchmark.

	Property	Units	Material
			Clay
Mechanical	Soil density, ρ_s	kg·m^{-3}	2 000
	Young's modulus, E	kPa	1 000
	Poisson's ratio, v	-	0
Hydrodynamics	Intrinsic permeability, $\boldsymbol{\kappa}$	m^2	1e-15
	Porosity, n	m^3·m^{-3}	0,3
	Storage, S	Pa^{-1}	1e-7
	Dynamic viscosity, μ*	Pa·s	0,001
	Liquid density, ρ_l*	kg·m^{-3}	1 000

** Water characteristic values.*

5.1.4 Results and discussion

The Figure 5.2 shows the drawdown curves at various times. The analytical solution of Terzagui's equation is depicted by solid blue lines, while the solution obtained with the simulation in COMSOL is represented by circles. A close agreement can be observed between simulated and the analytical solution.

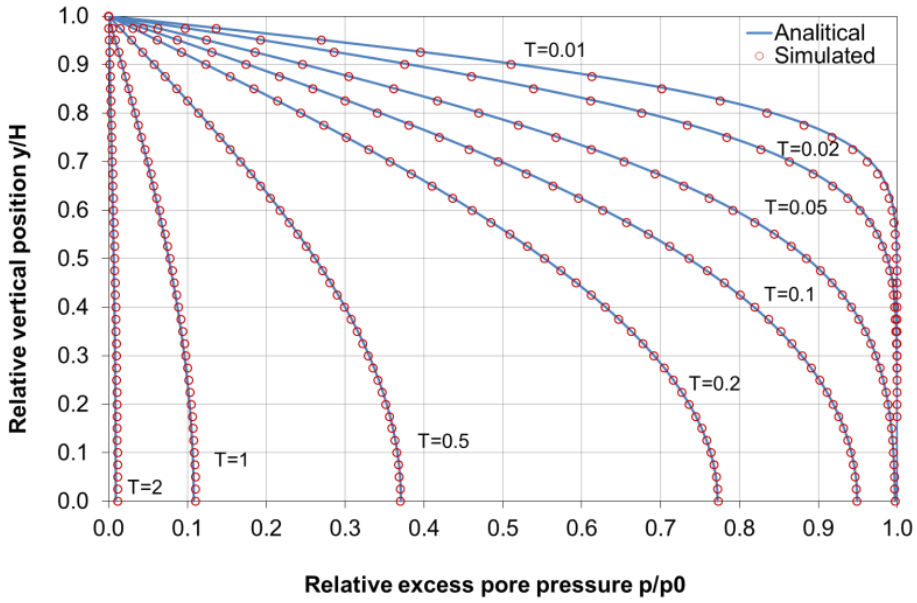

Figure 5.2: Isochrones simulated and analytical solution.

Figure 5.3 shows the dissipation of the liquid pressure distribution as a consequence of the soil drainage, at two different times.

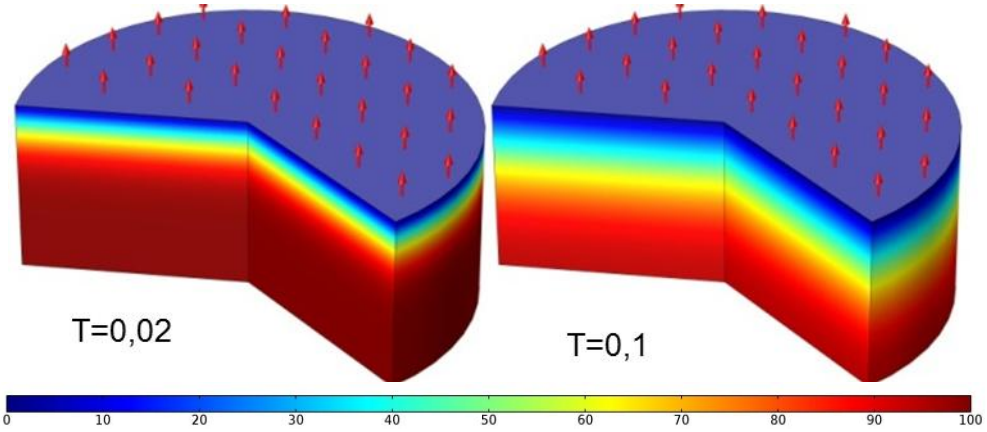

Figure 5.3: The liquid pressure distribution (kPa) at time T = 0,02 and T = 0,1 (dimensionless). The arrow represents the flow direction.

5.2 Triaxial test

5.2.1 Introduction

The triaxial test is one of the most common tests used in laboratory soil testing. The soil sample is normally placed inside a rubber membrane and then compressed maintaining a radial pressure.

In this benchmark, a vertical displacement and a confinement pressure are applied on the sample and the static response and the collapse load for a confinement pressure is studied. The material is modeled with 2 different constitutive model relationships: Mohr Coulomb and Cam-Clay criterion. The analysis is simplified by considering the intrinsic axial symmetry of the model.

The purposes of this benchmark are to demonstrate and verify the soil behavior in effective stress by simulate a triaxial test.

This example is adapted from SIGMA/W Manual (Krahn, 2004). The problem of axial symmetric triaxial test can be described by the equations 1, 6, 8 and 10.

5.2.2 Conceptual model

A triaxial apparatus of 1 m in diameter and 1 m in height, presses the soil sample from the top by a prescribed displacement (AB). A flexible membrane contains the soil radially, allowing changes in radial forces by setting the pressure of the confining water (BC). The stress and displacement was prepared in structure solid module of COMSOL Multiphysics.

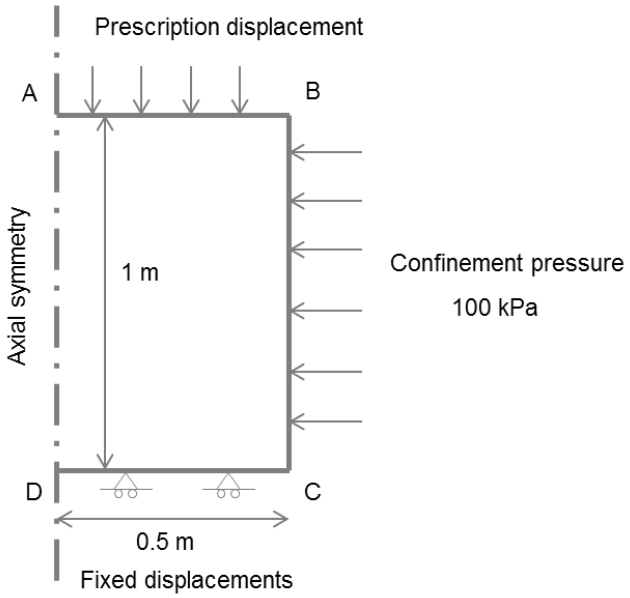

Figure 5.4: Dimensions and boundary conditions assumed to solve the triaxial test benchmark.

The boundary conditions if the problem are indicated in Table 5.3.

Table 5.3: Summary of boundary conditions assumed to solve the problem of triaxial test.

Boundary	Soil mechanics	Water flow
AB	Prescribed displacement	$\boldsymbol{q} \cdot \boldsymbol{n} = 0$
BC	$\boldsymbol{\sigma} \cdot \boldsymbol{n} = 100\ kPa$	$\boldsymbol{q} \cdot \boldsymbol{n} = 0$
CD	$u_x = u_y = 0$	$\boldsymbol{q} \cdot \boldsymbol{n} = 0$
DA	Axial symmetry	$\boldsymbol{q} \cdot \boldsymbol{n} = 0$

where $\boldsymbol{n}$ is the normal vector, $\boldsymbol{\sigma}$ is the stress tensor $\boldsymbol{q}$ is the flux vector and $\boldsymbol{u}$ is the displacement vector

5.2.3 Material properties

The soil properties are taken from standard clay.

Table 5.4 Abstract material properties for triaxial test.

	Property	Units	Constitutive Material	
			Mohr Coulomb	Cam-Clay
Mechanical	Young's modulus, E	kPa	1 000	1 000
	Angle of friction, φ	°	30	25,6
	Poisson's ratio, v	-	0,334	0,334
	compression index, λ	-	-	0,3
	swelling index, κ	-	-	0,05
	Initial void ratio	-	-	1,5
Hydrodynamics	Initial permeability, κ	m^2	-	1e-12
	Saturated liquid volume, θ_S	$m^3 \cdot m^{-3}$	-	0,5
	Residual liquid volume, θ_r	$m^3 \cdot m^{-3}$	-	0,03
	Storage, S	Pa^{-1}	-	1e-7
	Dynamic viscosity, μ*	Pa·s	-	0,001
	Liquid density, ρ_l*	$kg \cdot m^{-3}$	-	1 000

** Water characteristic values.*

5.2.4 Results and discussion

Figure 5.5 shows the stress path resulted assuming coupled drained/undrained conditions, both for Mohr Coulomb and Cam-Clay constitutive models.

The values obtained approach very well to numerical solution from other code. Total and effective stress path is developed due the two different kind of soil behavior with liquid.

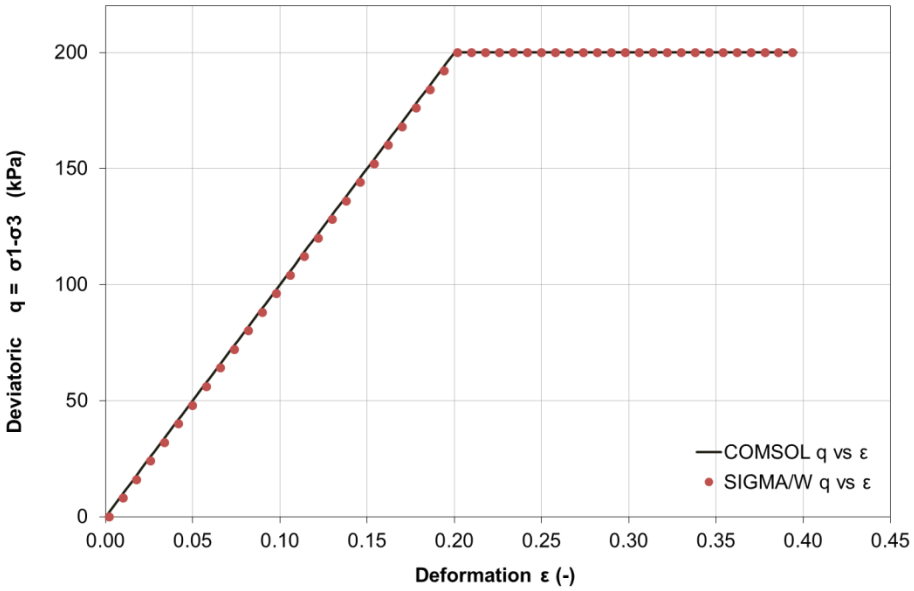
Deviatoric q = σ1-σ3 (kPa)
200
150
100
50
0
0.00
0.05
0.10
0.15
0.20
0.25
0.30
0.35
0.40
0.45
Deformation ε (-)
COMSOL q vs ε
SIGMA/W q vs ε

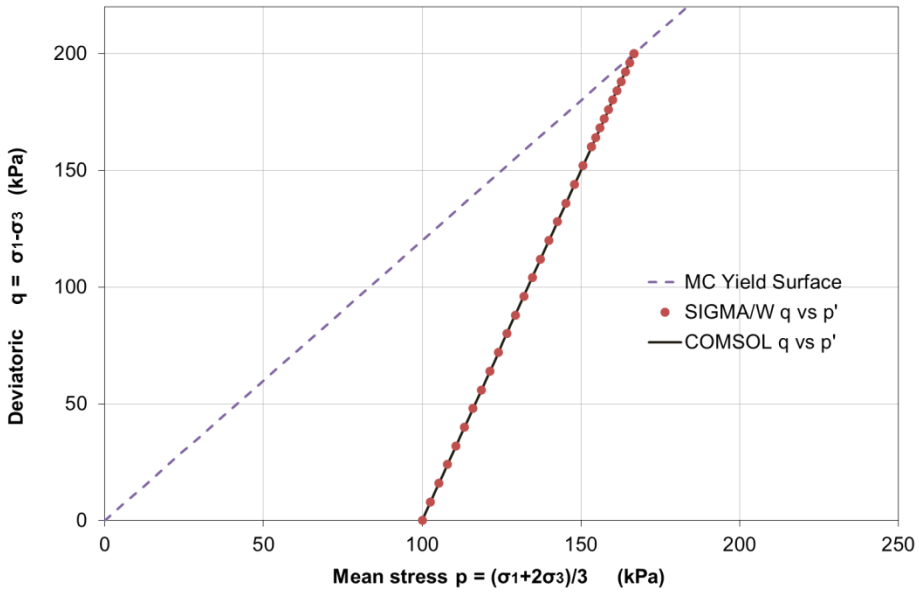
Deviatoric q = σ1-σ3 (kPa)
200
150
100
50
0
0
50
100
150
200
250
Mean stress p = (σ1+2σ3)/3 (kPa)
MC Yield Surface
SIGMA/W q vs p'
COMSOL q vs p'

(a)

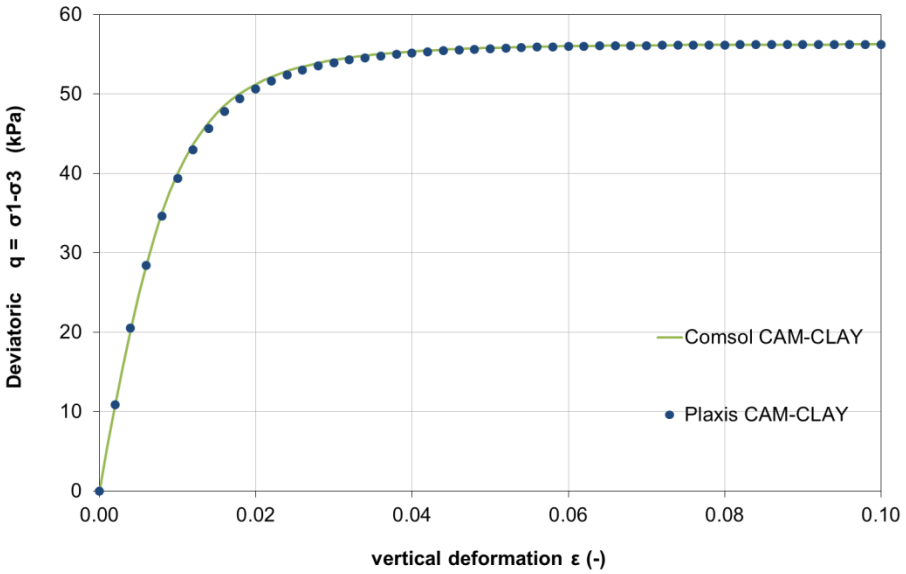

(b)

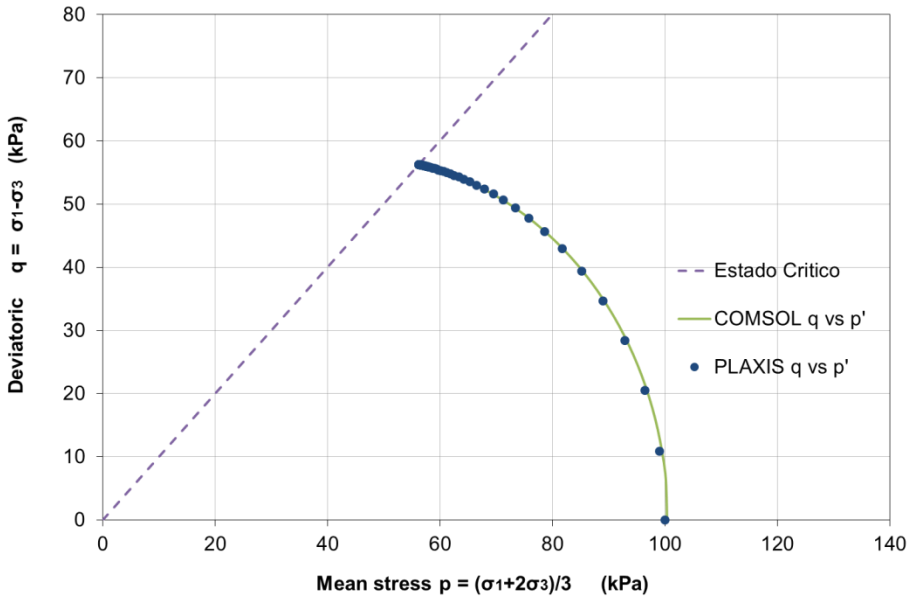

Figure 5.5: Stresses and axial strain resulted from the simulation of a drained/undrained triaxial test with SIGMA/W, PLAXIS and COMSOL. Two constitutive models were considered: (a) Mohr Coulomb model; (b) Cam-Clay model.

5.3 Dam construction by stages

5.3.1 Introduction

This simple example demonstrates the simulation of staged embankment construction on soft ground.

The purpose of this benchmark is to verify the vertical displacement due to construction process is accurate.

This example is adapted from SIGMA/W Manual (Krahn, 2004). The problem of two-dimensional dam construction is described by the equations 1, 6, and 10.

5.3.2 Conceptual model

Figure 5.6 shows the geometry of the problem. The fill is placed in eight successive one-metre lifts. The analysis starts by establishing the in-situ stress conditions and is followed by eight analyses representing the fill placement.

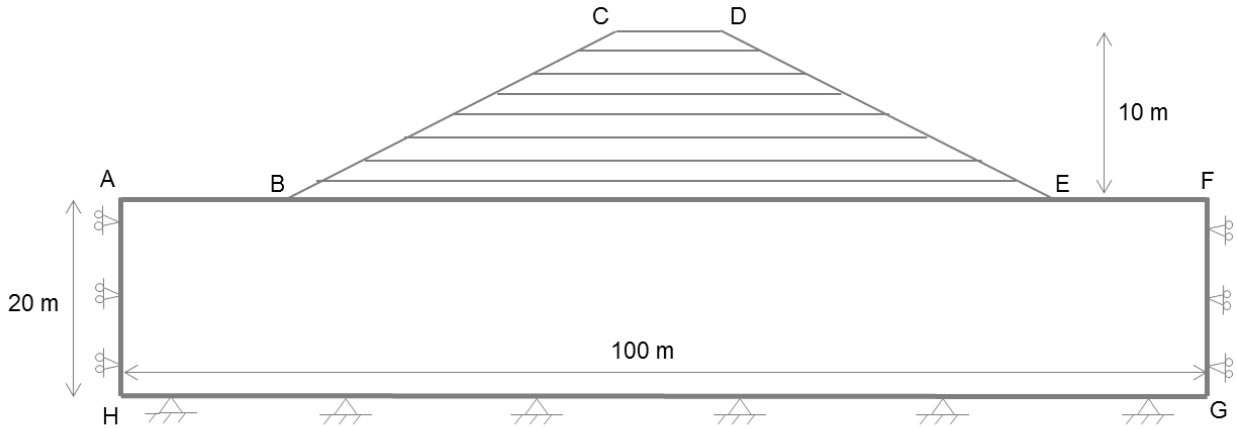

Figure 5.6: Model domain, geometry and boundary conditions assumed to solve the problem of dam construction.

The boundary conditions assumed to solve this benchmark are indicated in Table 5.5.

Table 5.5: Summary of boundary conditions assumed to simulate dam construction.

Boundary	Soil mechanics
AH	$u_x = 0$
ABCDEF	free
FG	$u_x = 0$
HG	$u_x = u_y = 0$

where $\mathbf{u}$ is the displacement vector.

5.3.3 Material properties

This benchmark was solved assuming the parameters specified in the following table.

Table 5.6 Summary of material properties for dam construction.

	Property	Units	Constitutive models	
			Lineal	Mohr Coulomb
Mechanical	Solid density, ρ_s	kg·m^{-3}	2 000	2 000
	Cohesion, c'	kPa	200	5
	Angle of friction, φ	°	30	35
	Young's modulus, E	kPa	200	5
	Poisson's ratio, v	-	0,49	0,40

5.3.4 Results and discussion

These are good approach for both codes. During dam construction vertical settlement occurs due the construction process. Contours of settlement obtained with both codes are shown in Figure 5.7.

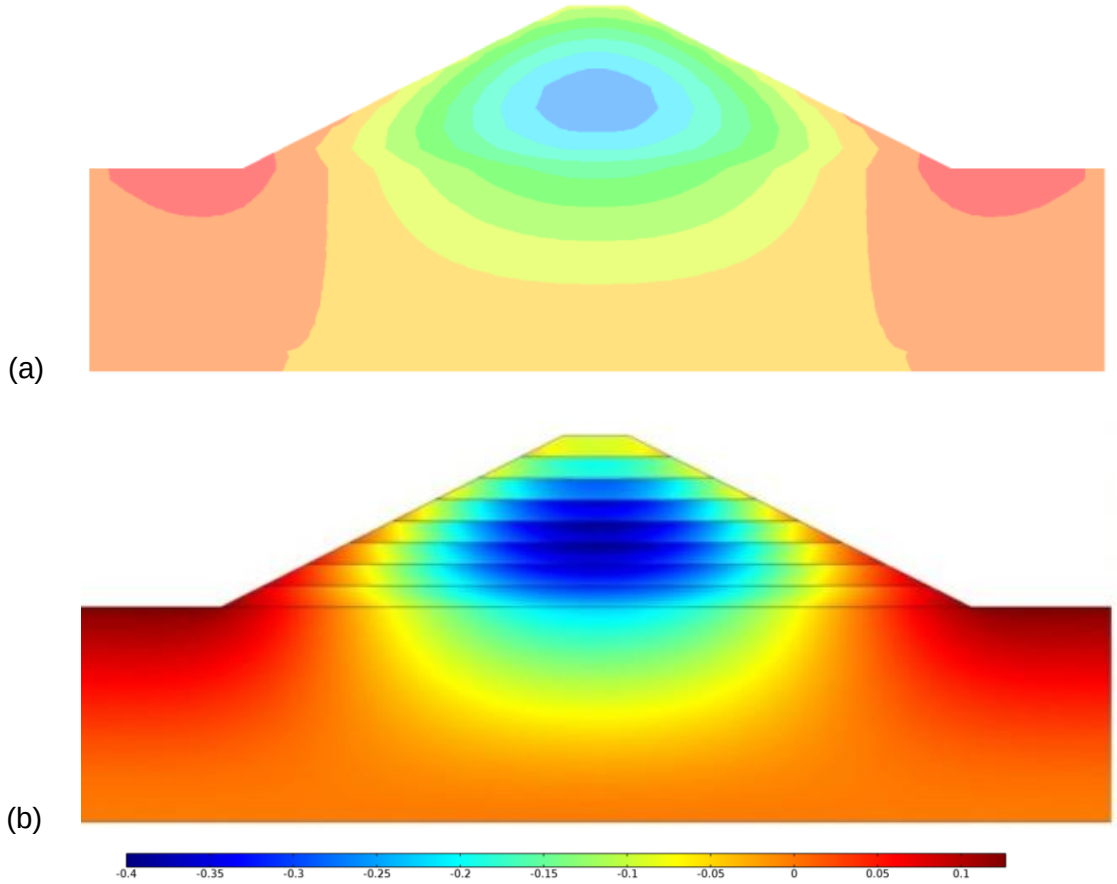

Figure 5.7: Contours of vertical settlement (m) simulated with SIGMA/W (a) and COMSOL (b).

Two profiles of vertical settlements developed within layers 6 and 8 of the dam and along the center-line of the embankment are shown in Figure 5.8. Note that the largest settlement is at the middle of dam as one could expect.

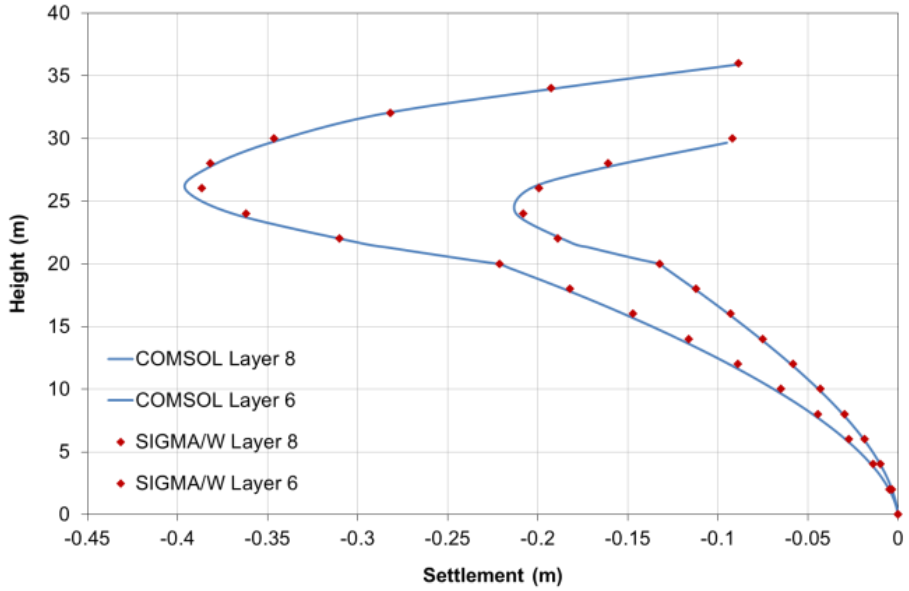

Figure 5.8: Vertical settlement profiles along the center line of the dam structure. Comparison between COMSOL and SIGMA/W simulations.

5.4 Contamination pond

5.4.1 Introduction

This benchmark is deals with the solute transport through a contamination pond.

The purposes of this benchmark are to demonstrate and verify the model advection and dispersion for a steady state seepage flow system.

The scope of this comparison will be two dimensional contamination transports model presented in the CTRAN/W User's Manual (Krahn, 2004). This example will use CTRAN/W to check COMSOL.

The problem of two-dimensional contamination pond is described by the Eq. 11 for unsaturated flow and Eq. 26 for solute transport.

5.4.2 Conceptual model

The system consists in an earth embankment with a pond. The seepage solution is prepared in COMSOL Subsurface-flow module. The COMSOL chemical-reaction-engineer module considers a constant concentration (AB) boundary condition along the pond floor of 10 kg/m^3. The model is run over a time of 2750 s.

Figure 5.9 shows the model geometry and the boundary conditions of the problem. A pond is located at the top left corner and is modeled using a hydraulic head condition (ABC). A potential seepage face has been applied along the slope (EF) and a pore-water pressure equal to zero is used at the toe of the slope (FG).

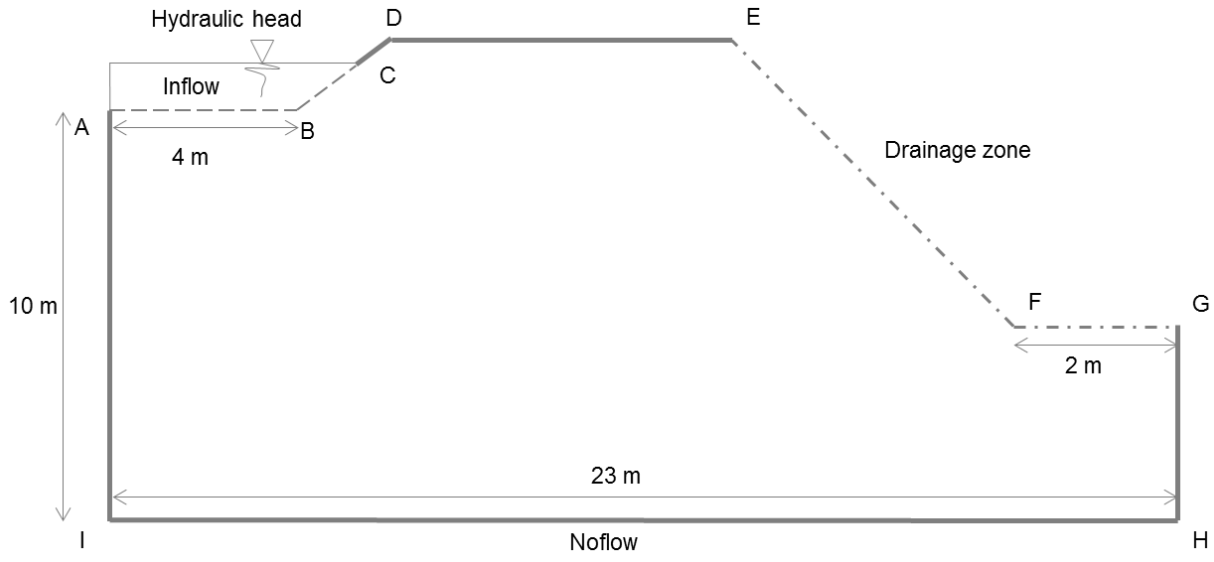

Figure 5.9: Model domain, geometry and boundary condition of pond contamination.

The boundary conditions are indicated in Table 5.7.

Table 5.7 Summary of boundary conditions assumed to solve the contamination pond problem.

Boundary	Liquid Flow	Solute transport
AB	$\overline{h_1} = 10{,}25\ m$	If $\boldsymbol{q} \cdot \boldsymbol{n} < 0 \rightarrow \mathrm{Q_{in}} = \boldsymbol{q}(\mathbf{m}_a - \mathbf{m}_a^*) \cdot \boldsymbol{n}$ If $\boldsymbol{q} \cdot \boldsymbol{n} \geq \mathbf{0} \rightarrow$ Outflow
BC	$\overline{h_1} = 10{,}25\ m$	Non-flow
CDE	$\boldsymbol{q} \cdot \boldsymbol{n} = 0$	Non-flow
EF	Outflow	Outflow
FG	$p - p_0 = 0$	Outflow
GHIA	$\boldsymbol{q} \cdot \boldsymbol{n} = 0$	Non-flow

where $\boldsymbol{n}$ is the normal vector, $\overline{h_1}$ is the hydraulic head and $\boldsymbol{q}$ is the flux vector.

5.4.3 Material properties

The material properties considered in this example are summarized in Table 5.8. Decay and adsorption is not included in model.

Table 5.8 Summary of material properties to solve the contamination pond problem.

	Property	Units	Silt
Hydrodynamics	Saturation permeability, $\boldsymbol{\kappa_s}$	m^2	1e-9
	Saturated liquid volume, θ_S	$m^3 \cdot m^{-3}$	0,35
	Residual liquid volume, θ_r	$m^3 \cdot m^{-3}$	0,03
	Storage, S	-	0
	Liquid density, ρ_l*	$kg \cdot m^{-3}$	1 000
	Dynamic viscosity, μ*	Pa·s	0,001
Conservative transport	Longitudinal dispersivity, α_l	m	2
	Transversal dispersivity, α_t	m	1

**Water characteristic values*

The hydraulic functions (SWCC and conductivity) shown in Figure 5.10 are based on sample functions (Krahn, 2004).

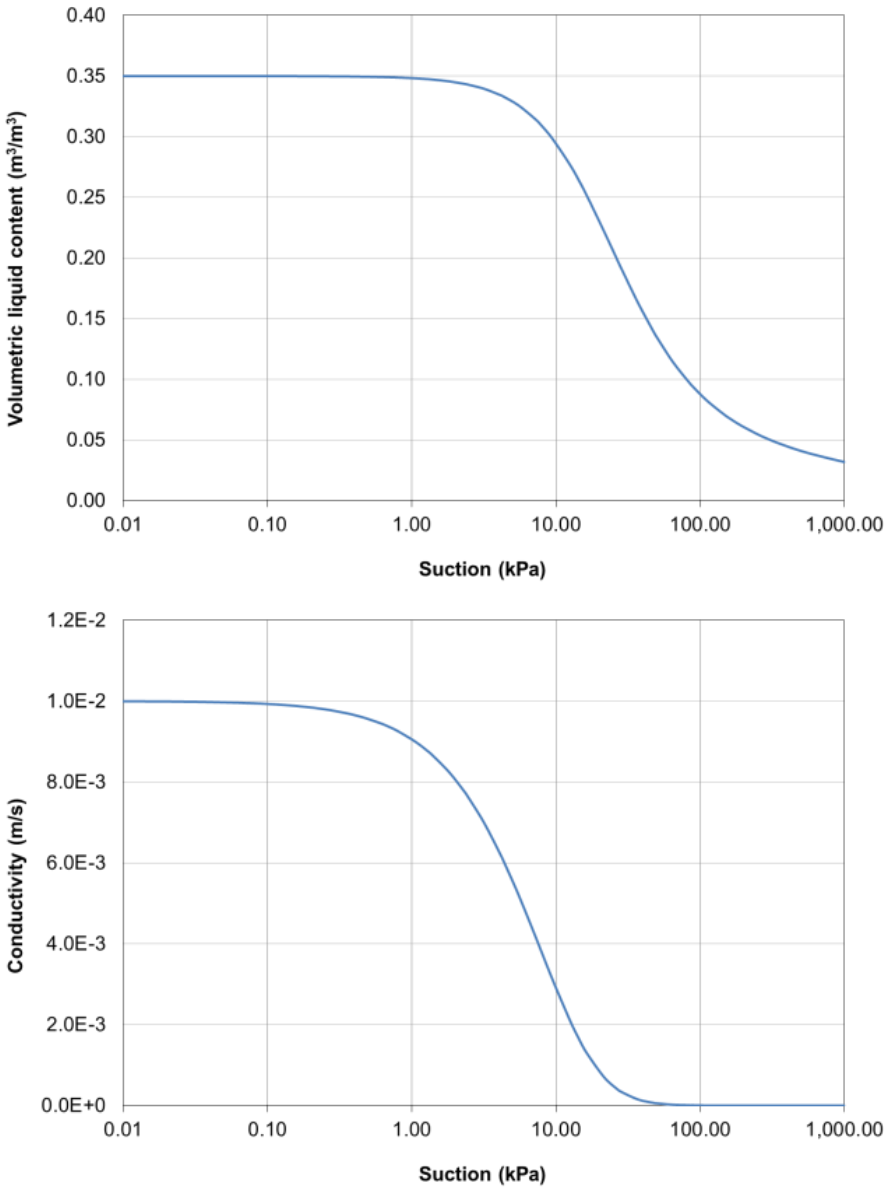

Figure 5.10: Soil water characteristic curve for silt soil from Krahn, 2004.

5.4.4 Results and discussion

From the figures below it can be seen that the results obtained from COMSOL are in close agreement with those obtained with CTRAN/W.

The results of the simulation of steady-state seepage show that a seepage face has developed near the toe of the slope (see Figure 5.11). Figure 5.11 also shows the phreatic level represented by blue line. This is expected flow behavior for the assumed material properties.

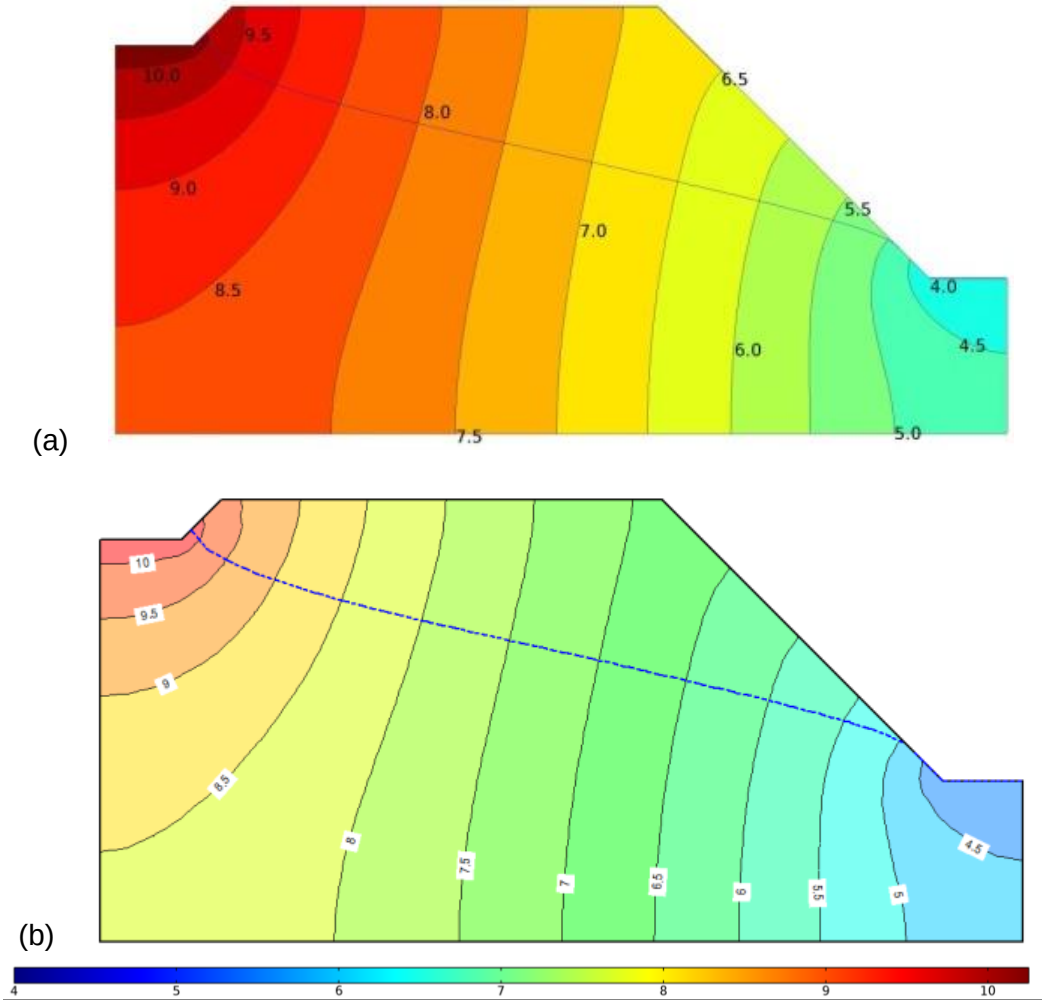

Figure 5.11 Head pressure contours (m) and phreatic level simulated with (a) COMSOL (b) CTRAN/W.

Figure 5.12 shows the concentration contours at the end of the simulation. Dispersion of the contaminant was considered in this analysis, which means it is possible that the contaminant will move ahead of the flowing water. The analysis demonstrates that the contaminant spread follow into the unsaturated zone above the phreatic surface.

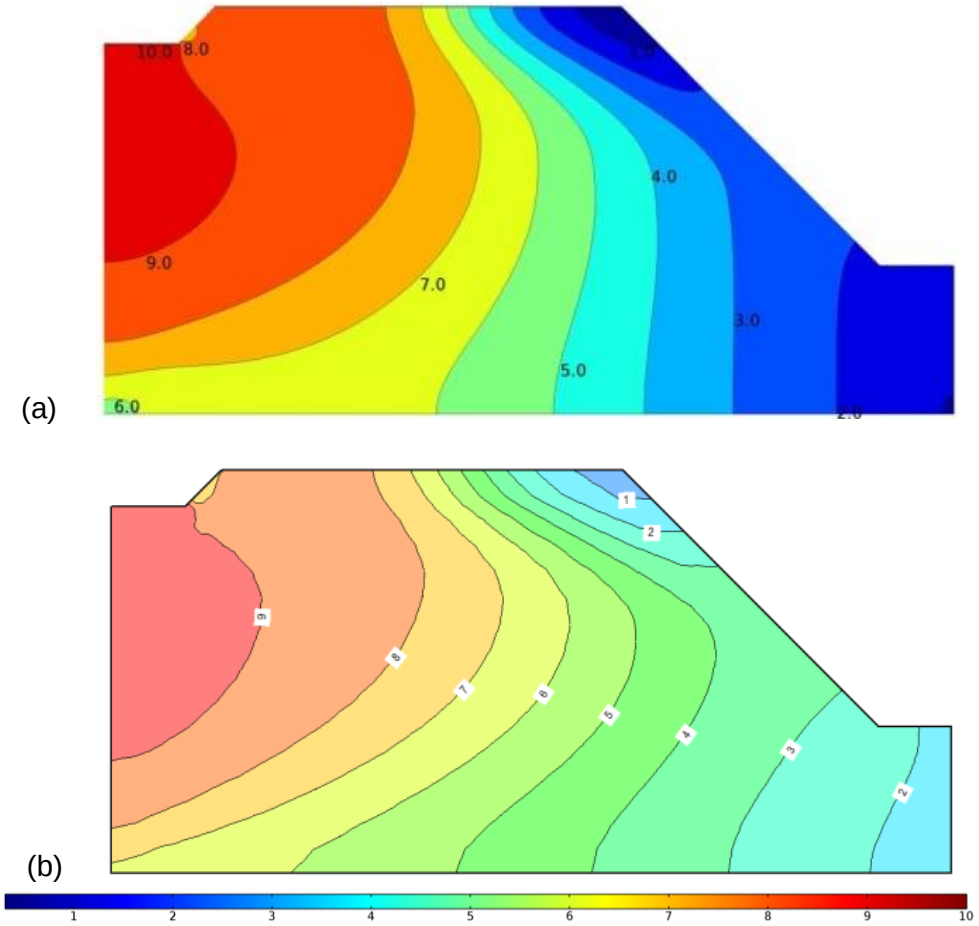

Figure 5.12: Concentration contours simulated with (a) COMSOL (b) CTRAN/W.

Figure 5.13 displays the evolution of the cumulative mass leaving the system through the drainage zone.

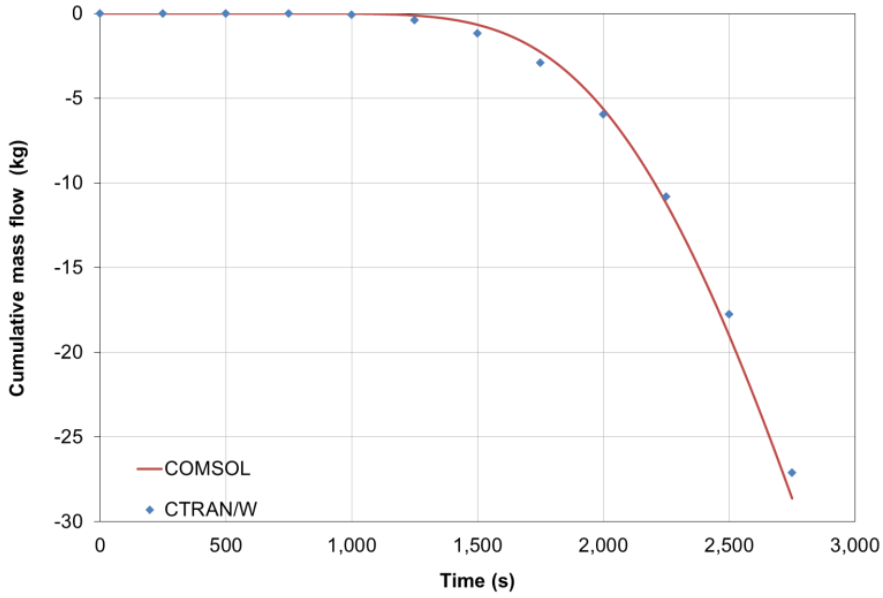

Figure 5.13: Evolution of the cumulative mass flow exiting the system.

6.0 APPLICATION CASE: HEAP LEACH PAD

6.1 Description

This chapter presents an application case of a copper heap leach pad. The objective is to analyze the different influence of hydrodynamics, mechanical and geochemical processes.

The heap leach pad simulation proposed involves the construction and operation of five ore layers settled on a terrain with a slight slope. It is a synthetic case, although geometry, properties and conditions are similar to real case (Anddes, 2012), (Amphos21, 2012).

Time analysis of the processes has been carried out for about a 100 days per layer.

6.2 Conceptual model

6.2.1 Overview

Geometry and dimensions try to reproduce a design typical heap leach pad (Figure 6.1). The model has been considered in two dimensions and is composed by three different domains:

- Five ore layers
- A liner system (underliner, geomembrane and drain)
- A foundation rock with 2% of slope.

The solution collection system composed by polyethylene network pipes and drainage gravel has been simplified to a drain layer domain.

The phenomena involved can been described by the Eq. 9 and 10 (soil behavior), the Eq. 18 (unsaturated flow), the Eq. 31 (reactive transport) and have been solved by the interface COMSOL-PHREEQC (see figure 4.2). It is worth mentioning that geochemical processes of mineral dissolution affect the porosity is also considered.

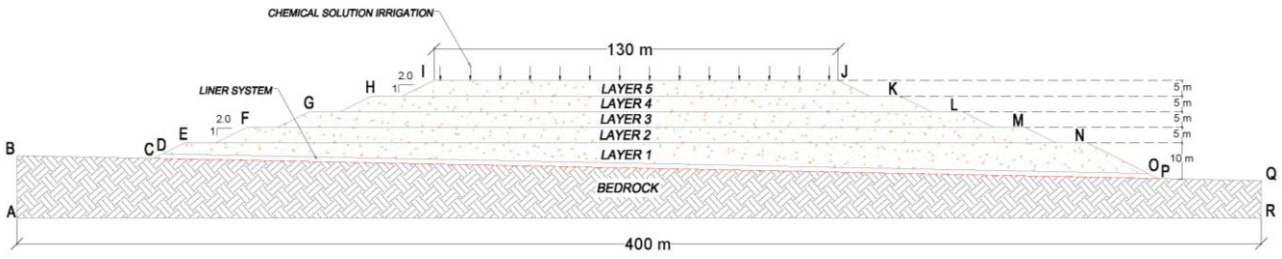

Figure 6.1: Sketch of the heap leach pad conceptual model with five layers.

6.2.2 Initial and boundary conditions

A constant net recharge rate (which accounts for the real amount of water which is infiltrated, taking into account i.e. the evaporation rate) applied on the top surface has been equal to 7,5 l/h/m^2 (Q_{in}). The layers have been irrigated during 90 days each one of them.

Construction process has been considered by applying a progressive load for each of ore layer. We have considered that the construction is performed during 10 days (see Table 6.1) for more details of construction and irrigation processes.

Table 6.1 Summary of time construction and irrigation of the heap leach pad.

	Construction		Irrigation	
	Initial time (day)	Final time (day)	Initial time (day)	Final time (day)
Layer 1	0	10	10	100
Layer 2	100	110	110	200
Layer 3	200	210	210	300
Layer 4	300	310	310	400
Layer 5	400	410	410	500

The Cam-Clay elasto-plastic criterion and plane strain conditions are assumed for simulating the geomechanical behavior. This is a compromise between the capabilities of COMSOL code and the representation of the real behavior. At the end of this chapter, some considerations about the behavior of real pads have been included.

Initial conditions are zero strains ($\boldsymbol{\varepsilon_0}$) and stresses ($\boldsymbol{\sigma_0}$) for each domain. Detailed information about boundary conditions is indicated in Table 6.2.

Table 6.2 Summary of boundary conditions for each phenomenon on heap leach pad.

Boundary	Soil mechanics	Liquid flow	Reactive solute transport
AB - QR	$u_x = 0$	$\boldsymbol{q} \cdot \boldsymbol{n} = 0$	Non-flow
BC	Free	$\boldsymbol{q} \cdot \boldsymbol{n} = 0$	Non-flow
CD	Free	$p - p_0 = 0$	Outflow
DEFGHI	Free	$\boldsymbol{q} \cdot \boldsymbol{n} = 0$	Non-flow
IJ – HK – GL - FM	Free	$\boldsymbol{q} \cdot \boldsymbol{n} = \mathrm{Q_{in}}$	If $\boldsymbol{q} \cdot \boldsymbol{n} < 0 \rightarrow \mathrm{Q_{in}} = \boldsymbol{q}(\mathbf{m}_a - \mathbf{m}_a^*) \cdot \boldsymbol{n}$ If $\boldsymbol{q} \cdot \boldsymbol{n} \geq \mathbf{0} \rightarrow$ outflow
JKLMNO	Free	$\boldsymbol{q} \cdot \boldsymbol{n} = 0$	Non-flow
OP	Free	$p - p_0 = 0$	Outflow
PQ	Free	$\boldsymbol{q} \cdot \boldsymbol{n} = 0$	Non-flow
RA	$u_x = u_y = 0$	$\boldsymbol{q} \cdot \boldsymbol{n} = 0$	Non-flow
CP	Free	$\boldsymbol{q} \cdot \boldsymbol{n} = 0$	Non-flow

where $\boldsymbol{n}$ is the normal vector, $\boldsymbol{q}$ is the flux vector and $\boldsymbol{u}$ is the displacement vector.

Initial natural moist of the ore material layer is considered equal to 5%. For the retention curve used this is equivalent to a negative pressure (suction) equal to 30kPa. An inflow condition ($\mathrm{Q_{in}}$) is considered for every layer (IJ, HK, GI, FM) to reproduce the irrigation process. An outflow condition is considered on the out sides of the drain domain.

Initial water ($\mathbf{m}_a^0$) and boundary of infiltration water ($\mathbf{m}_a^*$) concentrations used for the reactive solute transport are shown in Table 6.3. These values were provided by Amphos21, (2012).

Table 6.3 Chemical composition of pore water and leaching solution. Note: Concentrations are given in mol/l.

		m_a^0 pore water	m_a^* infiltrating water
	Temp(ºC)	25	25
	pH	5,95	0,94
	Eh (mV)	738	1 161
Master species (mol/l)	C	1,30 x 10^{-2}	1,04 x10^{-5}
	Ca	2,70 x10^{-2}	2,70 x10^{-3}
	Cl	8,80 x10^{-3}	9,63 x10^{-2}
	K	2,09 x10^{-2}	6,30 x10^{-4}
	Fe	2,62 x10^{-7}	7,50 x10^{-6}
	Mg	1,04 x10^{-5}	1,30 x10^{-5}
	Na	6,50 x10^{-5}	6,10 x10^{-4}
	S	3,08 x10^{-2}	4,50 x10^{-2}
	Si	9,90 x10^{-9}	3,20 x10^{-4}

The chemical reactions considered in the conceptual geochemical model are described in Table 6.4 and Table 6.5 (Amphos21, 2012).

Table 6.4 Summary of chemical reactions

Mineral	Volume fraction	Type of reaction	Reference
Jarosite-K	Initial condition = 0	Equilibrium conditions	(Charlton, 2011)
Jurbanite	Initial condition = 0	Equilibrium conditions	(Charlton, 2011)
Basaluminite	Initial condition = 0	Equilibrium conditions	(Charlton, 2011)
$Fe(OH)_{3(a)}$	Initial condition = 0	Equilibrium conditions	(Charlton, 2011)
Schwertmannite	Initial condition = 0	Equilibrium conditions	(Charlton, 2011)
Pyrite	1,08 x 10^{-2*}	Kinetic dissolution	(Williamson, 1994)
Chalcopyrite	2,68 x 10^{-4*}	Kinetic dissolution	(Saaltink, 2002)
K-Feldspar	1,58 x 10^{-1*}	Kinetic dissolution	(Palandri, 2004)
Albite	1,47 x 10^{-1*}	Kinetic dissolution	(Palandri, 2004)

* These parameter values were chosen arbitrarily.

Table 6.5 Description of chemical reactions

Mineral	Reactions
Jarosite-K	KFe3(SO4)2(OH)6 + 6 H+ = 3 Fe+3 + 6 H2O + K+ + 2 SO4-2
Jurbanite	AlOHSO4 + H+ = Al+3 + SO4-2 + H2O
Basaluminite	Al4(OH)10SO4 + 10H+ = 4Al+3 + SO4-2 + 10H2O
$Fe(OH)_{3(a)}$	Fe(OH)3 + 3 H+ = Fe+3 + 3 H2O
Schwertmannite	Fe8O8(OH)4,5(SO4)1,75 + 20,5H+ = 1,75SO4-2 + 8Fe+3 + 12,5H2O
Pyrite	FeS2 + 2 H+ + 2 e- = Fe+2 + 2 HS-
Chalcopyrite	CuFeS2 + 2H+ = Cu+2 + Fe+2 + 2HS-
K-Feldspar	KAlSi3O8 + 8 H2O = K+ + Al(OH)4- + 3 H4SiO4
Albite	NaAlSi3O8 + 8 H2O = Na+ + Al(OH)4- + 3 H4SiO4

6.3 Material properties

A list of parameters used can be found in Table 6.6. Isotropic properties for all the materials have been assumed. It is worth noting that the parameter values adopted have been taken from different information sources, such as laboratory tests, in situ tests and average field measurements for similar materials. The combination of all of them, however, could not correspond to a real case since they have been taken from different places (Anddes, 2012).

Van Genuchten retention curves (Van Genuchten, 1980) have been calculated by using the retention parameters provided by laboratory test information from (Pacheco, 2011).

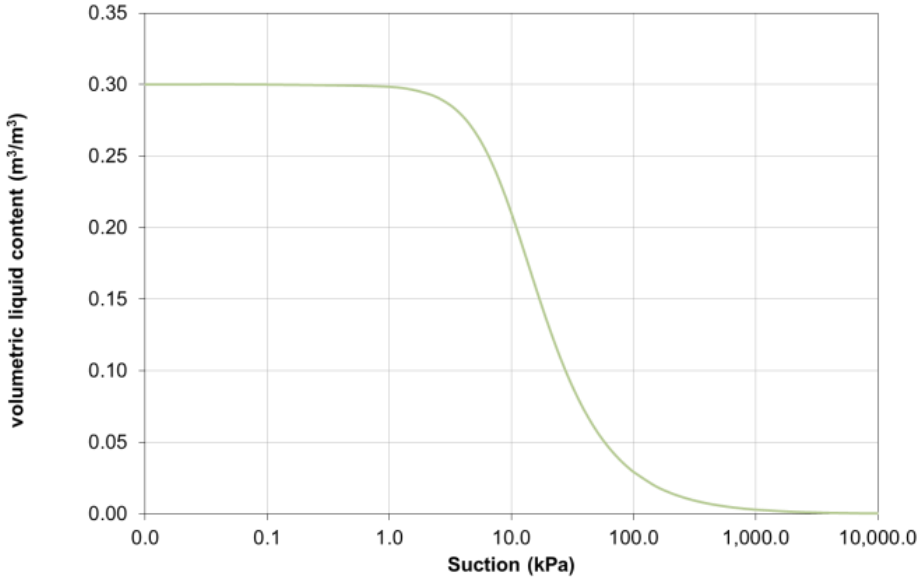

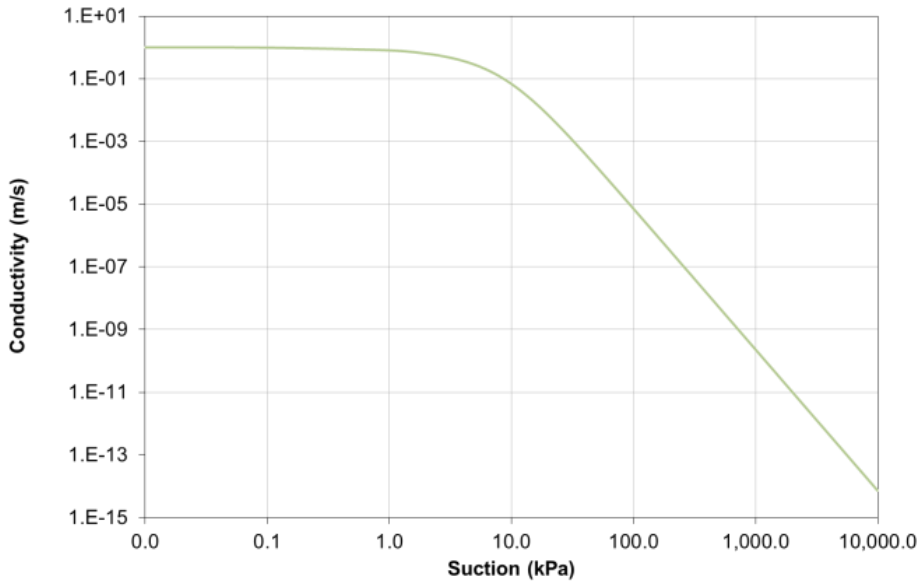

Figure 6.2: Soil water characteristic curve for ore material.

It is presented next the material property descriptions involved in the heap leach pad.

- The strength parameters of bedrock are estimated from RMR values (Anddes, 2012).

- The drain is composed of gravel which has high permeability. The strength parameters (cohesion and angle friction) of interphase among soil/geomembrane/drain (liner system) result from a direct shear test of a soil-geosynthetic interface for more detailed see ASTM D5312 (Anddes, 2012).

- The strength parameters and stiffness (cohesion, friction angle, kappa, lambda and Young's modulus) of the ore have been taken from a large triaxial test and some laboratory information available (Anddes, 2012).

Table 6.6 Summary of mechanical, liquid flow and reactive transport parameter values for heap leach pad.

	Property		Units	Material		
				Rock	Liner system	Ore
Mechanical	Solid density, ρ_s		kg·m^{-3}	3 000	2 600	2 600
	compression index, λ		-	-	0,007	0,007
	swelling index, κ		-	-	0,002	0,002
	Initial void ratio, n_0		m^3·m^{-3}	0,1	0,3	0,3
	Angle of friction, φ		°	-	30	35
	Angle of friction associated, φ^b		°	-	16	16
	Cohesion, c'		kPa	-	15	15
	Young's modulus, E		MPa	3 000	100	100
	Poisson's ratio, v		-	0,25	0,30	0,30
Hydrodynamics	Initial permeability, **κ**		m^2	-	5e-10	4e-11
	Initial porosity, n_0		m^3·m^{-3}	-	30	30
	Saturated liquid volume, θ_S**		m^3·m^{-3}	-	"Porosity"	"Porosity"
	Residual liquid volume, θ_r		m^3·m^{-3}	-	0,01	0,01
	Storage, S		Pa^{-1}	-	1e-7	1e-7
	liquid density, ρ_l*		kg·m^{-3}	-	1 000	1 000
	Dynamic viscosity, μ*		Pa·s	-	0,001	0,001
	Van Genuchten	α	kPa^{-1}	-	1	1
		n	-	-	2	2
		l	-	-	0,5	0,5
Reactive transport	Longitudinal dispersivity α_l		m	-	50	10
	Transversal dispersivity α_t		m	-	10	2

**Water characteristics values.*
*** "Porosity" is summation of initial porosity, changes of mechanical porosity and changes of chemical porosity.*

6.4 Spatial discretization

The mesh consists on 14 641 triangular first order elements. Its distribution around all the domains is shown in Figure 6.3.

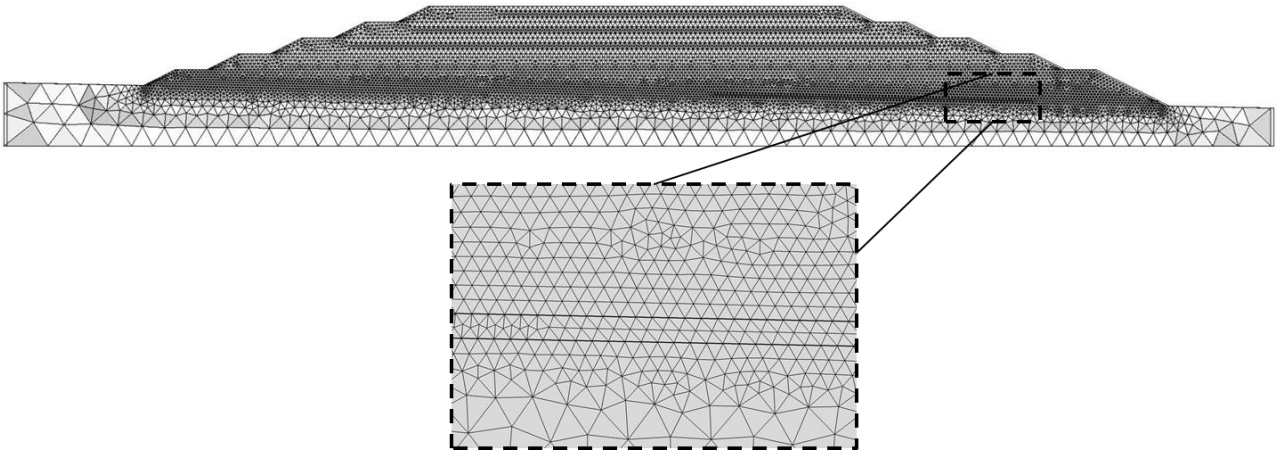

Figure 6.3: Finite element mesh used for spatial and time discretization.

6.5 Discussion and results

6.5.1 Mechanical displacements and stresses

The distribution of vertical total-stresses is shown in Figure 6.4a for every layer. A section (A-A') shows the vertical displacement distribution (see Figure 6.4b). The maximum vertical displacement is obtained at mid height. This is agreement with field observations.

(a)

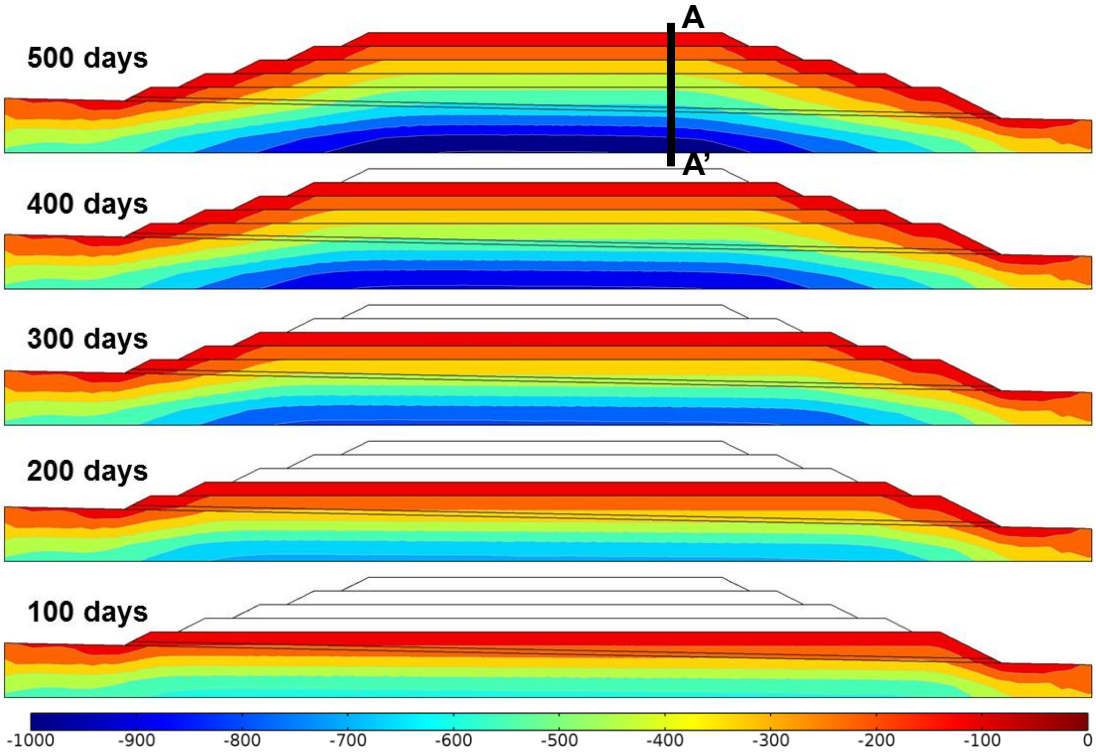

(b)

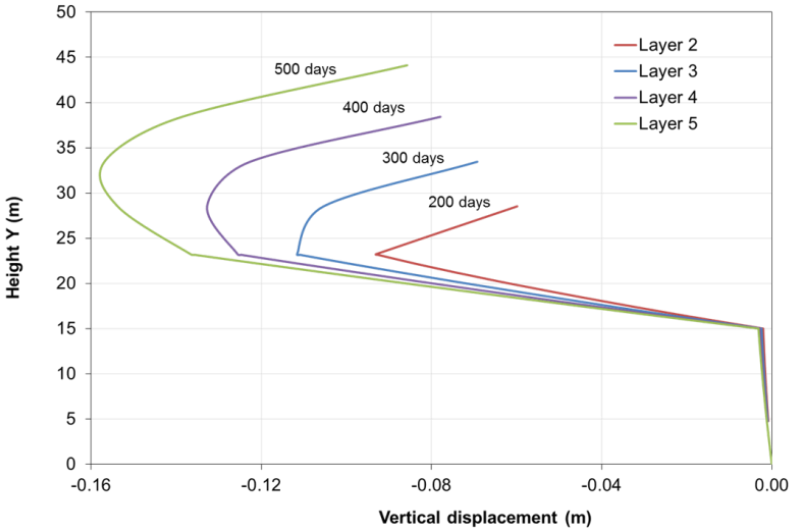

Figure 6.4: Vertical total-stress distribution (kPa) (a) vertical displacement distribution for the cross section A-A' for 200 days, 300 days, 400 days and 500 days due to self-weight (b).

6.5.2 Density evolution of soil

The evolution of density of soil is shown in Figure 6.5. This term is mainly affected by the degree of saturation liquid and the porosity as it is described in equation 1. The lower density is obtained in the slopes because degree of saturation has low values in those zones.

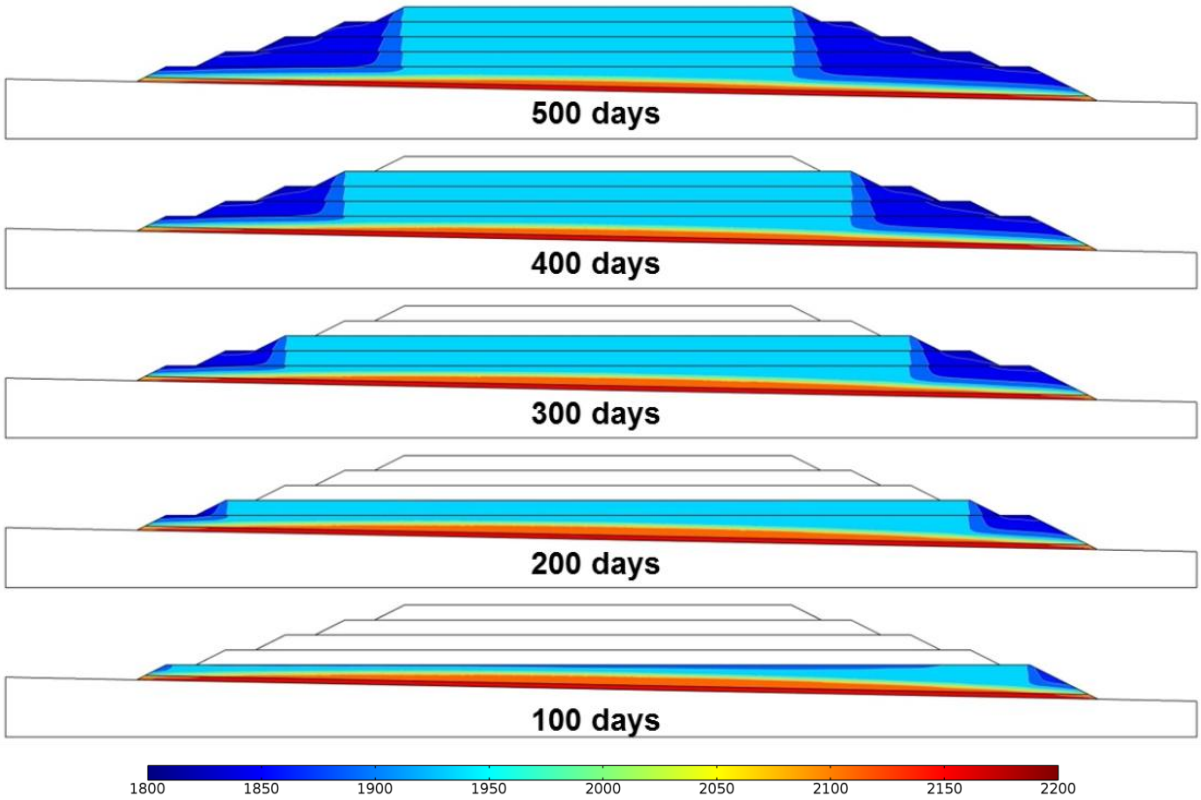

Figure 6.5: Evolution of the soil density (kg/m^3).

6.5.3 Safety factor regarding global failure

In general, slopes may exhibit global failures when destabilizing forces are greater than resisting forces. Limit equilibrium analyses are commonly used to assess this condition. In this case the COMSOL code has been used instead. A procedure called “c-phi” reduction methodology (Brinkgreve, 1991) was used in this work.

Cohesion in unsaturated conditions has two terms the effective cohesion (c') and the apparent cohesion ($c_{apparent}$), this last term is related to the matric suction ($p_a - p_l$) zero when is positive and increase when is negative.

The effect of suction is included by the apparent “cohesion”. This formulation is given in Eq. 9. It is assumed for this case the angle associated (φ^b) equal to 16° same for ore and system liner. This value is taken from (Fredlund, 1978) for Tappon Notch Hill silt.

Suction is reduced when irrigation takes place and thus the strength of the material reduces as well, following equations 9. The safety factor has been computed using COMSOL code by reducing progressively the shear strength until numerical collapse. “Effective Cohesion” and “tan(φ')” are divided by a number which becomes the safety factor when collapse is reached.

Figure 6.6a and Figure 6.6b show the shear stresses rate over all domains, when the red zone is bigger than blue it is representing low safety factor as it is shown in Figure 6.6c.

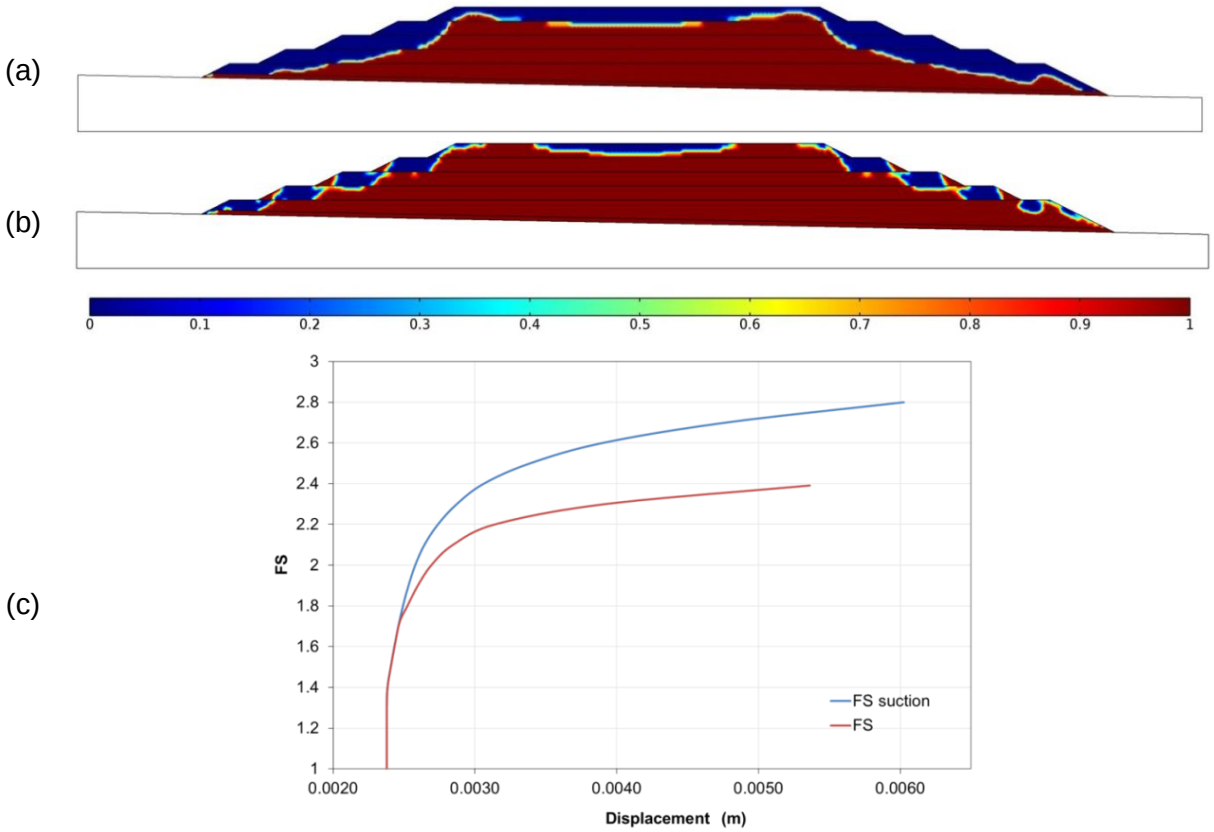

Figure 6.6: The shear strenght rate (Pa·Pa^{-1}) is represented with suction (a) and without suction (b). The safety factor by c-phi reduction methodology is sketched (c).

Figure 6.7 shows instability on first lift. This could be due to the increase of liquid pressure or to the lift thickness.

Figure 6.7: Case of slope failure in the first lift of heap leach pad (Anddes, 2012).

Often global failure occurs on the contact underliner, geomembrane and overliner (liner system). This interphase has probably lower shear strength than the ore itself. Some direct shear test on that interphase has been performed for private mining industries.

6.5.4 Liquid saturation evolution

The hydrodynamics behavior is conditioned by the time that takes the inflow water to saturate the heap ore in the path to the drainage system. The transient flow system is shown in Figure 6.8. After a short period of transient, a steady state is achieved for every layer; in our case it takes about 40 days since the layer construction (Figure 6.8).

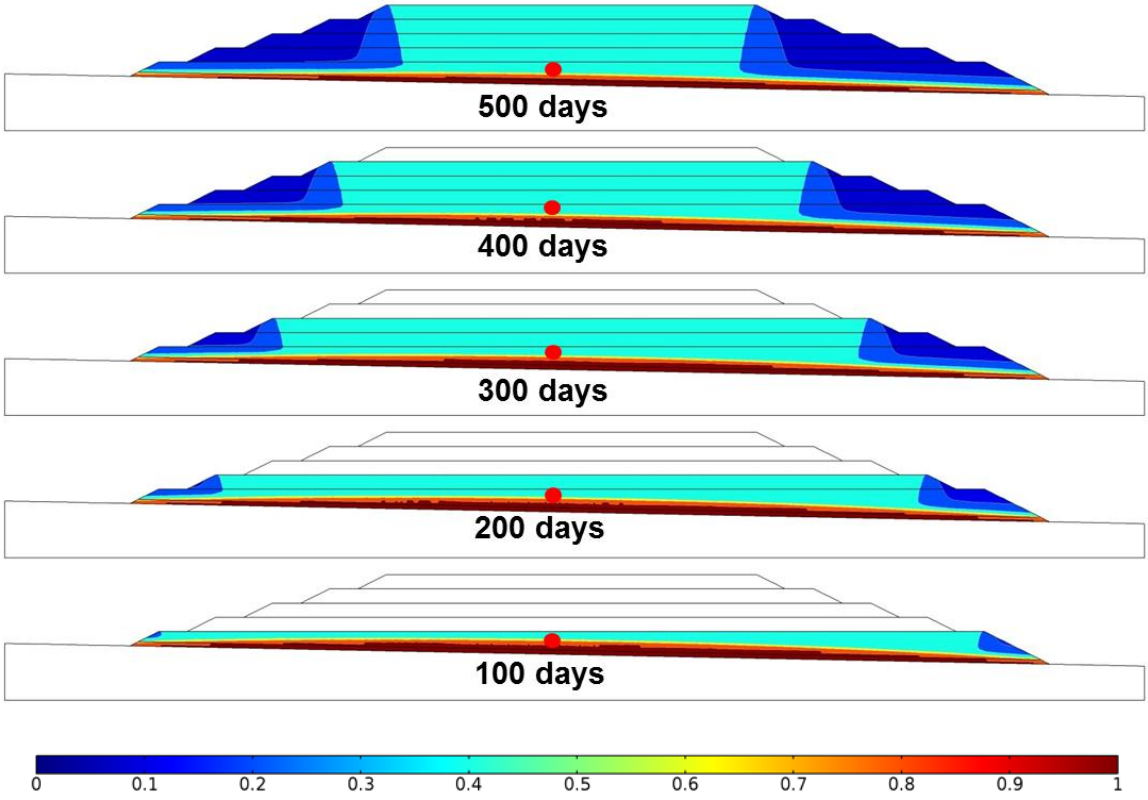

Figure 6.8: Degree of saturation and water level in different days ($m^3 \cdot m^{-3}$).

To understand the evolution of the liquid pressure one reference point has been chosen (see the red spot of figure 6.8) and has been drawn in Figure 6.9. There can be found two stages for every step: the construction and the irrigation.

The effect of construction does not generate pore water pressure (as in undrained conditions) due to two reasons: first ore is mainly unsaturated, and secondly construction has been simulated in a progressive manner.

The increase of liquid pressure is generated due to irrigation, but the decrease of liquid pressure with time is due to the minor amount of irrigation since it is proportional to each layer top surface.

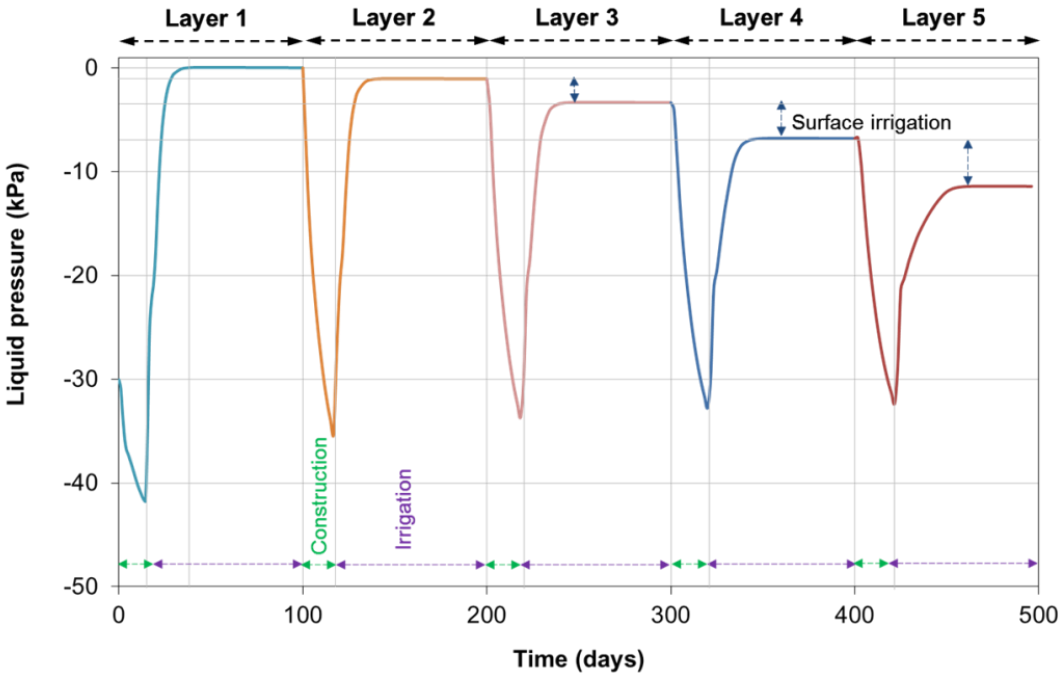

Figure 6.9: Evolution of the liquid pressure due to construction and irrigation processes.

6.5.5 Mass balance of liquid

The mass balance of liquid depends on the irrigation, the drainage and the mass retained in the media (storage). Figure 6.10 represents how the ratio of these different processes evolves over time.

The irrigation evolution is a known boundary condition. The drainage evolution is obtained from the analyses, at the drainage zone of the pad (see Table 6.2). Note that on this drainage zone the imposed boundary condition was a mixed one, so the outflow is provided by the computation. Finally the storage is computed by the COMSOL code by integration all the storage terms in the domain.

A feature observed is the decrease of mass flow over time. This is due to the surface irrigation.

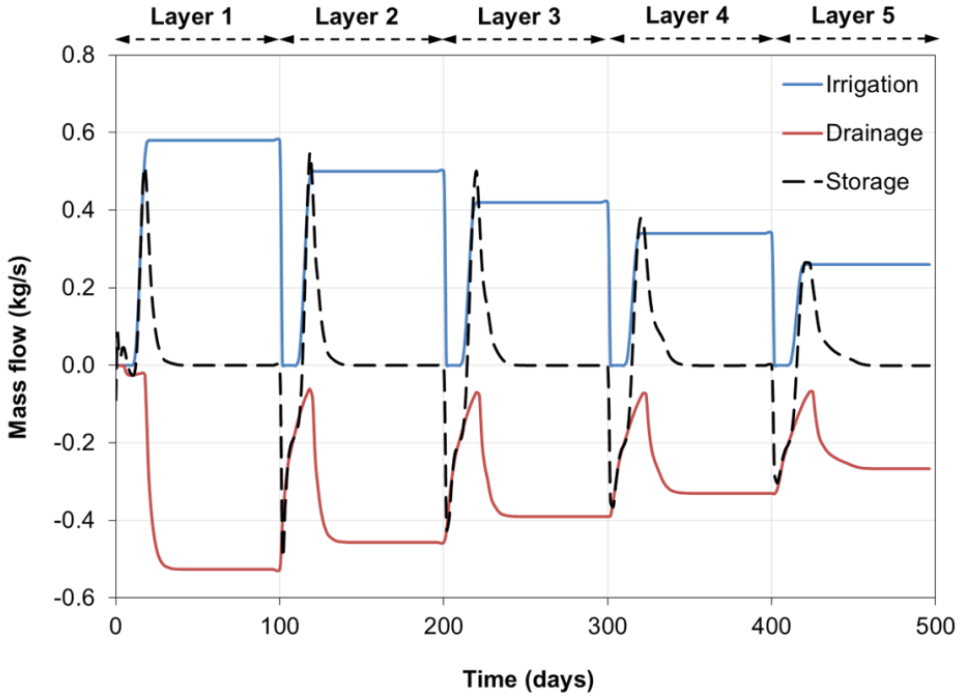

Figure 6.10: The ratio of different hydraulic processes over time.

To check the correct conservation of liquid mass a balance of mass of liquid has been done. Table 6.7 shows the values of each process and the totals accumulated. The relative error is equal to 8,7%, this is calculated as total input minus total output and plus total storage all of them divided by total input.

Table 6.7: Summary of mass balance of liquid.

States	Input (kg)	Output (kg)	Storage (kg)
Irrigation 1	4 259 520		
Irrigation 2	3 672 000		
Irrigation 3	3 084 480		
Irrigation 4	2 544 340		
Irrigation 5	1 916 272		
Drainage 1		3 622 843	
Drainage 2		3 383 623	
Drainage 3		2 916 400	
Drainage 4		2 484 851	
Drainage 5		1 930 657	
Initial amount of liquid			605 026
Final amount of liquid			818 370
Total	15 476 611	14 338 374	213 344

6.5.6 Chemical processes and mineral recovery

Figure 6.11a shows the evolution of selected dissolved species concentrations at the output of the drainage system. The evolution of pH shows the arrival of the acidic solution irrigated on the top boundary in a very short time (around 20 days). Kinetic dissolution of chalcopyrite is triggered by the infiltration of the acidic solution and, as a result, an increase of Cu concentrations is observed in the outlet flow (Figure 6.11b). The chemical evolution of Si and Al concentrations (Figure 6.11c and 6.11d) clearly shows that under this low pH conditions kinetic dissolution of aluminosilicates is also favored. This process is highly dependent of the pH and, over a long period of time, porosity can be significantly modified.

(a)

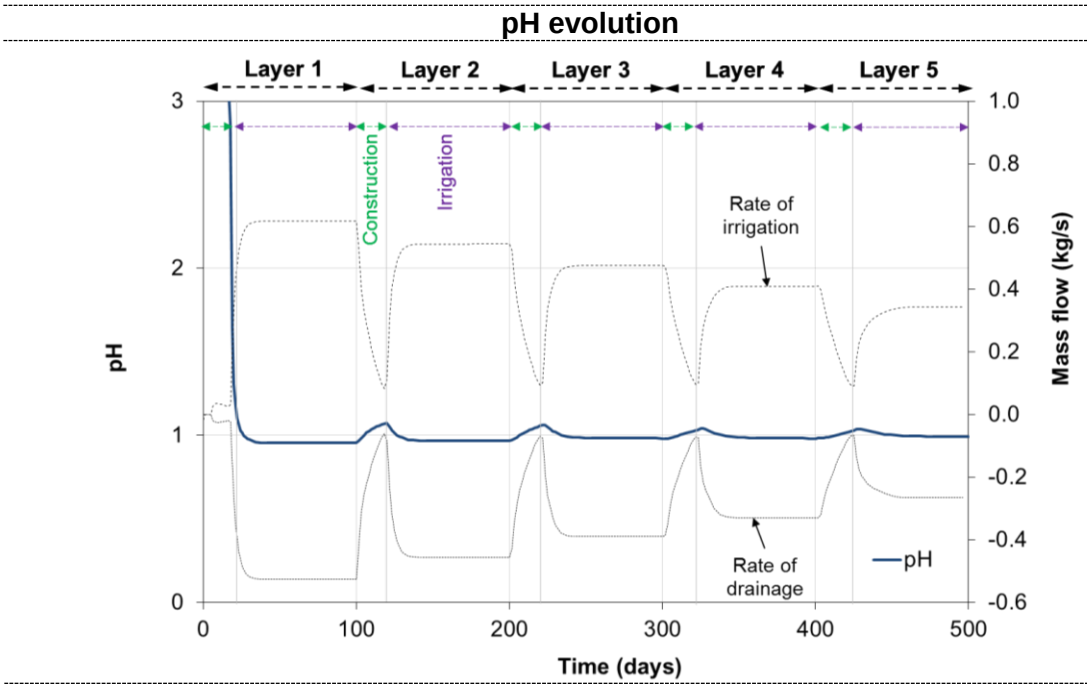

(b)

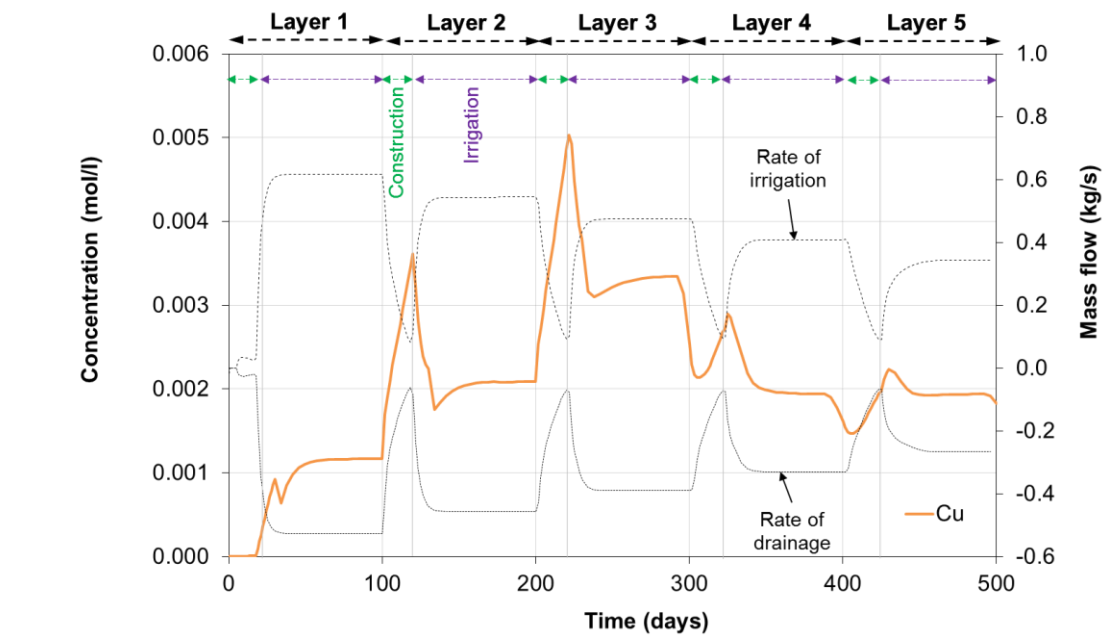

Dissolution of aluminosilicates

(c)

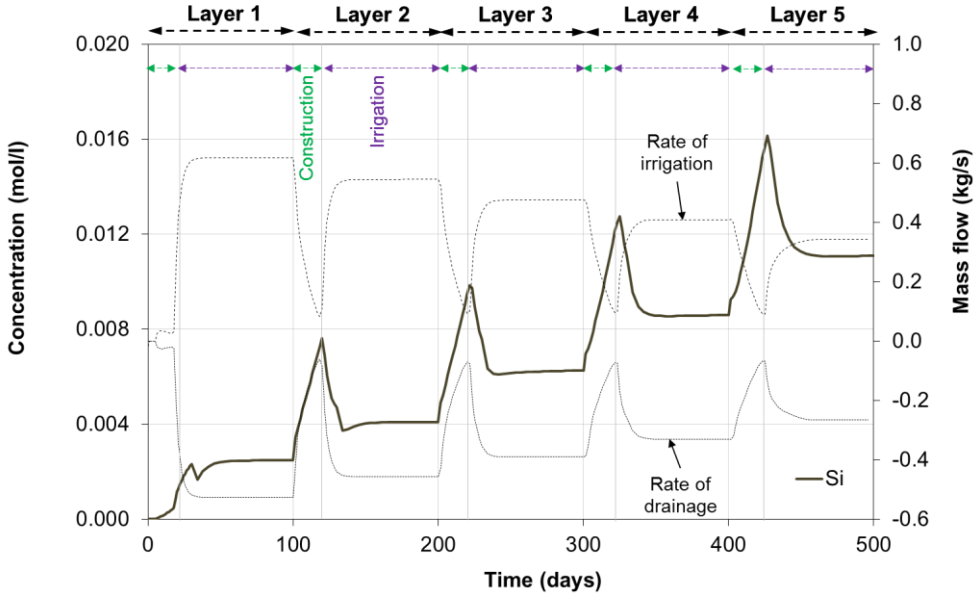

(d)

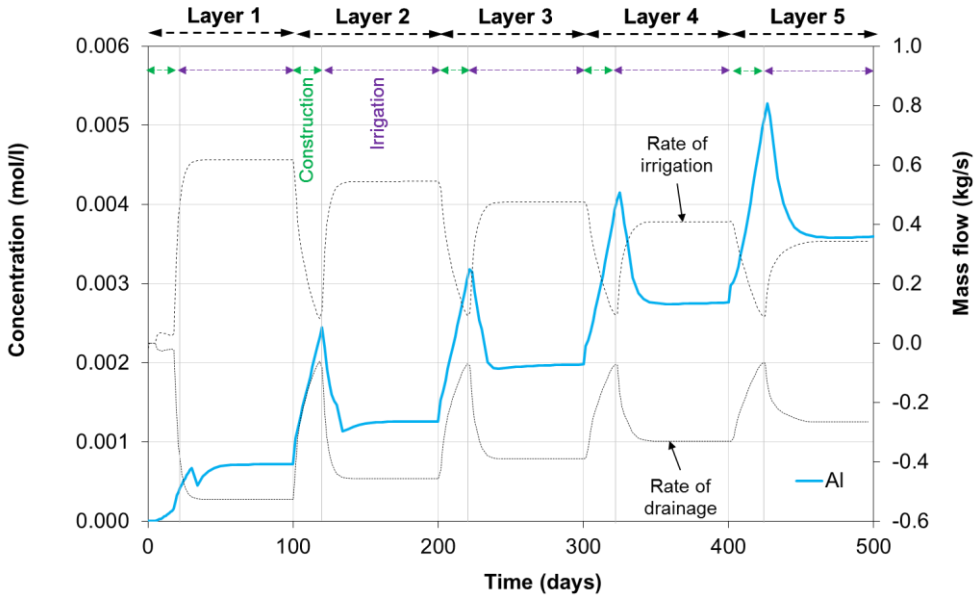

Figure 6.11: Chemical evolution of pH (a), Copper concentration (b), Silicon concentration (c) and Aluminum concentration (d) with respect to time in the drainage system outflow.

Primary copper ores like the chalcopyrite mineral is one of the main mineral where the copper is recovered. Figure 6.12 shows the evolution over time of chalcopyrite concentration. It can be observed how chalcopyrite is dissolved.

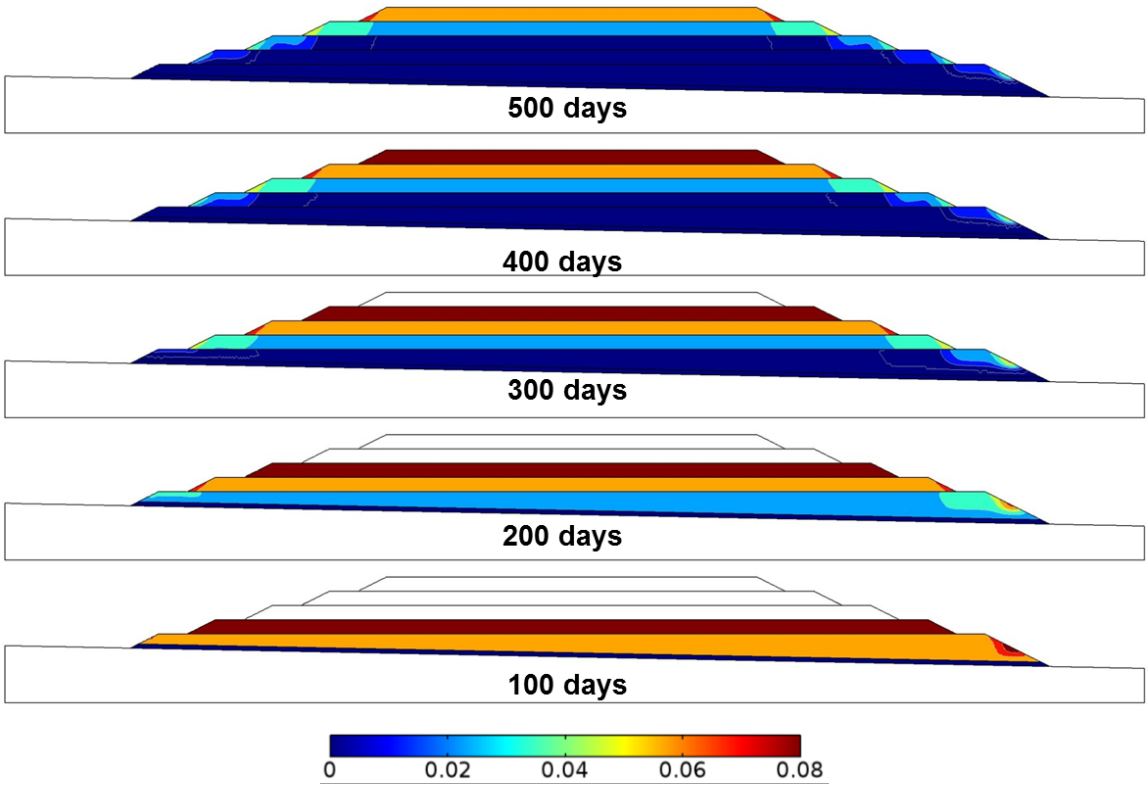

Figure 6.12: Evolution of chalcopyrite mineral for different times (volume fraction dimensionless).

Figure 6.13 presents a graph of mass copper recovered leaving the system through the drainage zone over time. The total mass of copper recovered for this simulation is equal to 2 280 kg per meter of pad the copper recovery of layer 3 has been of 700 kg per meter of pad. The recovered copper has been increased due to the leaching of residual mineral from previous layers. This effect depends on thickness of layers and irrigation time.

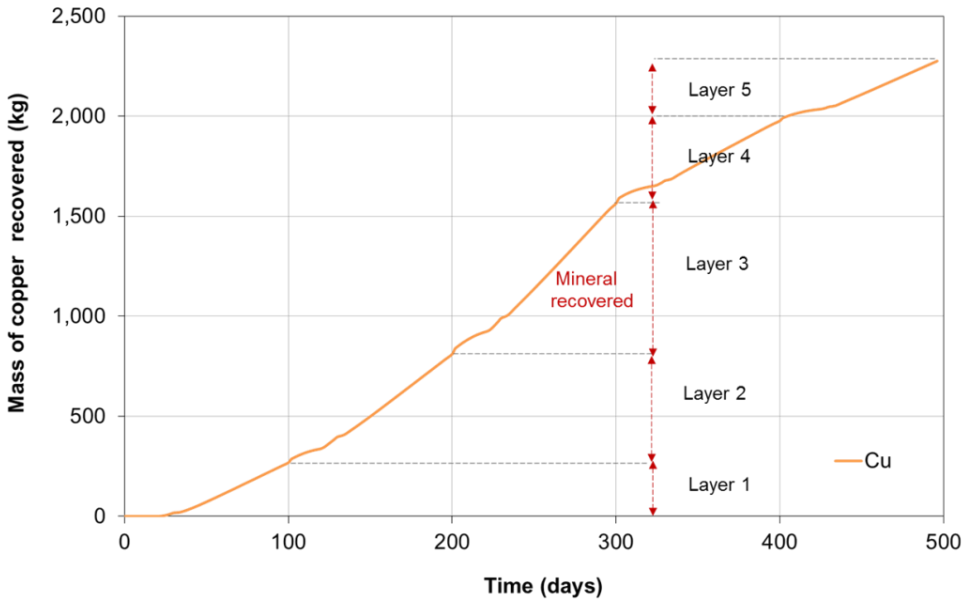

Figure 6.13: Mass of copper recovered at the exit over time per meter of pad.

6.5.7 Porosity changes

In Figure 6.14a and 6.14b, the changes of final mechanical and chemical porosity due to the mineral compaction and dissolution in the ore domain can be respectively observed. Note that porosity changes due to compaction are very small because compression index (λ) considered corresponds to a value for low compressibility. The only change over time which affects the volumetric strain is the increase of liquid pressure which only changes by loading and infiltration processes. These processes in this case are not relevant enough to provoke big displacements.

Global porosity only affects chemistry and hydrodynamics models. There is not coupling between the global porosity and the mechanical model. Considering that coupling is out of the scope of this work.

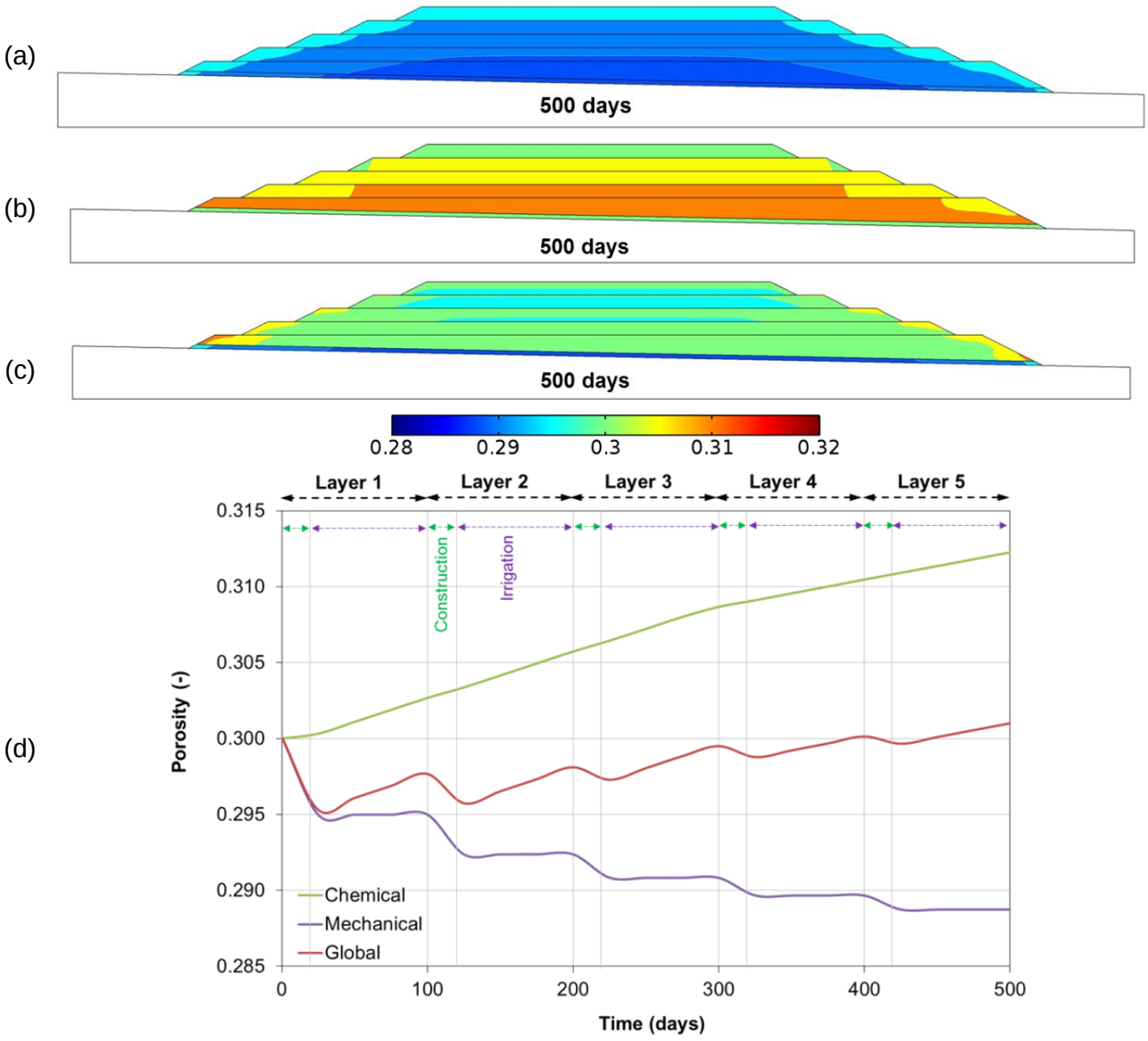

Figure 6.14: Final mechanical porosity (a), final chemical porosity (b), final global porosity (c), Temporal evolution of porosity (d).

6.5.8 Risk of soil collapse when wetting

We refer here to large settlements produced when wetting the pad. Unsaturated fill may collapse due to the suctions reduction.

Due to the difficulties obtained when attempting to implement the Barcelona Basic Model for unsaturated soils in COMSOL, a simplified “hand procedure” has been used to analyze the risk of soil collapse when wetting the behavior of a point located on the first layer is evaluated (see Figure 6.15). The information is taken from Figure 6.5 and Figure 6.9. The Barcelona Basic Model is considered to estimate the Loading Collapse curve (LC) which parameters is shown in Figure 6.15.

To analyze the risk of soil collapse, Figure 6.15 shows point “A” representing initial conditions. Then when the construction of the first layer is concluded the point is located on “B”. After that the first layer is irrigated, which produces a suction reduction to zero, moving to point “C”. The same process is repeated for next layers.

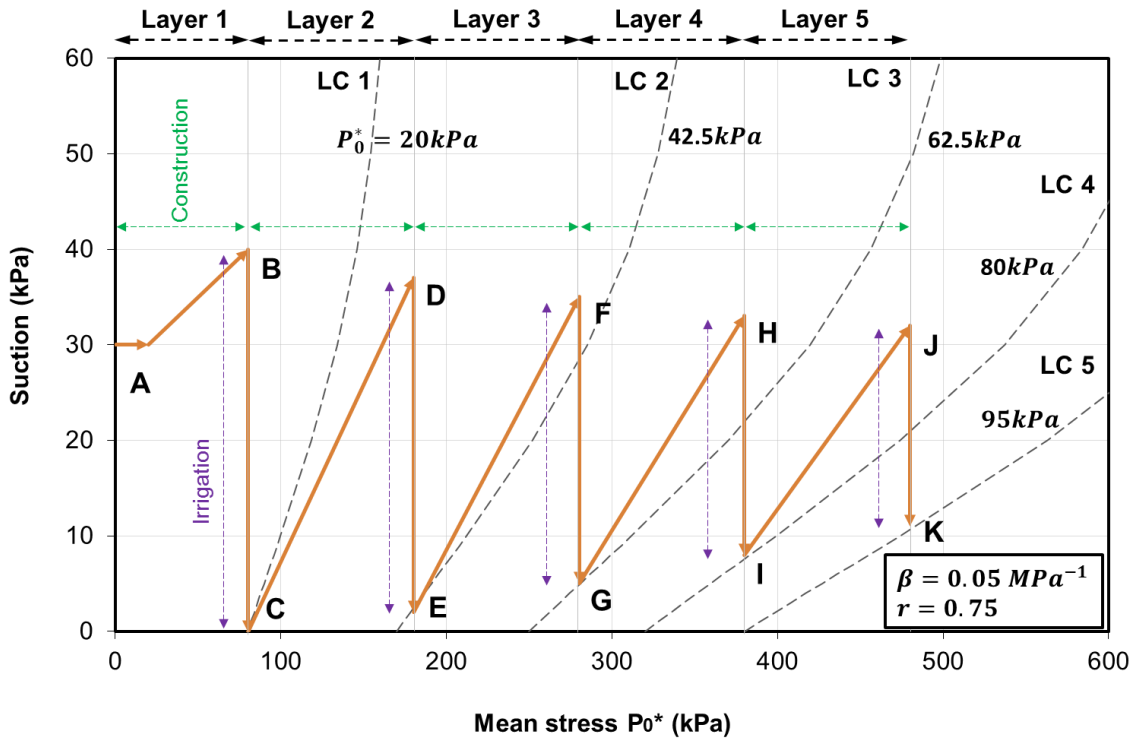

Figure 6.15: the soil collapse path developed during the simulated construction and operation

Figure 6.16 shows an example of soil collapse in a heap leach pad. Some indirect measurements by surveying indicate that collapse can be very small (under 1 or 2% of the depth of the lift) for hard competent ore, and much higher (>5%) for softer ores and those with higher fines content; for very fine laterite ores it might be 10% (Mark, 2013).

Figure 6.16: A case of soil collapse in heap leach pad (Anddes, 2012).

7.0 CONCLUSIONS AND RECOMMENDATIONS

Coupled hydromechanical and geochemical phenomena have been simulated in this work in the context of mining industry. The main aim of working such a complex hydrodynamics, mechanical and chemical problem has been to improve the understanding of a heap leach pad behavior.

Despite the importance of this type of analyses, the works published on this topic are scarce, probably due to the difficulties in taking into account all couplings.

The simulation has been carried out by the coupling of two standalone codes: COMSOL Multiphysics (which develops the geomechanical, the hydrodynamics part and the conservative solute transport part) and PHREEQC (which performs the geochemical reactive simulations).

The following conclusions can be drawn from this study:

- The proposed numerical tool allows integrating in a single framework hydromechanical and geochemical coupled phenomena and the processes involved in the construction and operation of heap leach pads.

- Although the simulation case has been restricted to five heap ore layers, simulation total time has been short (500 days) and parameter values used have been chosen arbitrarily, the illustrative example reported in this work shows that it is feasible to simulate the behavior of the ore leaching in a leach pad taking into account such coupled phenomena.

- It is possible to use the proposed numerical model in order to assess the risk of soil collapse during the construction and operation pad.

- The irrigation time plays an important role in the system behavior. This is due to the influence of irrigation on the liquid pressure and mass of recovered mineral.

- A better understanding of the relevant processes when designing a heap leach pad is needed, particularly on hydro-geochemical processes, coupled to the geo-mechanical aspects. Laboratory information on some parameters required in the simulations is not available yet and an effort should be developed in the near future to avoid this drawback.

- Mineral production is very sensitive to the number and thickness of layers. As abovementioned, it is also sensitive to the time of irrigation.

- For the case considered, it resulted that after 90 days of irrigating each layer, the copper recovery is greater at layer 3, when comparing the production between the 5 layers built. This is because irrigation on layer 3 also recovers residual mineral from previous layers.

- Some concentration of copper remains in the pad close to the slope limits, because irrigation is not very effective on those zones. Ideally those zones could be exploited as well.

- Construction process also plays an important role on the evolution of pore liquid pressure. Undrained pore liquid pressures are difficult to generate when loading because of the unsaturated state of the ore, but construction time of each layer influences the hydraulic response of the pad.

- This work proposes a tool for management of the three relevant features of heap leach pads: the engineering studies, the construction and the operation processes. The numerical model also illustrates that significant changes in porosity, due to mineral dissolution, can cause significant changes in the mechanical and hydrodynamics performance of the heap leaching and therefore they may compromise its long-term stability. The simulated example shows that the porosity due to chemical effects in the ore layer increases (up to 4%) mainly due to the dissolution of silicates. Changes of porosity due to mechanical effects may compensate this increment.

The following recommendations can be drawn from this study

- A better understanding of the ore material from a geomechanical point of view is required. As a proposal, at least some oedometer tests with suction control should be carried out to obtain the corresponding mechanical parameters. Additionally, some strength experiments (direct shear or triaxial with suction control) could be carried out. Obviously, the grain size distribution of the ore constitutes a challenge on this work. Changes on the mechanical parameters during the chemical evolution of the ore could be determined as well, by testing the material at different stages of the process.

- To get an accurate control, it is recommended to monitor the different variables that are involved in the construction and operation of the pad.

- The rate of irrigation and the irrigation time seems to be very important regarding production characteristics of the pad. Therefore, a sensitivity analysis on this variable could be performed using this numerical model.

- A fully coupling of the chemical and mechanical porosity could be developed in the framework of an elastoplastic model. Cam-clay has been just an initial step and the use of further models including the unsaturated behaviour should be attempted.

8.0 FUTURE WORKS

The analyses of heap leaching pads using coupled HMC formulations are scarce and usually they use staggered approaches or not fully coupled formulations. This work is a preliminary attempt in this direction. Future works may include some of the following topics:

- Improve the mechanical description of the ore by using a model for unsaturated soils, Barcelona Basic Model could be a good starting point, but a model more appropriate for the ore should be finally adopted.
- The stability analysis must be studied to design the pad for earthquake conditions, because it is critical in many places.
- To assess the risk of static liquefaction on heap leach pads.
- Energy conservation should be considered. Chemical reactions induce temperature changes and the influence of this effect is not well known.
- An Analysis 3D could be performed for a more realistic approach.

9.0 REFERENCES

Alonso, E. E., Gens, A., & Josa, A. (1990). A constitutive model for partially saturated soils. *Géotechnique,* 40(3), 405-430.

Amphos21 Consulting S.L. **(2013).** Personal communication: unpublished, Spain, Barcelona.

Anddes Asociados S.A.C. (2013) Personal communication: unpublished, Peru, Lima.

Bea Jofré S. A., Carrera J., Ayora C., Batlle F., Jan Slooten L., Saaltink M. (2008) .CHEPROO (CHEmical PRocesses Object-Oriented) A User's Guide, UPC, Barcelona.

Biot M.A. (1956). General solutions of the equations of elasticity and consolidation for a porous material. *Journal of Applied Mechanics*, 23(1), 91-96.

Breitenbach A. J. (1999). The good, the bad, and the ugly lessons learned in the design and construction of heap leach pads. *Society of Manufacturing Engineers, Copper Leaching, Solvent Extraction, and Electrowinning Technology (USA),* pp. 139-147.

Brinkgreve R.B.J., & Bakker H.L. (1991). Non-linear finite element analysis of safety factors. *Proc. 7th Int. Conf. on Comp. Methods and Advances in Geomechanics*, Cairns, Australia, 1117-1122.

Brooks R. H., & Corey A. T. (1964). Hydraulic properties of porous, *Hydrology Papers*, Colorado State University.

Carman P.C. (1937). Fluid flow through granular beds. *Transactions-Institution of Chemical Engineers*, 15, 150-166.

Charlton S. R., & Parkhurst D. L. (2011). Modules based on the geochemical model PHREEQC for use in scripting and programming languages, *Computers & Geosciences*, 37(10), 1653-1663.

Chen W.F., & Mizuno E. (1990). *Nonlinear analysis in soil mechanics: theory and implementation (Developments in Geotechnical Engineering*, 3er ed., Elsevier Science.

COMSOL, (2011a). COMSOL Multiphysics Version 4.2a (www.comsol.com).

Decker, D. L., & Tyler, S. W. (1999). Hydrodynamics and solute transport in heap-leach mining. *Closure, remediation and management of precious metals heap-leach facilities*. *Univ. of Nevada, Reno*, 1-13.

Fredlund, D. G., Morgenstern, N. R., & Widger, R. A. (1978). The shear strength of unsaturated soils. *Canadian Geotechnical Journal,* 15(3), 313-321.

Guimarães, L., Gens, A., & Olivella, S. (2002). Modelling the geochemical behaviour of an unsaturated clay subjected to heating and hydration. *In Proc. 3rd Int. Conf. on Unsaturated Soils* (pp. 71-76).

Kappes, D. W. (2002). Precious metal heap leach design and practice. *Proceedings of the Mineral Processing Plant Design, Practice, and Control,* 1, 1606-1630.

Krahn, J. (2004). Stress and deformation modeling with SIGMA/W, *an engineering methodology. GEO-SLOPE International Ltd., Calgary, Alberta*.

Krahn, J. (2004). Transport Modeling with CTRAN/W: *an engineering methodology. GEO-SLOPE International Ltd., Calgary, Canada.*

Lichtner, P. C. (1985). Continuum model for simultaneous chemical reactions and mass transport in hydrothermal systems. *Geochimica et Cosmochimica Acta,* 49(3), 779-800.

Liu, J., & Brady, B. H. (2004). Simulations of a coupled hydro-chemo-mechanical system in rocks. *Geotechnical & Geological Engineering*, 22(1), 121-133.

Smith M.E. (2013). Personal communication, unpublished.

Mata, C., Guimarães, L. D. N., Ledesma, A., Gens, A., & Olivella, S. (2005). A hydro-geochemical analysis of the saturation process with salt water of a bentonite crushed granite rock mixture in an engineered nuclear barrier. *Engineering geology*, 81(3), 227-245.

Mohajeri, A., Muhlhaus, H., Gross, L., & Baumgartl, T. (2011). Coupled Mechanical-Hydrological-Chemical Problems in Elasto-plastic Saturated Soils and Soft Rocks Using escript. *In Advances in Bifurcation and Degradation in Geomaterials (pp. 269-275).* Springer Netherlands.

Nardi, A., Trinchero, P., de Vries, L., Idiart, A., & Molinero, J. (2012). Coupling multiphysics with geochemistry: The COMSOL-PHREEQC interface. *In COMSOL Conference, October.*

Pacheco P.G. M., Purizaga, M., Huertas, J., Romanel, C. (2011). Flow analysis and dynamic slope stability in a copper ore heap leach, *Geotechnical Conference*, 7.

Palandri J. L., & Kharaka Y. K. A. (2004). Compilation of rate parameters of water-mineral interaction kinetics for application to geochemical modeling, *Tech. rep. / U. S. Geological Survey Open File Report 2004-1068*.

Parkhurst, D. L. en CAJ Appelo, (1999). User's guide to PHREEQC (version 2)-a computer program for speciation, batch-reaction, one-dimensional transport and inverse geochemical calculations. *Water-Resources Investigations Report,* 99-4259.

Potts, D. M., & Zdravković, L. (1999). *Finite Element Analysis in Geotechnical Engineering: Theory* (Vol. 1), 304-310,Thomas Telford Services Limited.

Saaltink, M. W., Ayora, C., & Carrera, J. (1998). A mathematical formulation for reactive transport that eliminates mineral concentrations. *Water Resources Research,* 34(7), 1649-1656.

Saaltink, M. W., Carrera, J., & Ayora, C. (2001). On the behavior of approaches to simulate reactive transport. *Journal of Contaminant Hydrology*, 48(3), 213-235.

Saaltink, M. W., Domenech, C., Ayora, C., & Carrera, J. (2002). Modelling the oxidation of sulphides in an unsaturated soil. *Geological Society, London, Special Publications,* 198(1), 187-204.

Smith, M. E., & Giroudt, J. P. (2000). Influence of the Direction of Ore Placement on the Stability of Ore Heaps on Geomembrane-Lined Pads. *Slope Stability in Surface Mining,* 435.

Smith, W. R., & Missen, R. W. (1982). *Chemical reaction equilibrium analysis: theory and algorithms* (pp. 204-13). New York: Wiley.

Steefel C. I., & MacQuarrie K. T. (1996). Approaches to modelling reactive transport in porous media. Reviews in Mineralogy and Geochemistry, 34(1), 85-129.

Terzaghi, V. K. (1936). The shearing resistance of saturated soils and the angle between the planes of shear. *In Proceedings of the 1st International Conference on Soil Mechanics and Foundation Engineering*, Vol. 1, pp. 54-56.

Thiel, R., & Smith, M. E. (2004). State of the practice review of heap leach pad design issues. *Geotextiles and Geomembranes*, 22(6), 555-568.

Timoshenko, S., & Goodier, J. N. (1951). *Theory of elasticity*. New York, 412.

Van Genuchten, M. T. (1980). A closed-form equation for predicting the hydraulic conductivity of unsaturated soils. *Soil Science Society of America Journal,* 44(5), 892-898.

Williamson, M. A., & Rimstidt, J. D. (1994). The kinetics and electrochemical rate-determining step of aqueous pyrite oxidation. *Geochimica et Cosmochimica Acta,* 58(24), 5443-5454.

Wissmeier, L., & Barry, D. A. (2011). Simulation tool for variably saturated flow with comprehensive geochemical reactions in two-and three-dimensional domains. *Environmental Modelling & Software*, 26(2), 210-218.

Wood, D. M. (1990). *Soil behaviour and critical state soil mechanics*. Cambridge university press.

Annex A – Brief description of the problem implementation in COMSOL

In this annex, the procedure to set an analysis HMC by COMSOL is described.

COMSOL has a tree structure that organizes the different analysis. The used information is shown in the next pictures:

GENERAL INFORMATION

Parameters

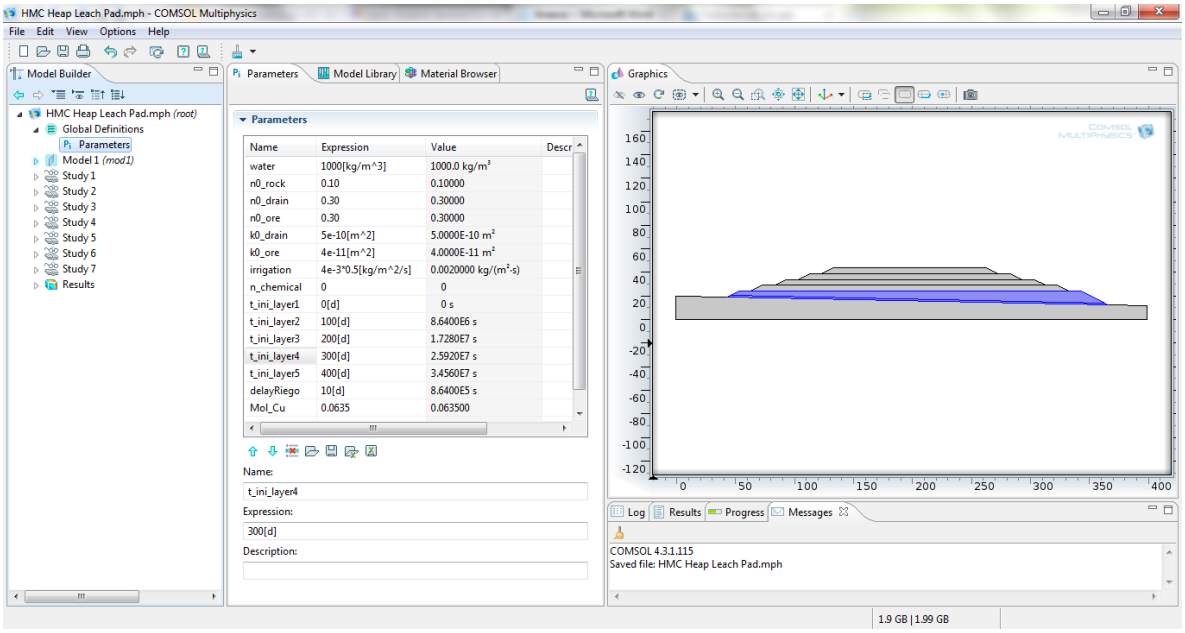

The model

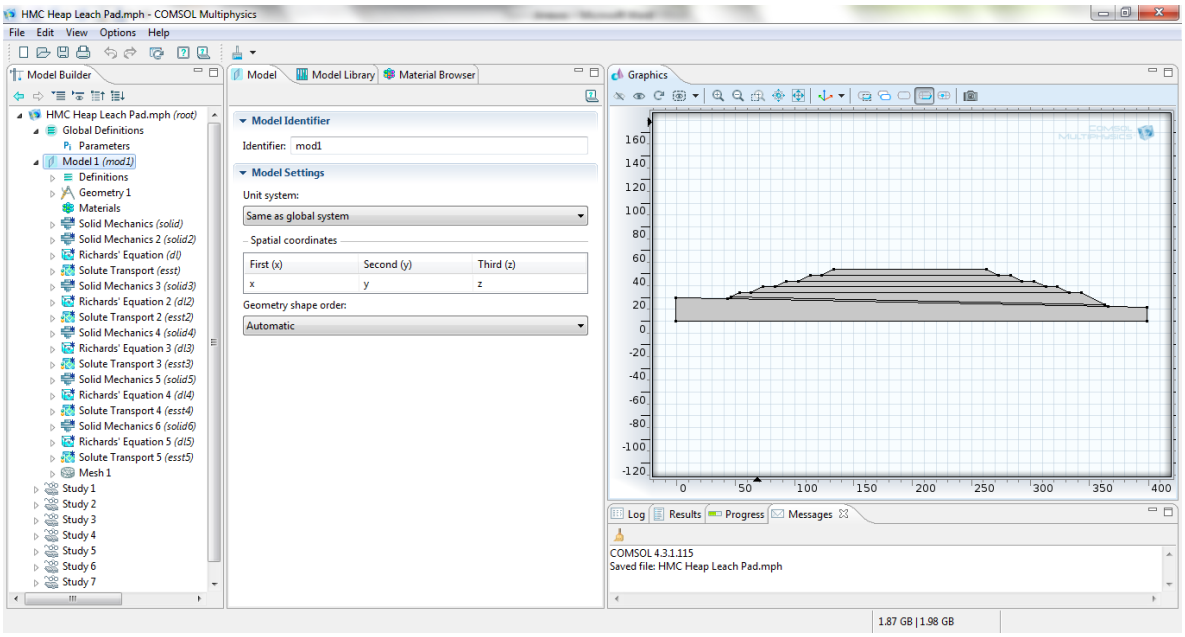

The definitions of each domain is defined for the different properties.

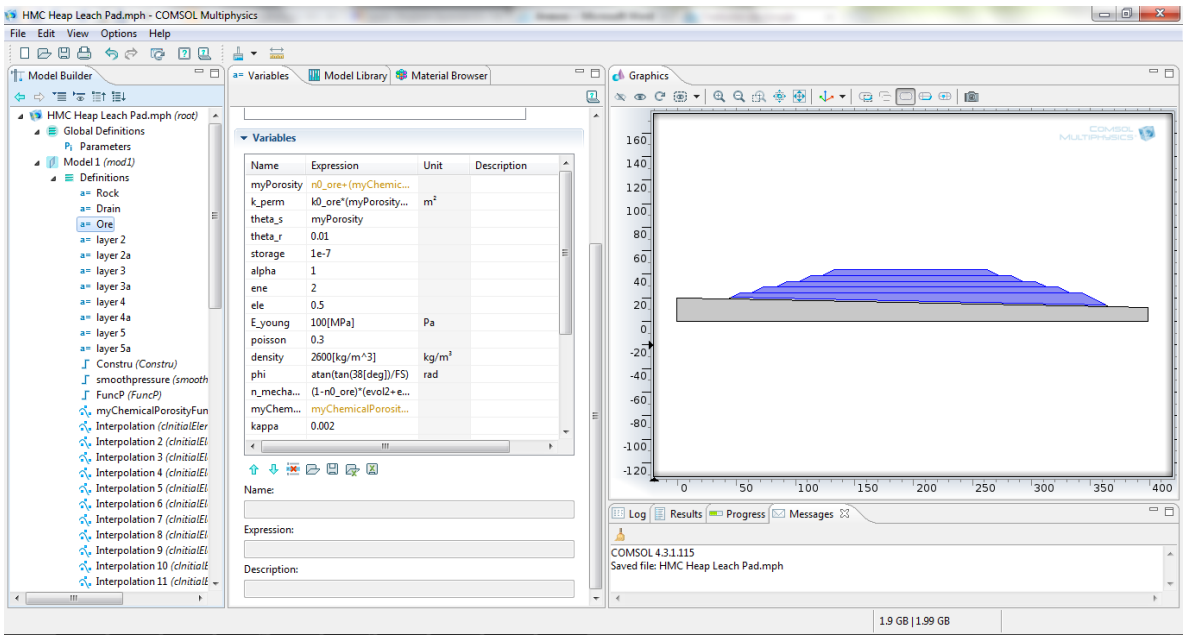

The geometry is imported from an AutoCAD file

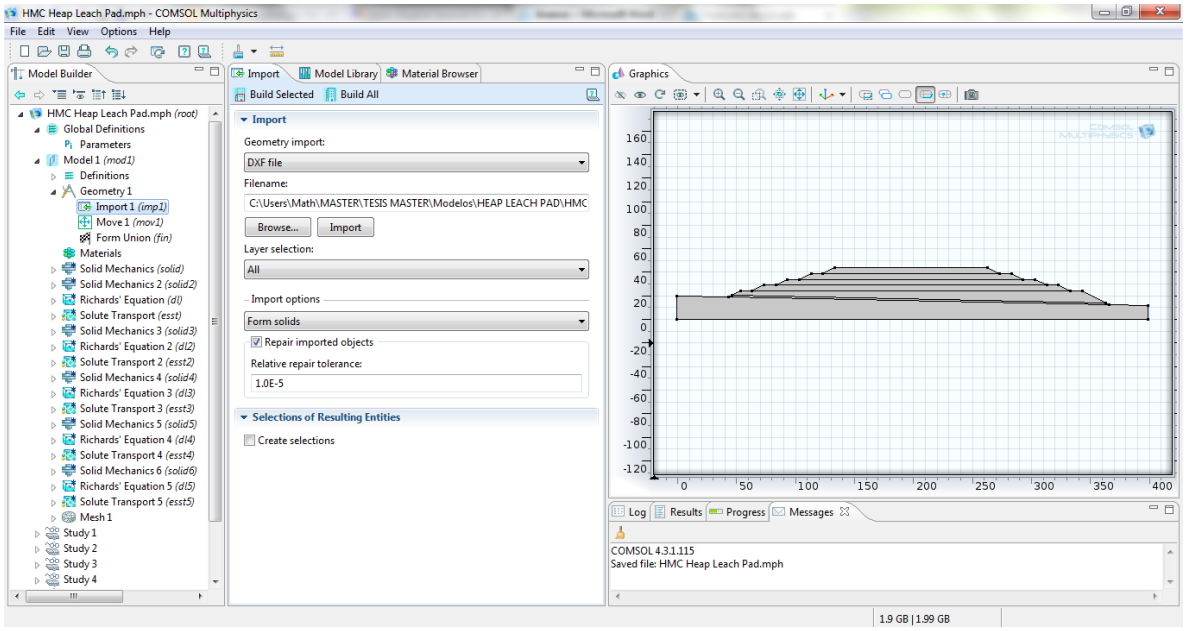

MECHANICAL ANALYSIS

The first domain (blue shaded zone) represents a rock (Solid Mechanics).

Lineal elastic model was used

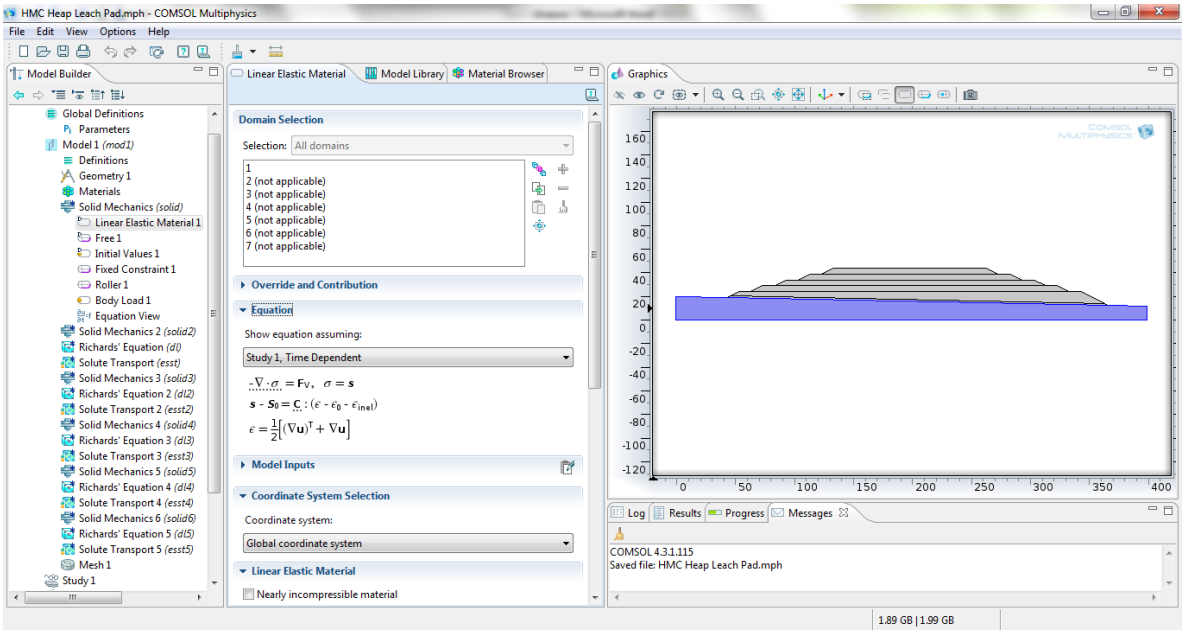

Free boundary to displacement (blue line)

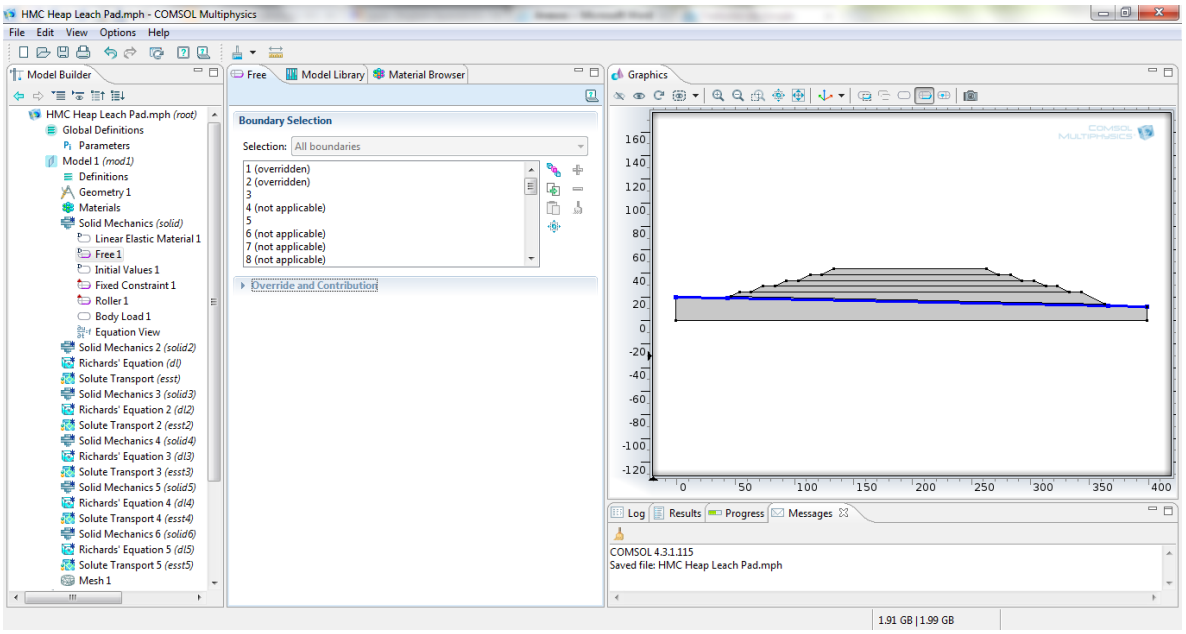

Initial values (blue shaded zone)

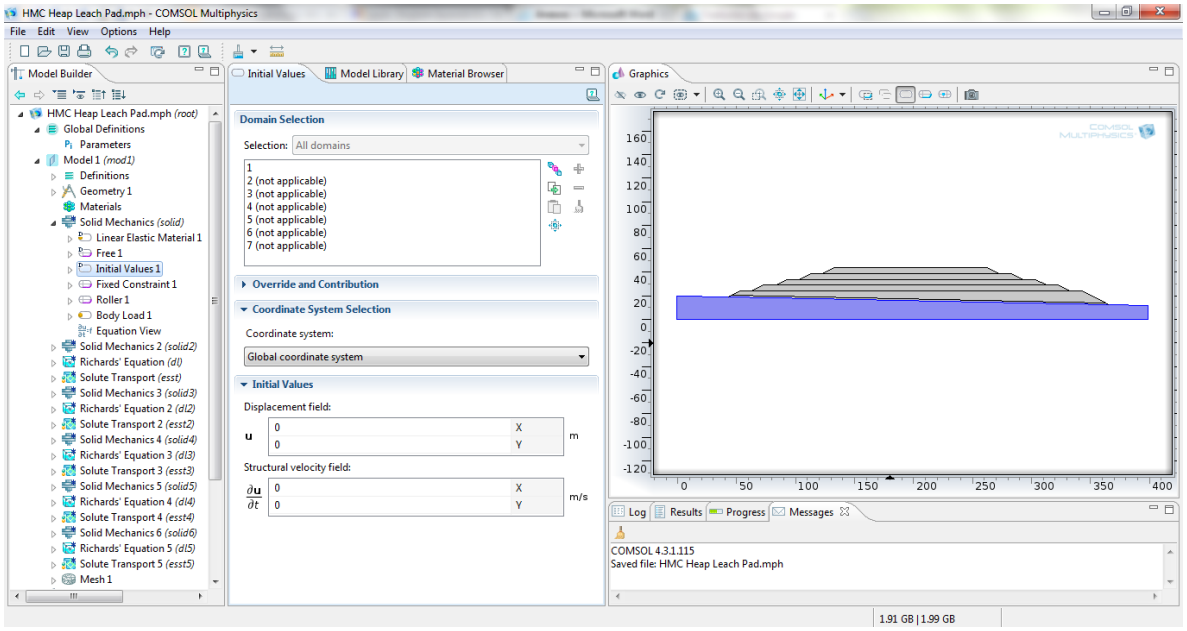

Fixed condition (blue line)

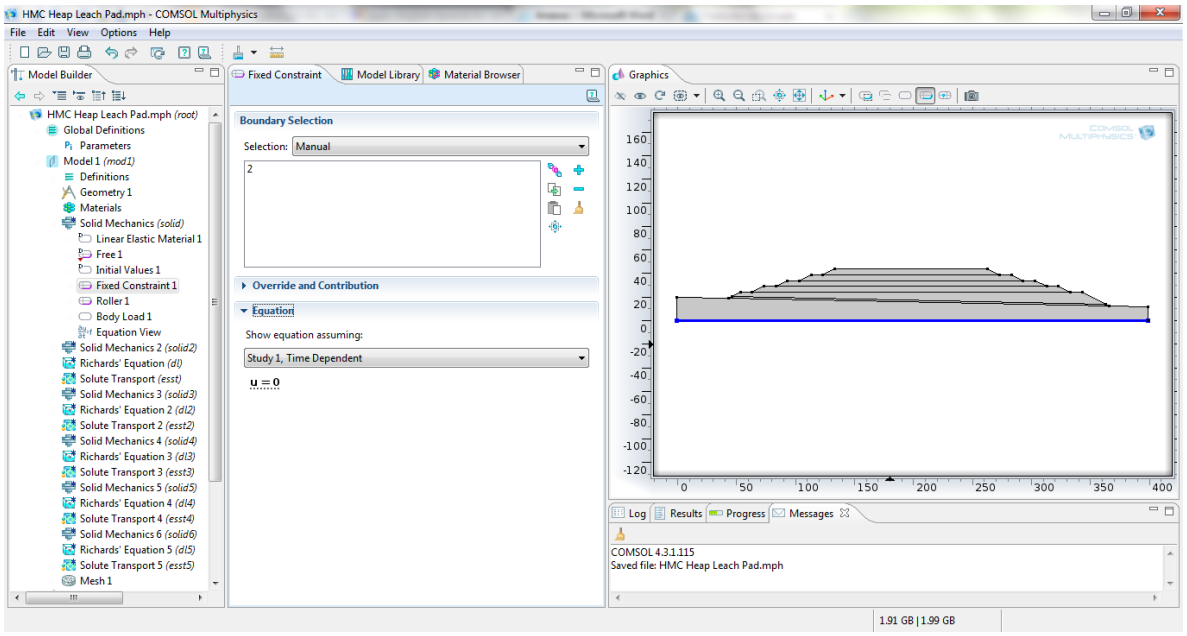

Fixed conditions to displacement horizontal (blue line)

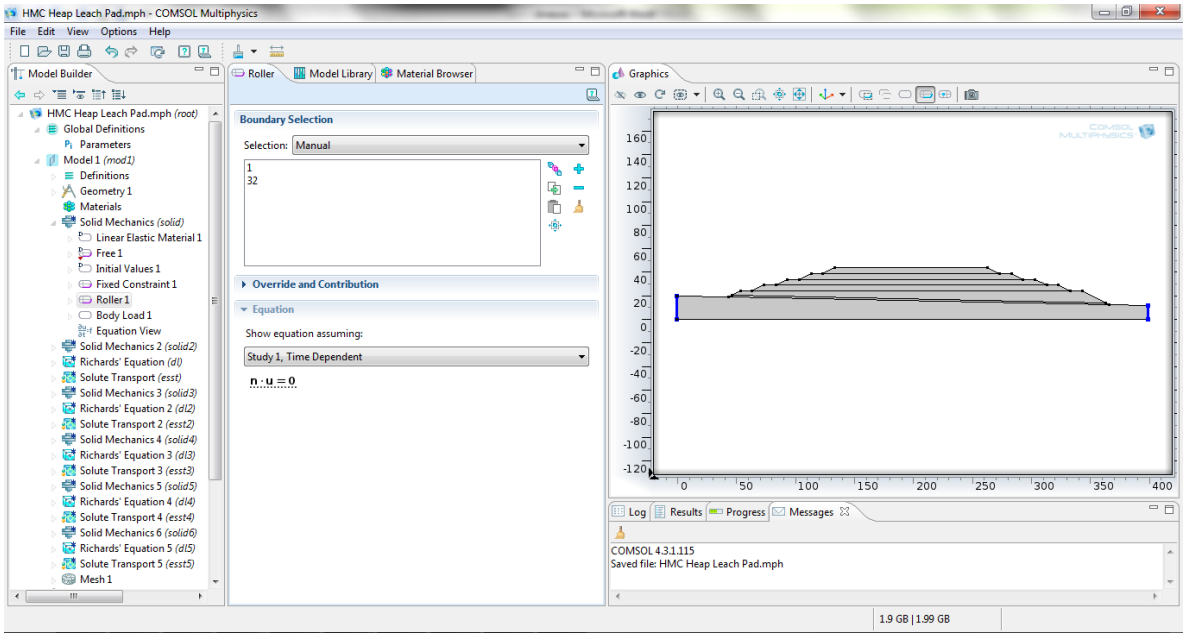

Body load for rock (blue shaded zone).

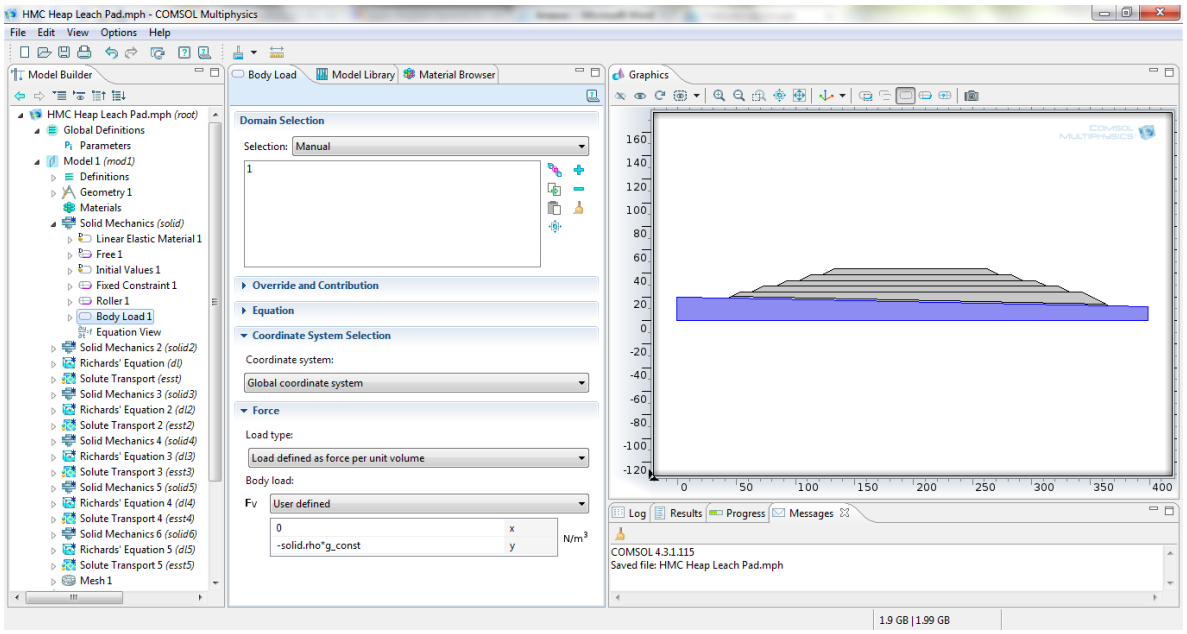

The second domain (blue shaded zone) represents an ore layer (Solid Mechanics 2).

Cam-Clay model is used (Solid Mechanics 2)

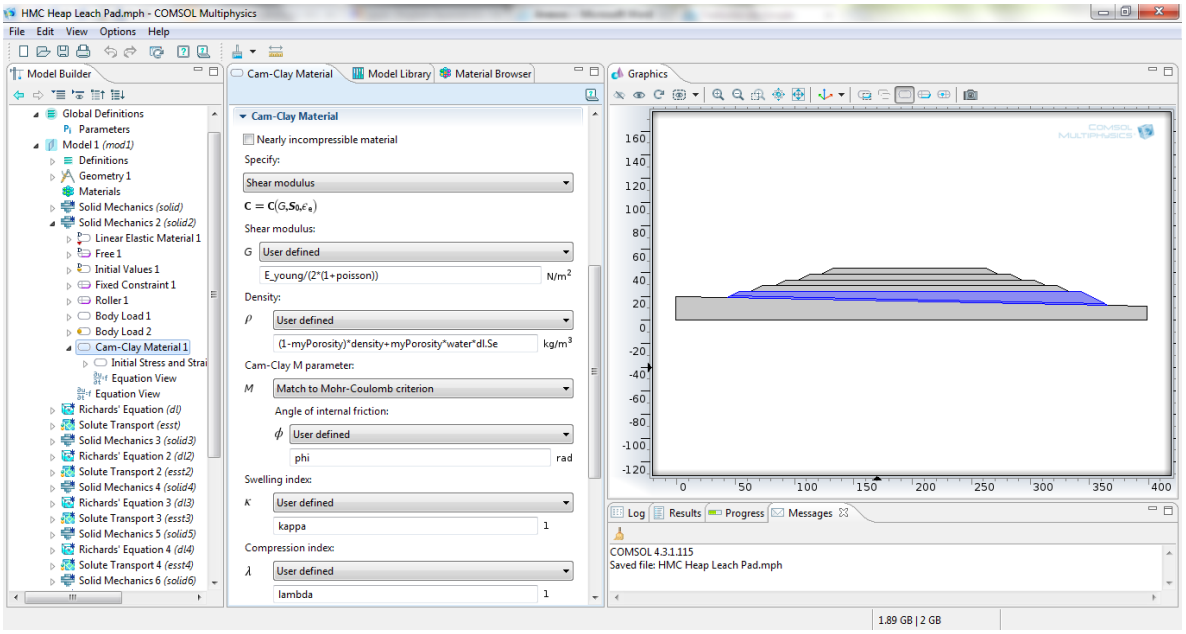

Body load for ore (blue shaded zone)

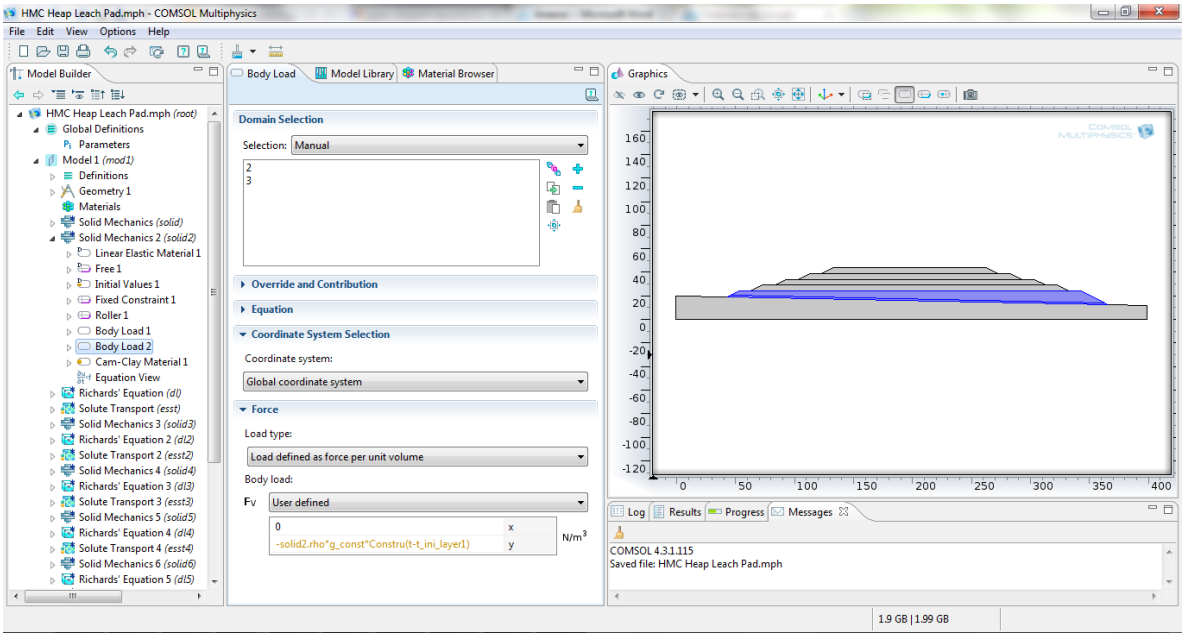

FLOW ANALYSIS

The second domain (blue shaded zone) represents an ore layer (Richard's equation).

Richard's equation is used.

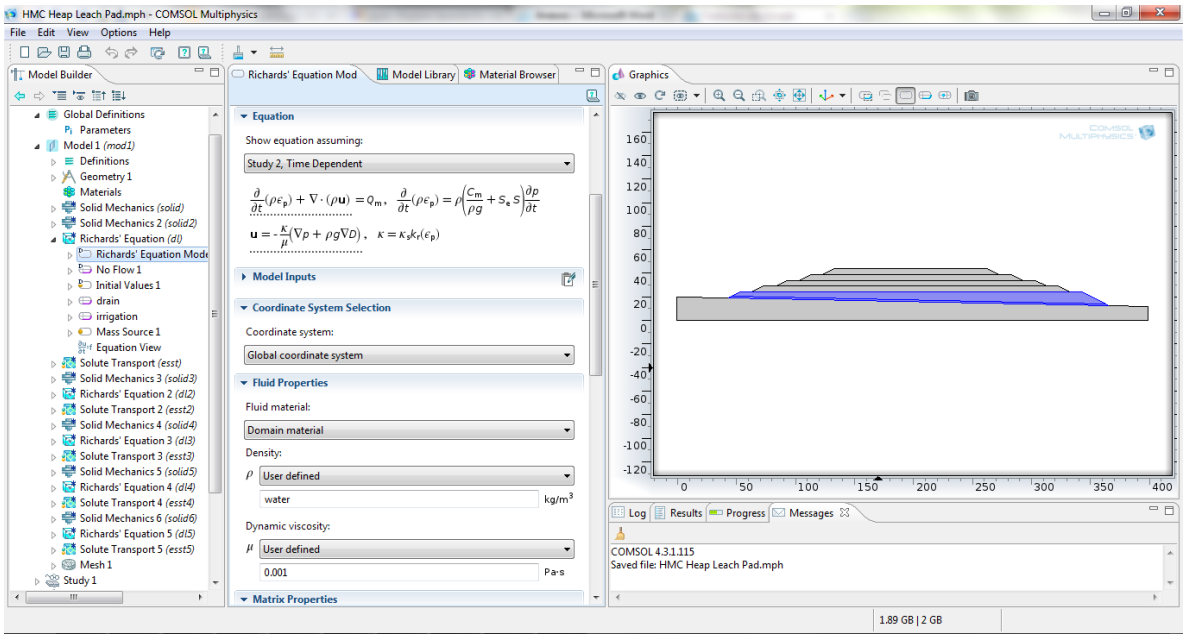

Non-flow boundary (blue line)

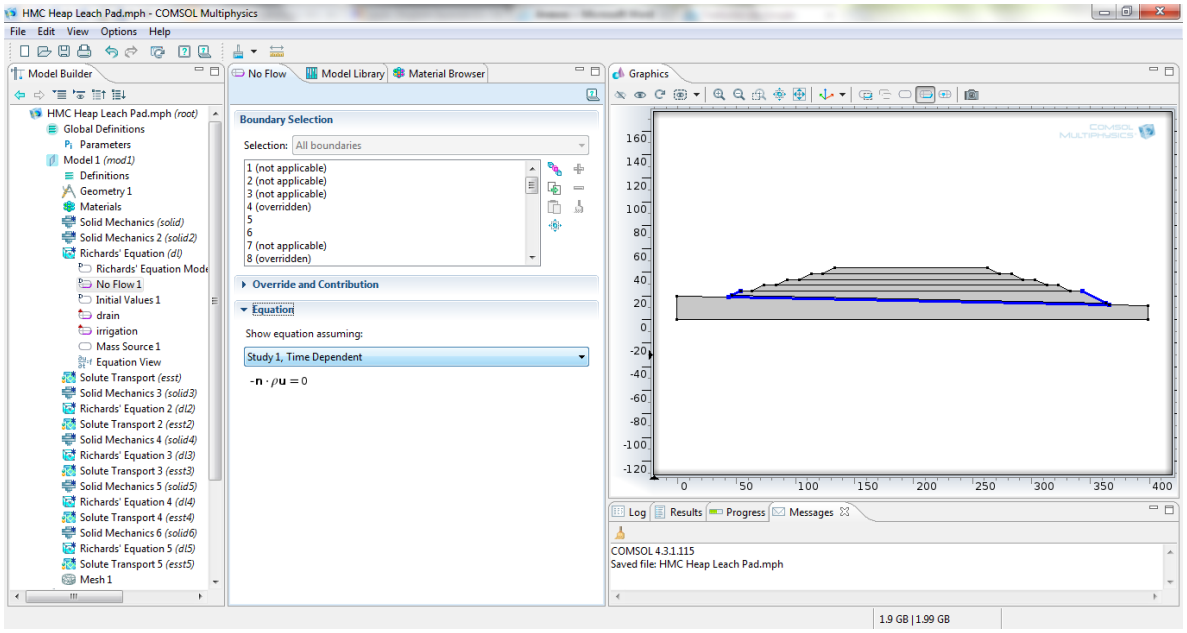

Initial values (blue shaded zone)

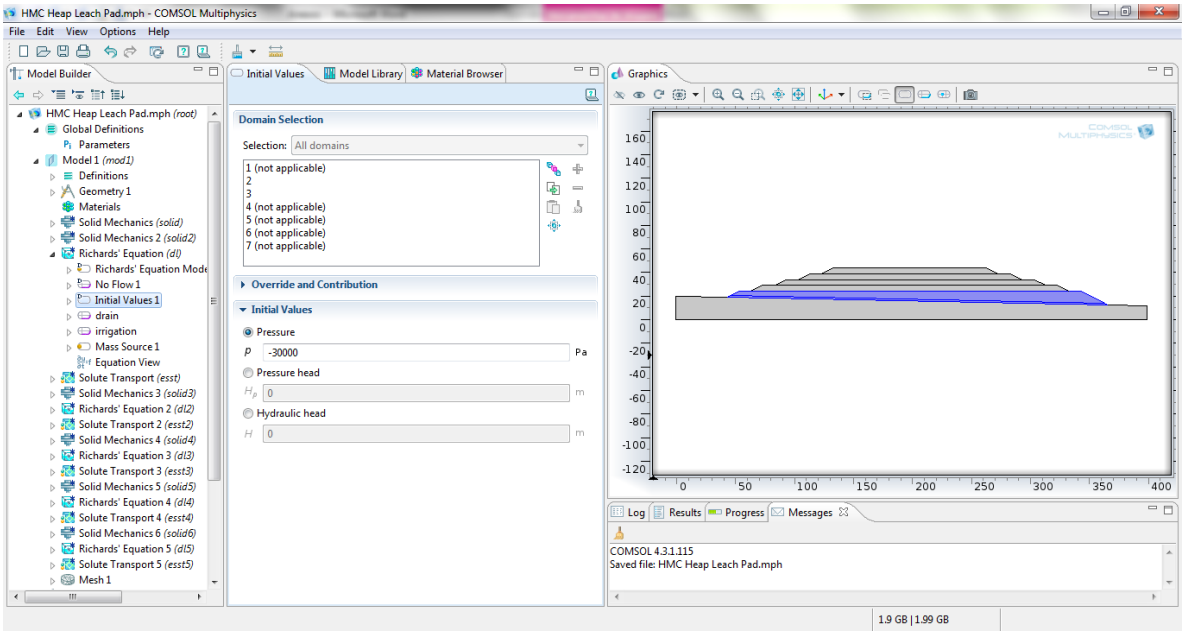

Mixed condition for drainage (blue line)

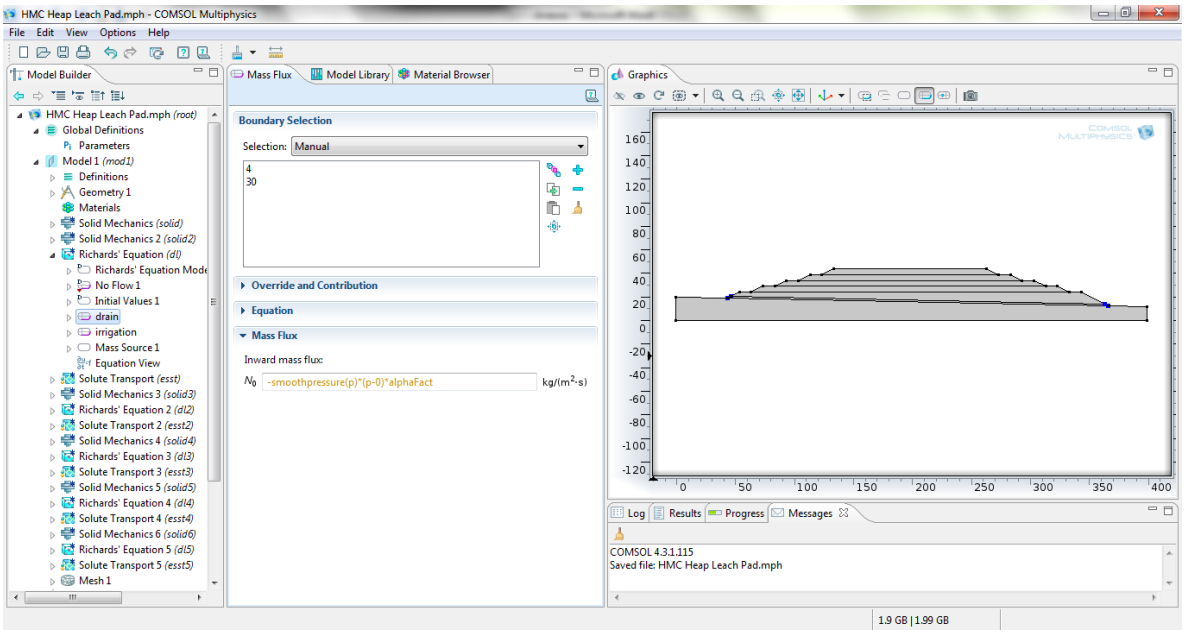

Inflow condition (blue line)

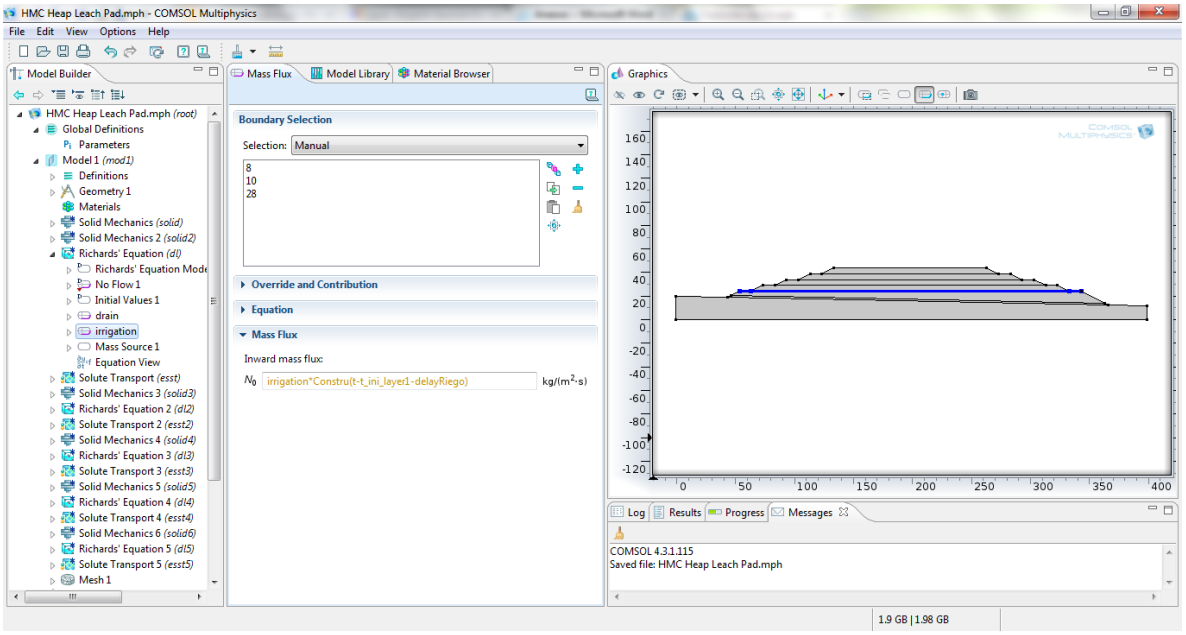

Coupling term (blue shaded zone)

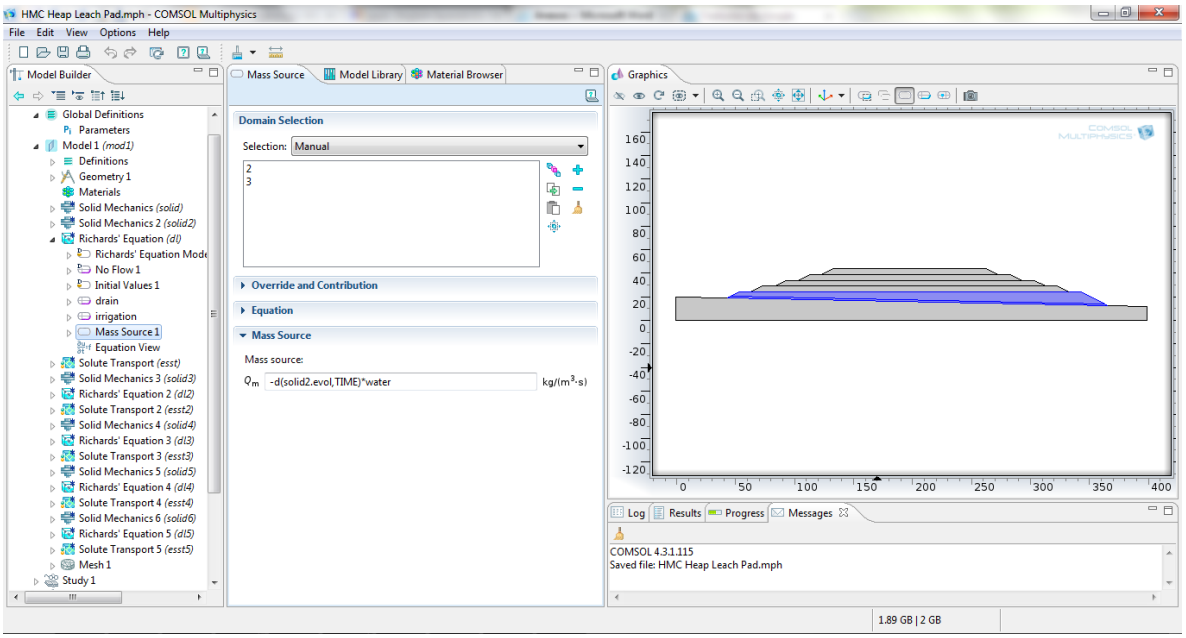

SOLUTE TRANSPORT ANALYSIS

The second domain (blue shaded zone) represents an ore layer (Solute Transport).

Conservative equation is used.

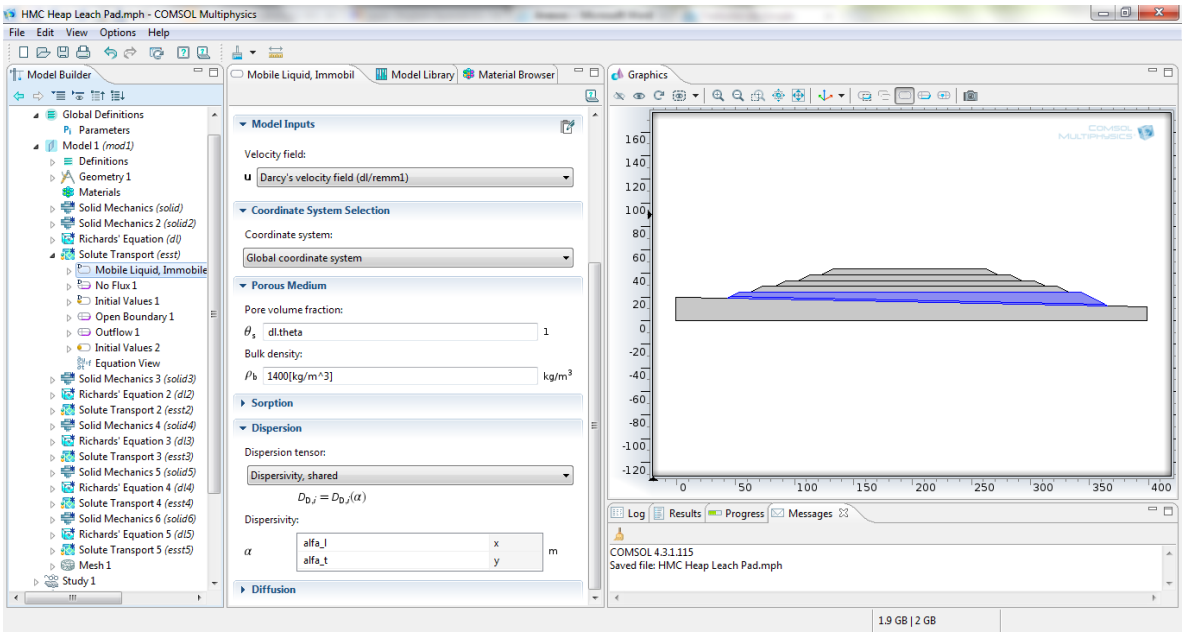

Non-flux condition (blue line)

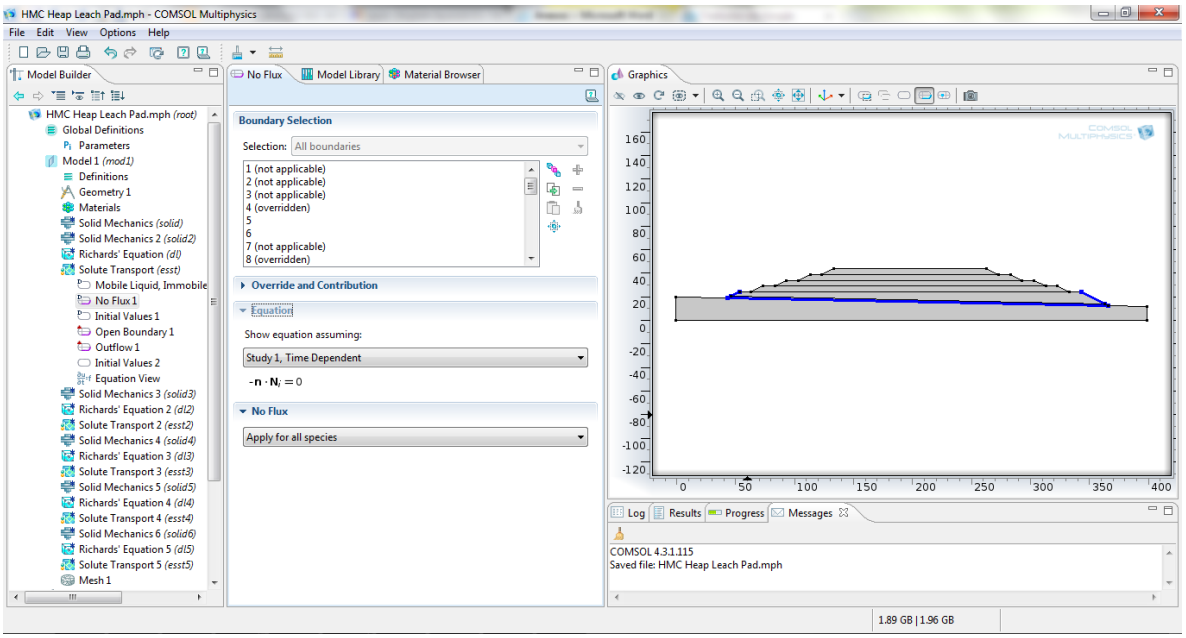

Initial values of concentration (blue shaded zone)

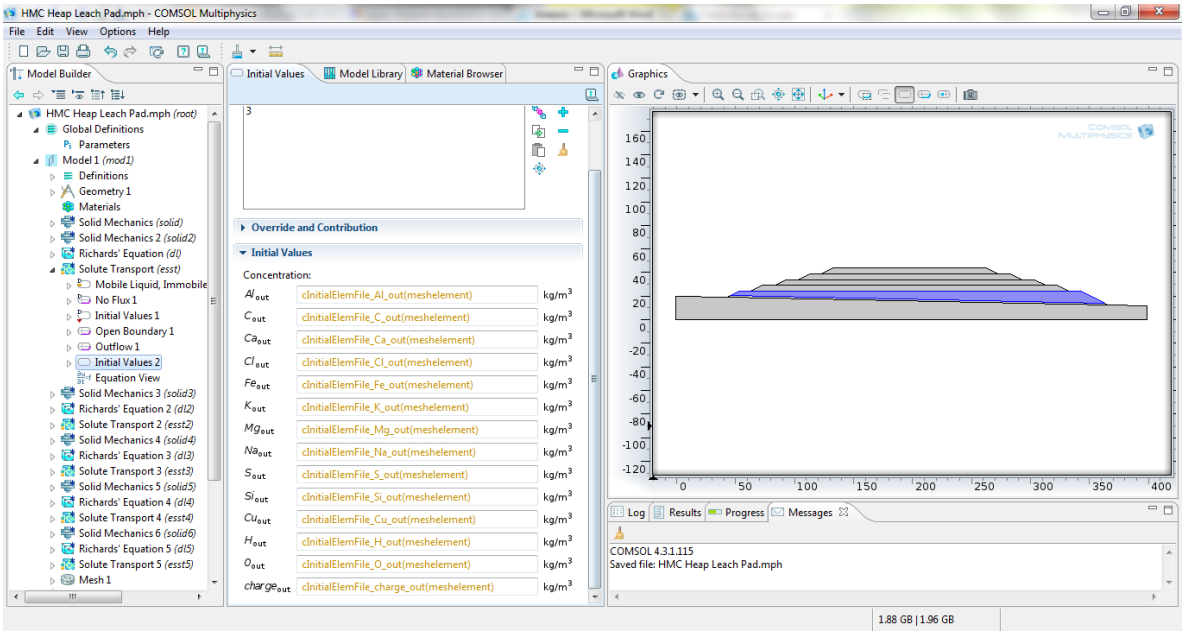

Inflow condition of concentration (blue line)

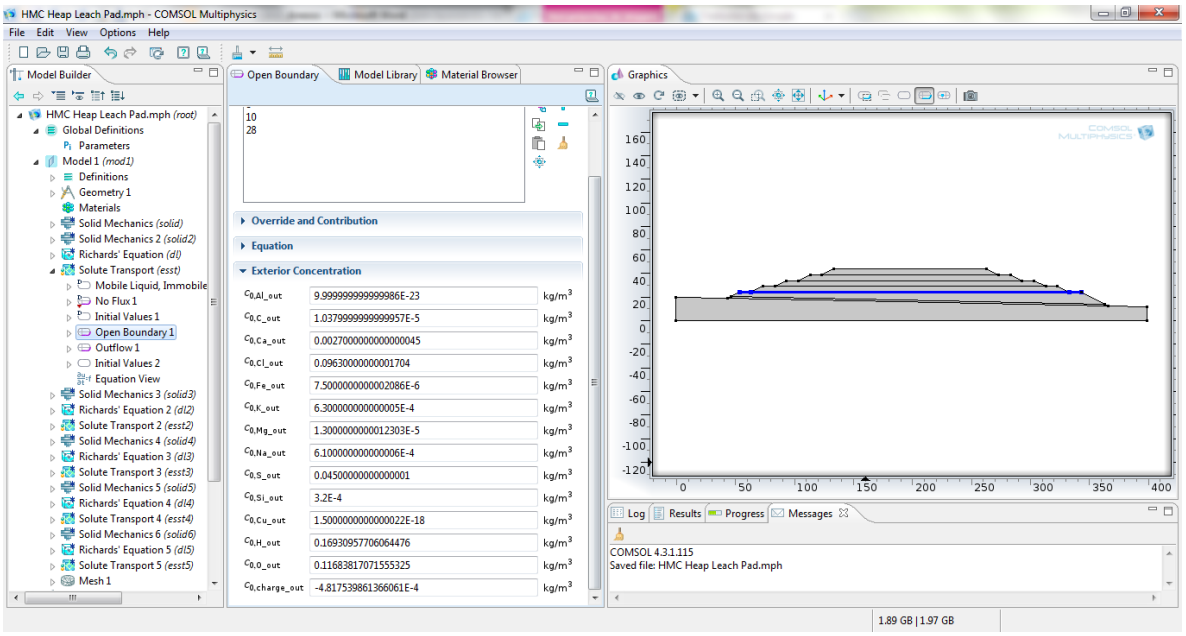

Outflow condition of concentration (blue line)

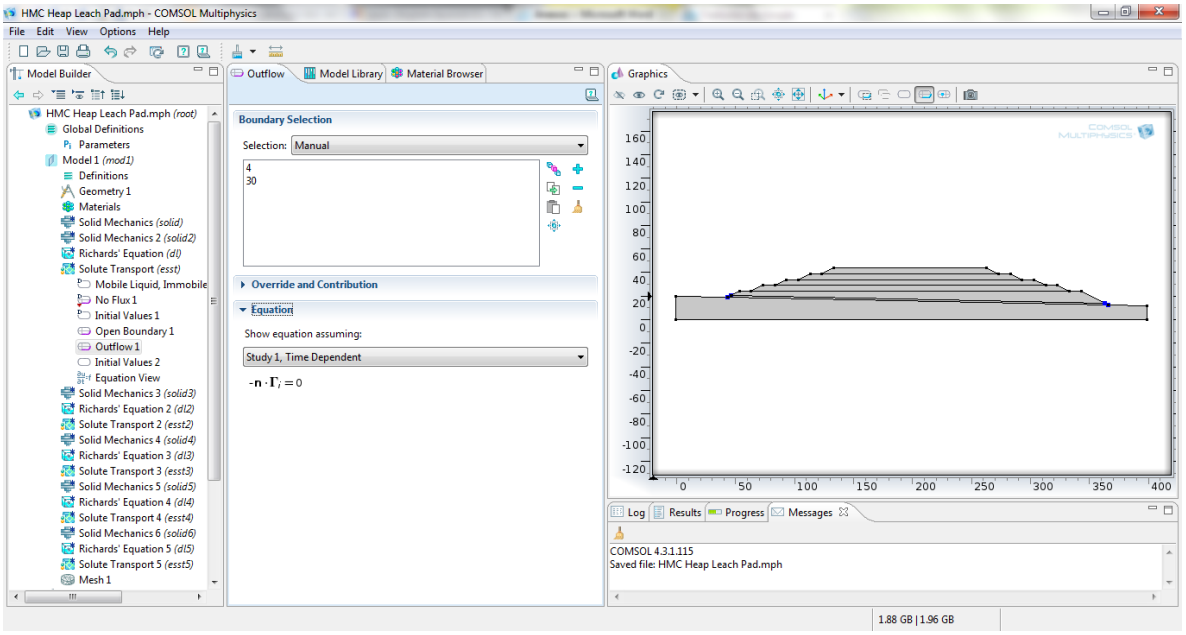

Meshing

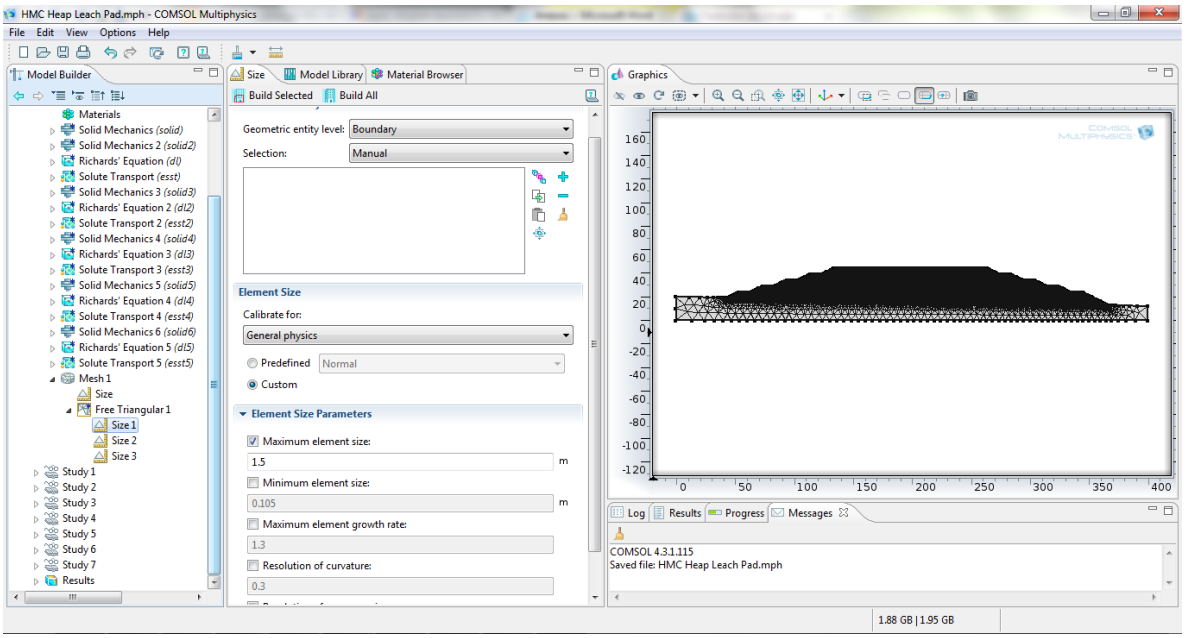

Study time

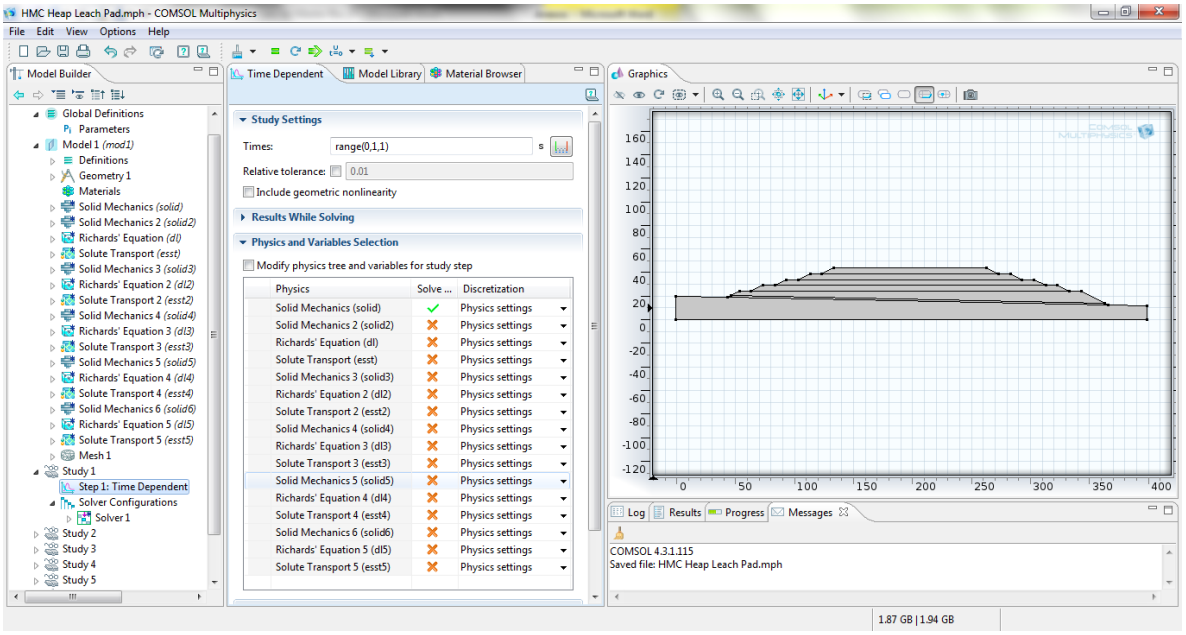

Results

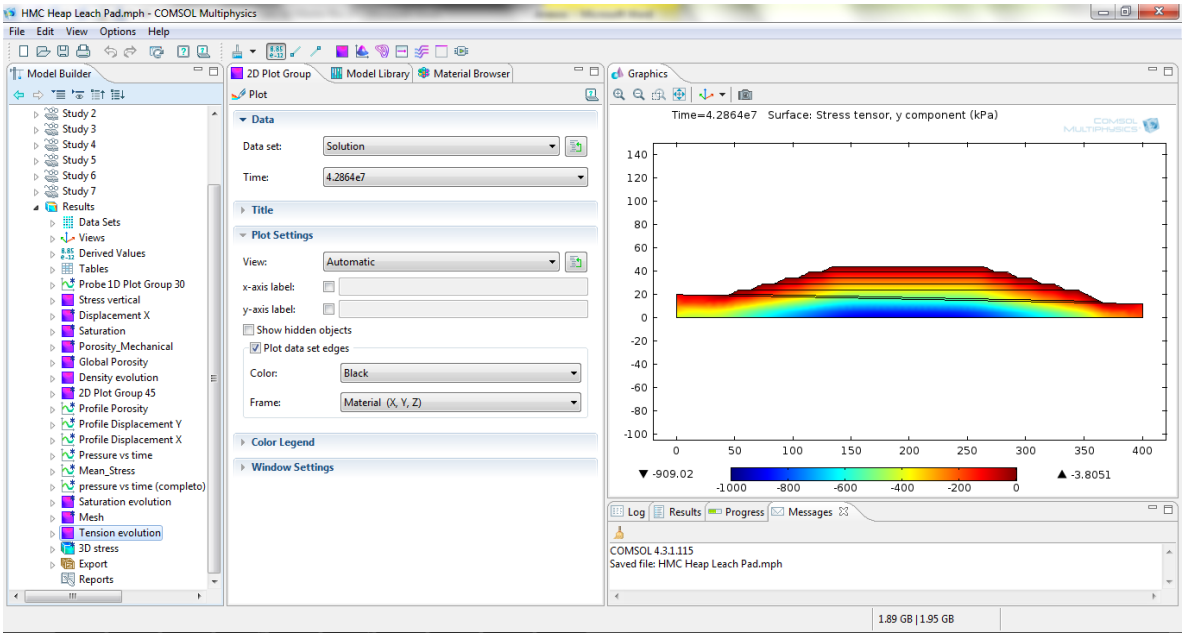

Annex B –COMSOL-PHREEQC interface: example of verification

1. VERIFICATION OF THE IMPLEMENTATION: TEST CASE

This annex presents a verification example to test the reliability of the implementation of the coupling procedure. To this end, the capability of PHREEQC to simulate reactive transport under saturated conditions in 1D has been exploited to compare the results with those obtained with the COMSOL-PHREEQC interface.

1.1 Example of 1D reactive transport with PHREEQC

To test the reliability of the COMSOL-PHREEQC interface, an example using the PHREEQC capability of performing 1D reactive transport has been used. Example number 11 of the PHREEQC manual has been simulated with PHREEQC and with the COMSOL-PHREEQC interface.

The example consists of advective transport in a 1D column in the presence of a cation exchanger. The chemical composition of the effluent from a column containing a cation exchanger is simulated. Initially, the column contains a sodium-potassium-nitrate solution in equilibrium with the cation exchanger. The column is then flushed with three pore volumes of calcium chloride solution. Calcium, potassium, and sodium react to equilibrium with the exchanger at all times. The problem is run using the TRANSPORT data block, which simulates advection and dispersive mixing. The input data set is listed in Table 1. The column has 40 cells in the PHREEQC simulation, and all cells contain the same solution (the definition of a solution for each cell is mandatory). The number of the exchanger corresponds to the number of the cell in a column. In this example, an identical exchanger composition is prescribed for all cells.

The solution filling each of the 40 cells of the column is defined with the SOLUTION 1-40 data block. The infilling solution for the column is defined as SOLUTION 0, and it is a calcium chloride solution. The amount and composition of the exchanger in each of the 40 cells is defined by the EXCHANGE 1-40 data block. The number of exchange sites in each cell is 1.1 mmol, and the initial composition of the exchanger is calculated such that it is in equilibrium with SOLUTION 1. Note that the initial exchange composition is calculated assuming that the composition of SOLUTION 1 is fixed (the composition of SOLUTION 1 is not changed during the initial exchange-composition calculation).

Table 1. Input data set for example 11 in PHREEQC format.

```
TITLE Example 11.--Transport and ion exchange.
SOLUTION 0 CaCl2
temp 25.0
pH 7.0 charge
pe 12.5 O2(g) -0.68
Ca 0.6 mmol/kgw
Cl 1.2  mmol/kgw

SOLUTION 1-40 Initial solution for column
temp 25.0
pH 7.0 charge
pe 12.5 O2(g) -0.68
Na 1.0  mmol/kgw
K 0.2   mmol/kgw
N(5) 1.2  mmol/kgw

EXCHANGE 1-40
Equilibrate with solution 1
X 0.0011 # moles of sites

TRANSPORT
-cells 40
-length 0.002  # meters
-shifts 120   # total simulation time = 120 x 720 sec = 86400 sec = 1 day
-time_step 720.0  #seconds
-flow_direction forward
-boundary_cond flux flux
-diffc 0.0e-9  #diffusion coefficient
-dispersivity 0.002  #meters
-correct_disp true
END
```

The results for example 11 are shown by the curves in Figure 1. The concentrations in cell 40, the end cell, are plotted against time (breakthrough curve). Chloride is a conservative solute and arrives in the effluent at about one pore volume (1/3 day). The sodium initially present in the column exchanges with the incoming calcium and is eluted as long as the exchanger contains sodium. The midpoint of the breakthrough curve for sodium occurs at about 1.5 pore volumes (half a day). Because potassium exchanges more strongly than sodium (larger log K in the exchange reaction), potassium is released after sodium. Finally, when all of the potassium has been released, the concentration of calcium increases to a steady-state value equal to the concentration in the infilling solution.

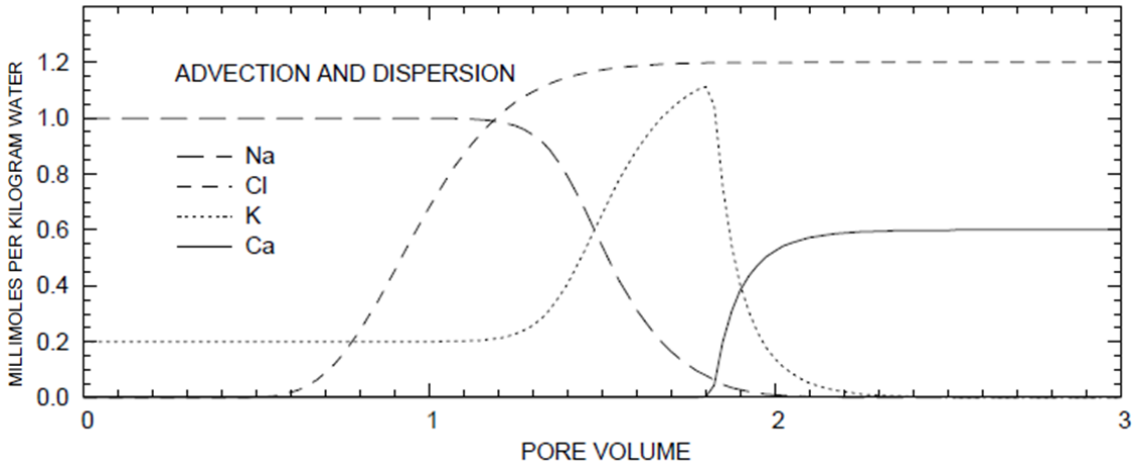

Figure 1. Results of the 1D reactive transport in a column obtained with PHREEQC. Note that the x-axis can be transformed to time by multiplying the pore volume with the number of cells (40) and the time-step length (720 sec), yielding a final value of 1 day.

1.2 Simulation using the COMSOL-PHREEQC interface

1.2.1 Setup of the simulation

The same simulation problem described in the previous section has been repeated with the COMSOL-PHREEQC interface, to test the reproducibility of the results and therefore build confidence on the implementation of the interface. The main differences are that in this case the 1D problem has been simulated using a 3D mesh of the column with tetrahedral (linear) finite elements. However, the mean size of the finite elements with respect to the total column length is maintained the same as in the PHREEQC simulation. The total simulation time is also kept to 1 day. The finite element mesh is shown in Figure 2. It consists of 3,173 nodes (15,470 tetrahedral elements).

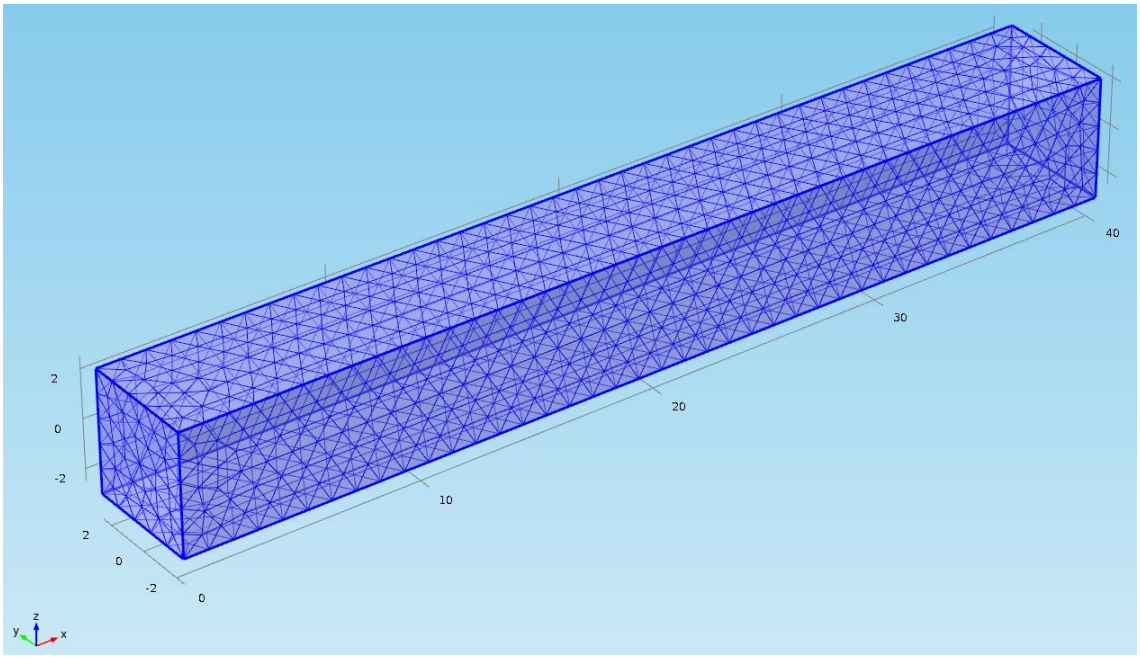

Figure 2. Finite element mesh used in the COMSOL-PHREEQC simulation of the verification case. The number of nodes is 3,173 (which is the number of times that a PHREEQC batch calculation is performed at each time step).

The geochemical setup is based directly on the PHREEQC input files (*.pqi) format. A SOLUTION 0 block is defined for the boundary condition (if more than 1 boundary condition is present, then additional SOLUTION blocks maybe defined), and a SOLUTION 1 block is defined for the initial conditions of the aqueous concentrations in the 1D column. Finally, an EXCHANGE 1 block is considered for the initial ion exchanger composition. Of course, the TRANSPORT block used in PHREEQC is not used in the COMSOL-PHREEQC interface, since this operation is performed by COMSOL. Therefore, the PHREEQC input files for the coupled COMSOL-PHREEQC is equivalent to the input file used for the PHREEQC simulation, except for the transport part.

The setup of the parameters and boundary conditions for the transport part is done in COMSOL, where the same boundary conditions, advective and dispersive data have been considered.

1.2.2 Comparison of the results with PHREEQC simulation in 1D

The concentration of the conservative tracer chlorine is shown in Figure 3 at a simulation time of 0.66 days. It can be observed that the 3D simulation evolves as in the 1D case, with homogenous concentrations in any YZ cross-section.

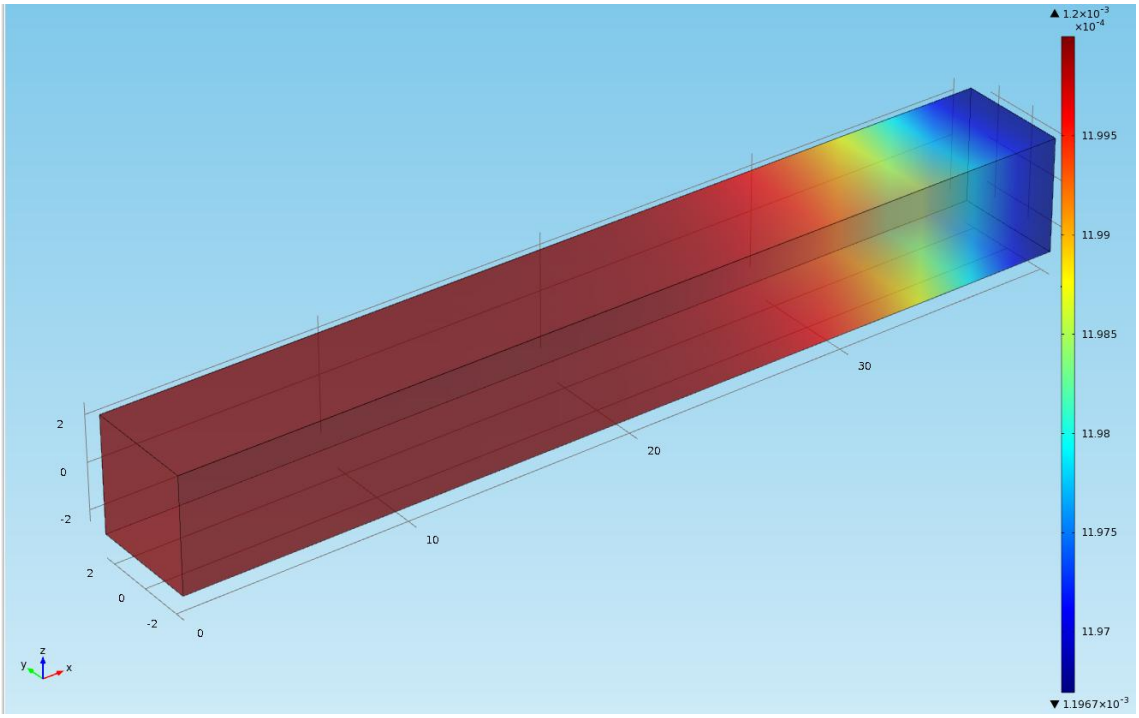

Figure 3. Concentration of chlorine at time = 0.66 days obtained with the COMSOL-PHREEQC interface, showing the transport of a conservative tracer.

The results of the simulation regarding the breakthrough curve at the column outlet are compared with those obtained with the PHREEQC simulation in 1D in Figure 4. An almost perfect agreement is observed for the time evolution of Na^+, Ca^{2+}, K^+, Cl^- between the two simulations. This serves as a verification of the implementation and operability of the COMSOL-PHREEQC interface for saturated conditions.

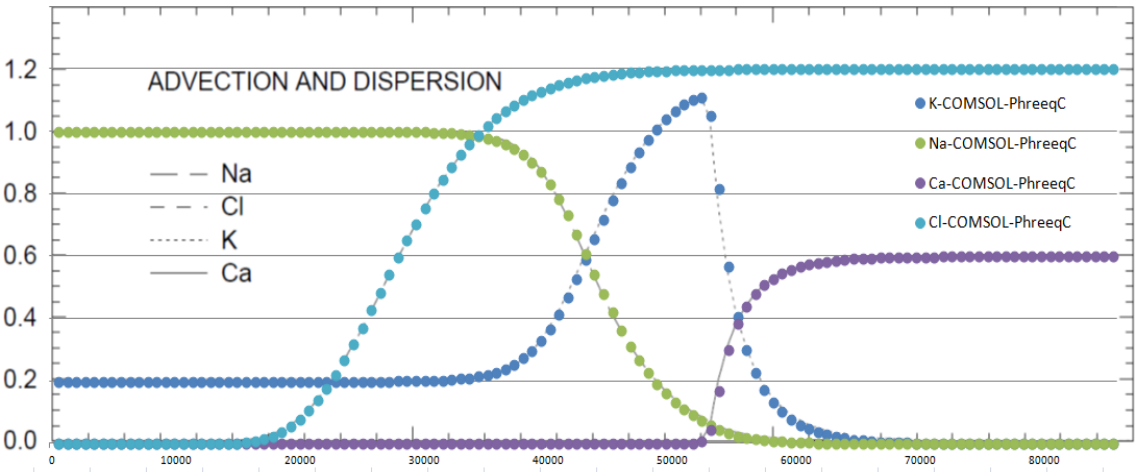

Figure 4. Breakthrough curves of aqueous species concentrations in solution (Na^+, Ca^{2+}, K^+, Cl^-) as a function of time (total time is 1 day). Comparison of results obtained with PHREEQC and COMSOL-PHREEQC interface.